EFFECT OF INFILL WALL STIFFNESS VARIATIONS ON THE BEHAVIOR OF REINFORCED CONCRETE FRAMES UNDER EARTHQUAKE DEMANDS

**A Thesis Submitted to
the Graduate School of Engineering and Sciences of
İzmir Institute of Technology
in Partial Fulfillment of the Requirements for the Degree of**

MASTER OF SCIENCE

in Civil Engineering

**by
Egemen SÖNMEZ**

**July 2013
İZMİR**

We approve the thesis of **Egemen SÖNMEZ**

Examining Committee Members:

_____
Assist. Prof. Dr. Cemalettin DÖNMEZ
Department of Civil Engineering, İzmir Institute of Technology

_____
Assoc. Prof. Dr. Engin AKTAŞ
Department of Civil Engineering, İzmir Institute of Technology

_____
Assist. Prof. Dr. Özgür ÖZÇELİK
Department of Civil Engineering, Dokuz Eylül University

11 July 2013

_____
Assist. Prof. Dr. Cemalettin DÖNMEZ
Supervisor, Department of Civil Engineering
İzmir Institute of Technology

_____
Prof. Dr. Gökmen TAYFUR
Head of the Department of Civil Engineering

_____
Prof. Dr. R. Tuğrul SENGER
Dean of the Graduate School of
Engineering and Sciences

ACKNOWLEDGEMENTS

First and foremost, I offer my sincerest gratitude to my supervisor Assist. Prof. Dr. Cemalettin Dönmez who has supported me throughout my thesis with his knowledge and experience. I would never have been able to complete my dissertation without his guidance and encouragement.

I would like to thank the members of my dissertation committee, Assoc. Prof. Dr. Engin Aktaş and Assist. Prof. Dr. Özgür Özçelik for providing useful suggestions for my dissertation.

Special thanks to my colleagues who helped me in any way they could; especially Mehmet Alper Çankaya for providing me with the data of his experiments whenever I needed.

Last but not least, I would like to express my deepest gratitude to my parents and to my beloved sister who have always believed in me and sacrificed so much throughout my life.

ABSTRACT

EFFECT OF INFILL WALL STIFFNESS VARIATIONS ON THE BEHAVIOR OF REINFORCED CONCRETE FRAMES UNDER EARTHQUAKE DEMANDS

Reinforced concrete (RC) structures with infill walls are the most common building types in earthquake-prone regions of Turkey. Due to the complications in modeling the infill wall - frame interaction, they are generally neglected in structural design. However, presence of the infill walls has been proved to affect stiffness, strength and behavior of the structures significantly. Effects of infill walls may be either beneficial or detrimental under seismic demands. Infill walls typically increase the stiffness and strength of the structures. This situation may be advantageous for non-ductile buildings up to a certain limit. However, brittle nature and variety of failure modes of infill walls may cause unforeseen and irreversible damages. Particularly, soft-story mechanisms may occur due to drift concentrations at lower stories. An organized stiffness distribution along the height of the structure may help mitigating these negative effects.

The main purpose of the study is to investigate the effects of stiffness variations in infill walls to the behavior of the frames. In order to achieve the purpose, an analytical software that supports an infill model, was selected. The software is calibrated and verified by simulating a series of experiments. Afterwards, a planar, five-story, five-bay reinforced concrete frame was designed with common deficiencies observed in residential buildings in Turkey. The performance of the bare frame (BF) was determined using pushover analysis. Then, two types of infilled frames were obtained by introducing infill walls into two bays. The infill walls of the first infilled frame (IF-1) had a uniform stiffness and strength distribution along the height of the frame. In the second infilled frame (IF-2), the stiffness and strength of the infill walls had a decreasing profile from the bottom to the top story. By this distribution, drift concentration at the lower stories was aimed to be mitigated. Nonlinear dynamic and pushover analyses were performed on the frames. The results indicated that the organized stiffness distribution of IF-2 mitigated the drift concentrations and improved the seismic performance of the frame.

ÖZET

BETONARME ÇERÇEVELERDE DOLGU DUVAR RİJİTLİK DEĞİŞİMLERİNİN DEPREM TALEPLERİ ALTINDAKİ DAVRANIŞA ETKİSİNİN İNCELENMESİ

Dolgu duvarlı betonarme binalar, ülkemizin deprem bölgelerinde en sık rastlanan yapı tipleridir. Dolgu duvarlar duvar-çerçeve etkileşiminin modellenmesindeki sorunlardan dolayı yapısal tasarım sürecinde çoğunlukla hesaba katılmazlar. Fakat dolgu duvarların, yapının rijitlik, dayanım ve davranış özelliklerini önemli ölçüde etkilediği bilinmektedir. Bu etkiler, deprem talepleri altında yapı için faydalı olabilecekleri gibi, zararlı da olabilirler. Dolgu duvarlar, yapının rijitlik ve dayanımını artırırlar ve bu durum sünek olmayan binalar için belirli bir seviyeye kadar yararlı olabilir. Fakat dolgu duvarlar, gevrek doğaları ve çok çeşitli göçme şekilleri sebebiyle öngörülemez ve geri dönüşü olmayan hasarlara yol açabilir. Özellikle alt katlarda yoğunlaşan ötelenme talepleri, yapılarda yumuşak kat mekanizmalarının oluşmasına neden olabilir. Binanın yüksekliği boyunca sağlanacak planlı bir rijitlik dağılımı, bu tip olumsuz etkilerin azaltılması yönünde kullanılabilir.

Bu çalışmanın temel amacı, dolgu duvarların rijitliklerindeki değişimlerin çerçevelerin davranışına etkisinin incelenmesidir. Bunun için dolgu duvar modeline sahip bir analiz programı seçilmiş ve bu program, önceden yapılmış bir grup deney modellenerek doğrulanmıştır. Daha sonra, Türkiye'deki yapılarda sıkça görülen kusurlara sahip beş katlı, beş açıklıklı ve düzlemsel bir betonarme çerçeve tasarlanmıştır. Boş çerçevenin performansı artımsal itme analizi kullanılarak belirlenmiştir. Daha sonra boş çerçevenin iki açıklığı dolgu duvarlarla doldurularak iki tip dolgu duvarlı çerçeve elde edilmiştir. Birinci çerçevenin açıklıklarına tek tip dolgu duvarlar yerleştirilirken ikinci çerçevenin açıklıklarına aşağıdan yukarıya gittikçe azalan rijitlik ve dayanım değerlerine sahip duvarlar yerleştirilmiştir. Çerçeveler, doğrusal olmayan statik itme ve dinamik analiz yöntemleriyle analiz edilmiştir. Sonuçlar, binanın yüksekliği boyunca sağlanan planlı rijitlik dağılımının alt katlarda yoğunlaşan ötelenme taleplerini azalttığını ve binanın deprem performansını iyileştirdiğini göstermiştir.

TABLE OF CONTENTS

LIST OF FIGURES

LIST OF TABLES

CHAPTER 1

INTRODUCTION

1.1. Overview

Reinforced concrete frames with masonry infill walls are widespread systems in many earthquake-prone regions of the world. The infill walls are used for insulation and partition purposes rather than structural purposes and generally considered as non-structural elements in structural design. The inherent uncertainties of the infill walls introduce difficulty to regard them as structural members. These uncertainties are associated to both the infill wall and the surrounding frame.

The variability in the material properties of the constituent elements and high nonlinearity of the masonry panels make it difficult to predict/calculate the behavior of the infill walls. Moreover, the properties of the infill walls highly depend on the quality of the bricks, mortar and the workmanship. Typically, quality control of these factors is poor in most applications. In addition, the properties of the frames, i.e. reinforcement detailing, member capacities, number of bays and stories are the factors that influence the behavior of the infilled frames.

In many studies, it is proven that infill walls affect the behavior of structures significantly. If separation joints between infills and bounding frame are not provided, interaction of the frame and the infill wall reveals a different behavior than what is expected. This interaction can be advantageous, if the infill walls are located appropriately throughout the structure and taken into account in the analysis process, if possible. It is known that presence of infill walls lead to considerable increases in lateral strength and stiffness of the frames compared to those of the bare frames while decreasing the average drifts. However, these effects may or may not be advantageous depending on the case. Infill walls are stiff but brittle elements. If the surrounding frame is not strong enough, infill walls can cause unforeseen damages such as premature failures in columns such as shear, compression or tension failures. Another negative effect may be the development of soft-story mechanism in the structure. This mechanism is more likely to occur in the structures without infill walls at bottom story.

However, it is not uncommon to have formation of soft stories after loosing the lower story infill walls due to the high drift concentration in lower stories.

1.2. Background Study

Bertero and Brokken (1983) performed a series of monotonic and quasi-static cyclic tests on 1/3-scale models of the lower three and a half stories of an 11-story, three-bay reinforced concrete frame infilled in the outer two bays. The layout of the model is shown in Figure 1.1.
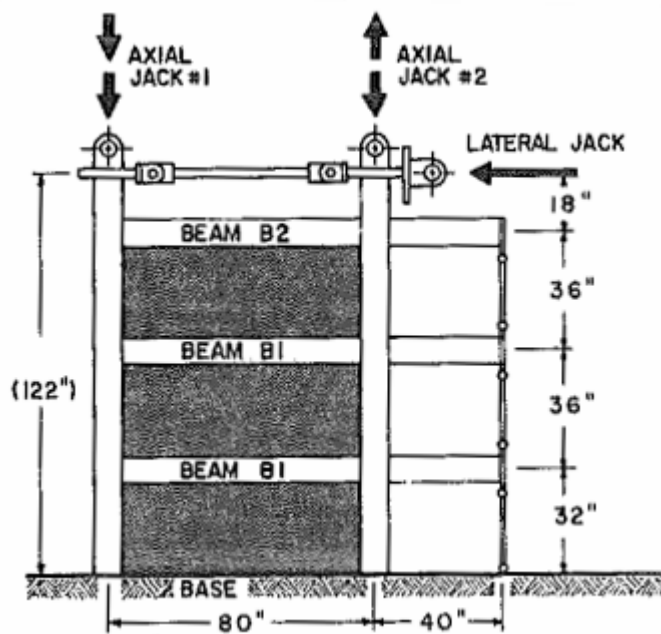
Figure 1.1. Specimens tested by Bertero and Brokken
(Source: Bertero & Brokken, 1983)

Four different infill materials, namely, unreinforced hollow clay panels, reinforced concrete block panels, lightweight concrete panels and solid brick panels with welded-wire reinforcement and a mortar cover, were tested. The results indicated that the lateral stiffness of the infilled frames was 5.3 to 11.7 times that of the bare frame, depending on the infill material. In addition, the lateral strength of the virgin infilled frames was 4.8 to 5.8 times that of the bare frame, while repaired infilled frames yielded 2.8 to 8.0 times higher strength than that of the bare frame. The results also indicated that the lateral strength of an infilled frame is not the sum of the strengths of the infill walls and the confining frame, because the frame may not always reach its lateral load capacity at the same time with the infill. Bertero and Brokken also stated

2

that the infill walls tend to exhibit brittle failure. As a result, the majority of the infilled frames failed with a soft-story mechanism. It was also observed that the properties of the infills highly depend on material quality and workmanship.

Saneinejad and Hobbs (1995) proposed a method to design and analyze concrete or masonry infilled steel frames subjected to in-plane lateral loads. The method depended on the results of previous experiments and finite element analyses. It accounted for two possible infill damage modes, i.e. diagonal compression and corner crushing. The stress distributions along the contact surface between the infill wall and the frame were assumed to be rectangular. The lateral resistance of an infill panel was expressed as a function of these contact stresses and plastic moment capacities of the frame elements. The peak lateral resistance of an infilled frame was defined by a combination of normal and shear contact stresses using a Tresca failure criterion. The paper provides comparisons between the former modeling methods and the proposed method. It was stated that the proposed method gave rationally reliable results. In conclusion, the method proposed design equations to model multistory infilled frames by replacing the infill walls with equivalent diagonal struts. The study includes a design example, as well.

Negro and Verzeletti (1996) conducted a series of pseudo-dynamic tests on a full-scale, two-bay, four-story reinforced concrete frame. The layout of the specimen is given in Figure 1.2. The frame was designed in accordance with the 1988 EC2 and EC8 codes to exhibit high ductility. Initially, the bare frame was subjected to a simulated ground motion generated from 1976 Friuli earthquake with a nominal acceleration scaled by 150%. The frame acted as expected and only minor damage was observed. Then, infill walls made of hollow bricks were added into two external frames in all stories. The infilled frame subjected to the same input signal. The maximum base shear recorded for the infilled frame was 50% higher than that of the bare frame, while the maximum displacement was 40% of the maximum displacement recorded for the bare frame. The infill walls of the first and the second stories entirely collapsed, while the ones at the third story exhibited major damage. The walls at the fourth story remained almost undamaged. Subsequently, a third test was performed by replacing the damaged infill panels and leaving the bottom story bare to create a soft-story mechanism. The maximum base shear in this frame was slightly higher than that of the bare frame, while the maximum displacement is slightly lower. Though, the spatial distribution of the interstory drifts was noticeably different. The maximum interstory drift ratios were

2.4%, 1.1% and 3.5% for the bare frame, uniformly infilled frame and soft-story frame, respectively. The bare frame exhibited a strong-column weak-beam mechanism, while a side-sway mechanism formed in the soft-story frame. It is concluded that the presence of the infill walls affect the behavior of the structure significantly. Additionally, the irregularities in the infill panel distribution can cause major damages to the structure.
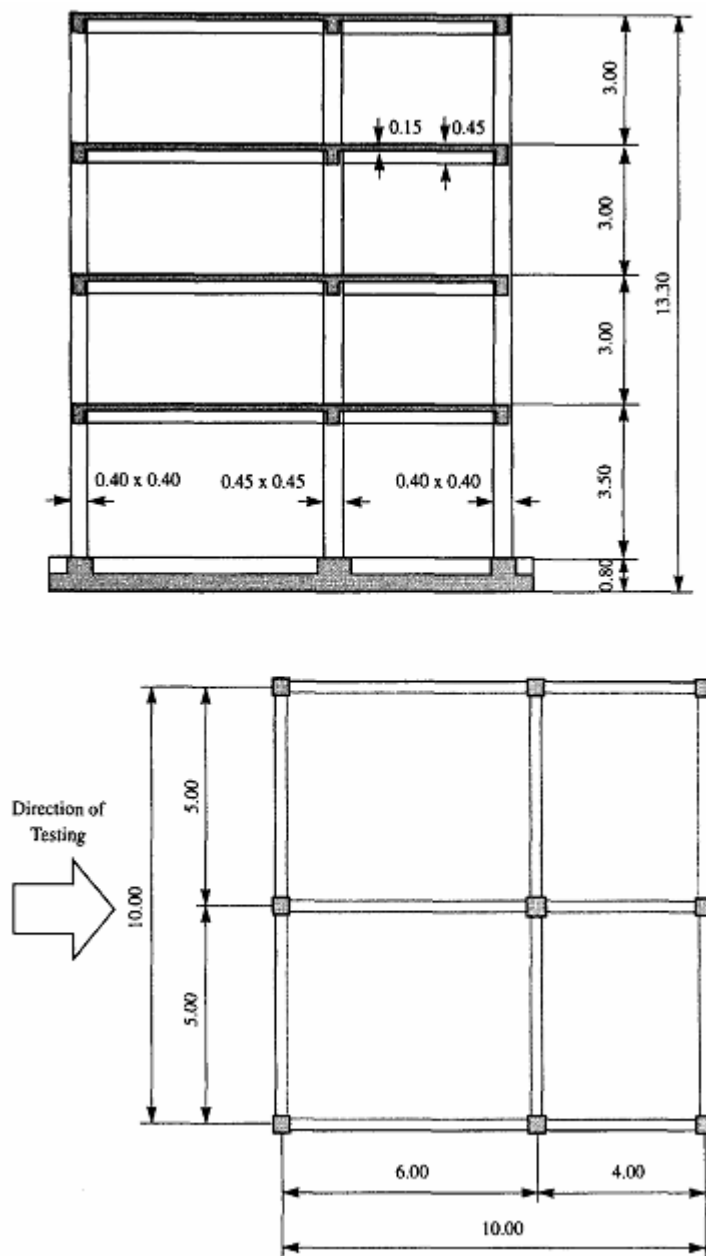
Figure 1.2. Layout of the specimen tested by Negro and Verzeletti
(Source: Negro & Verzeletti, 1996)

4

Madan et al. (1997) proposed a macro-model based on the "equivalent strut" approach to represent the behavior of infilled frames. The equivalent strut model was taken from the work of Saneinejad and Hobbs (1995). However, the formulations proposed in that study furnished only extreme or boundary values. Therefore, a hysteretic model was necessary to perform step-by-step static or dynamic analyses. In order to satisfy this need, the equivalent strut approach was integrated with the smooth hysteretic model proposed by Bouc (1967) and enhanced by Baber and Wen (1981). Characteristic hysteretic properties of the infill walls such as stiffness degradation, strength deterioration and pinching were taken into account in the proposed model. In the following sections of the study, verifications of the proposed method were presented. Firstly, the experimental and analytical results of a one-bay steel frame were compared. The analyses were performed using IDARC-2D Version 4.0 (Valles et al., 1996). The comparisons showed a good agreement in terms of hysteresis curves. Then, dynamic analyses of a previously tested three-story and three-bay reinforced concrete frame with and without infill walls were performed using IDARC-2D. The authors stated that the proposed hysteretic rule was satisfactory after comparing the experimental and analytical results.

Erdem et al. (2006) investigated the effects of two strengthening methods on the response of infilled frames and compared the results to the previously tested bare frame. Two 1/3-scale, two-story, three-bay reinforced concrete frames were constructed. The dimensions and the reinforcement details are given in Figure 1.3. The frames were designed to represent the common deficiencies encountered in most of the residential buildings in Turkey.
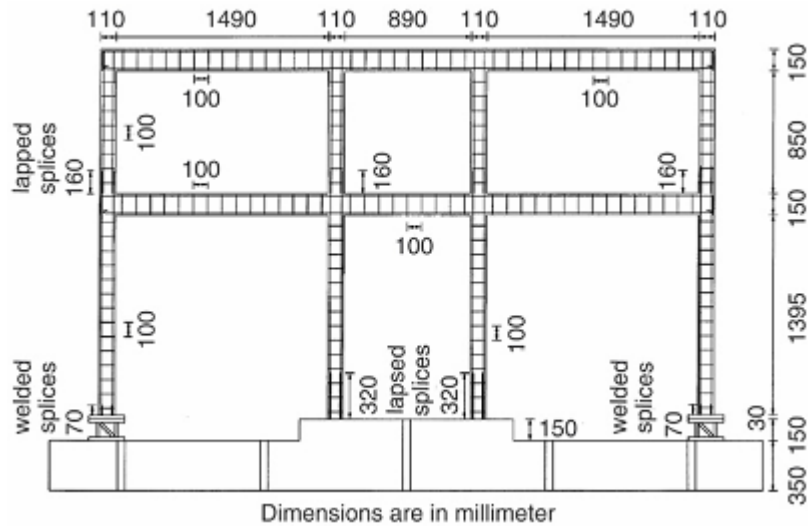
Figure 1.3. Dimensions and reinforcement details
(Source: Erdem et al., 2006)

The first strengthening method was to provide 70 mm reinforced concrete infills in the middle bay of the frame. The connection between the infill and the frame was provided with steel dowels. In the second strengthening method, the middle bay of the frame was filled with hollow clay tile infill walls. The walls were plastered and anchored to the frame using carbon fiber anchor dowels. Total thickness of the infill panel was 90 mm with 10 mm being the plaster at both sides. In addition, carbon fiber reinforced polymer (CFRP) strips were applied diagonally on the infill walls for strengthening purposes. The specimens were subjected to quasi-static cyclic loadings at the second stories. The results indicated that both methods increased the lateral strength of the frames by approximately 500%. The stiffness of the infilled frames was ten times of that of the bare. The strength degradation in the second specimen was more significant, although the peak strength values of both specimens were nearly the same. It was also observed that 90% of the base shear was carried by the infill walls. Therefore, low ductility of the frame elements had no significant effect on the capacity of the test specimens.

Dolšek and Fajfar (2008) studied the effects of infill walls on a four-story, planar reinforced concrete frame. They used the N2 method which is a performance-based nonlinear analysis technique developed by Fajfar. A partially-infilled frame which has openings in the infill walls and a fully-infilled frame without openings were analyzed and the results were compared to that of a bare frame. The frames were designed to represent the typical building types built in European and Mediterranean

countries forty to fifty years ago. Details of the tested frames are presented in Figure
1.4. The infill walls, made of clay hollow bricks, were modeled using the equivalent
strut approach. The analytical models were calibrated and validated using the results of
previously performed experiments of the analogous frames.
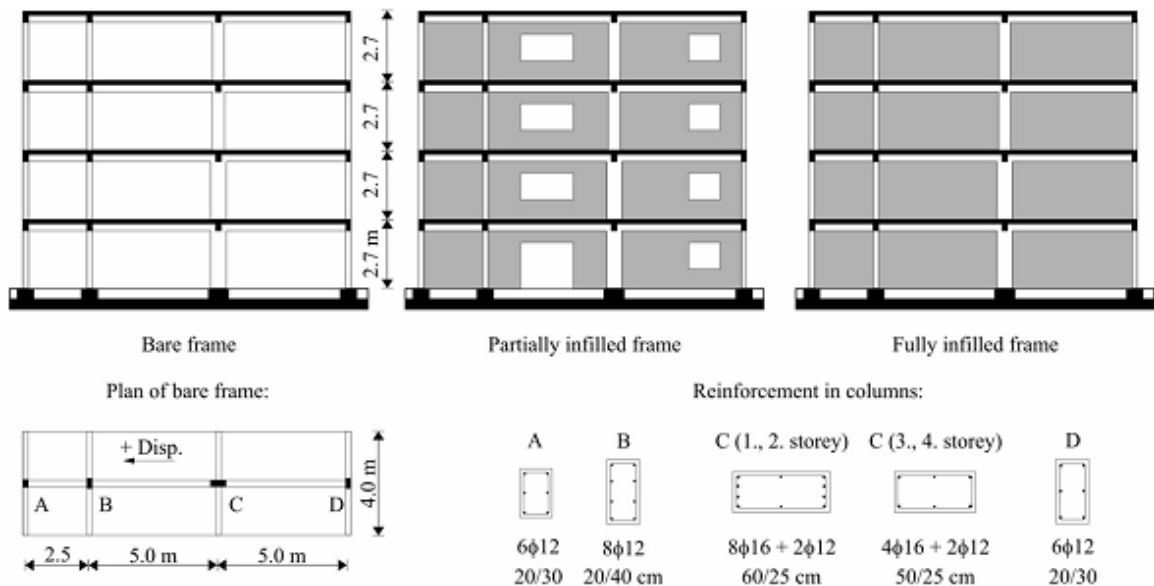
Figure 1.4. Layout of the frames and reinforcement details of the columns
(Source: Dolšek and Fajfar, 2008)

Afterwards, capacities of the frames were determined by pushover analyses. The
analyses were performed by considering the structures that were located in moderate
seismic hazard region and high seismic hazard region. It was observed that the presence
of the infill walls increased the stiffness and the strength of the structures significantly.
The base shear coefficients of the frames were calculated as 0.13 for the bare frame,
0.43 for the partially-infilled frame and 0.73 for the fully-infilled frame. Dramatic
strength degradation was observed after all the infill walls in the first stories had
collapsed. The degradation amounted to 57% and 77% of the maximum base shear for
the partially-infilled and fully infilled frames, respectively. The roof drift ratios
measured at the near-collapse state were approximately 0.75% for both of the infilled
frames, while it was 1.14% for the bare frame. Soft-story mechanism was observed in
all the frames. The collapse mechanism occurred in the third story of the bare frame
where the cross-sections of the columns change at. The mechanisms of the infilled
frames occurred in the first stories due to the brittle failure of the infill walls. As a
result, the maximum interstory drifts were observed in the mentioned stories.

Demands corresponding to limited damage, significant damage and near-collapse states were calculated for each frame for ground motions with 225, 475 and 2475-year return periods in moderate and high seismic hazard regions. The analysis results and the demands were compared for seismic assessment of the structures. Considering the comparisons, it was stated that infill walls could improve the behavior up to a certain intensity of ground motion, though a slight increase in the amplitude of the ground motion may lead the structure to significant damage. The study showed that the stiffness and the strength of the structures increase noticeably, provided that the demand does not exceed the deformation capacity of the infill walls. Subsequent to this situation, the global stiffness and strength of the system rapidly decreases. It is also seen that the contribution of the infill walls strongly affects the damage distribution and behavior and should be taken into account in design process. The effects of the infill walls deemed advantageous, unless the placement of the walls cause an irregularity in elevation or plan. In addition, shear failures in the column ends should be avoided.

Pujol and Fick (2010) performed pseudo-static tests on a full-scale, three-story, flat-plate reinforced concrete building which was designed according to modern codes only for gravity loads. Initially, the bare frame was subjected to four cycles of lateral loading showing a triangular distribution. The structure was pushed to roof drifts of 0.22%, 0.45%, 1.5% and 3.0% in consecutive cycles. After the roof drift ratio reached to 2.8%, shear failure observed at a column-slab connection on the third story. After the first test was completed, the infill walls were added into one of the two bays in each story. The structure with infill walls is shown in Figure 1.5. The walls were made out of modular-cored clay bricks and type N mortar. The infilled structure was subjected to twenty cycles of increasing roof drift ratios ranging from 0.025% to 1.25%. Each drift target was applied twice.

Diagonal cracks, sliding planes and corner crushing in the infilled bays can be observed from the crack maps in Figure 1.6. The results of the experiments indicated that the added infill walls increased the lateral strength of the structure by approximately 100% and the lateral stiffness by approximately 500%. The infilled structure maintained its lateral load capacity up to a roof drift ratio of 1.5%. That drift capacity was deemed satisfactory. The study implied that infill walls could be able to improve the performance of older buildings by controlling interstory drifts.
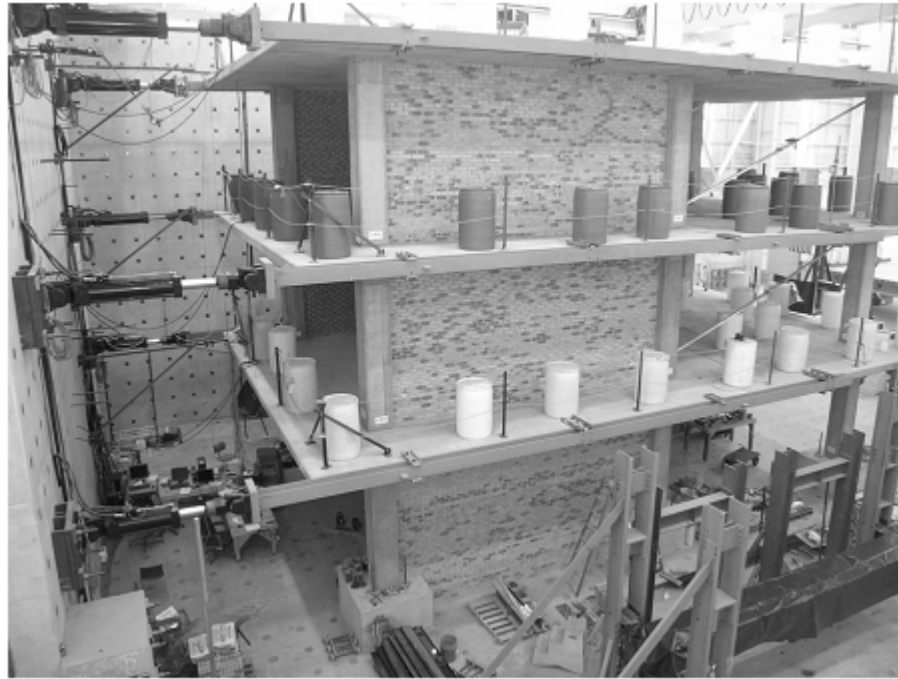
Figure 1.5. Infilled frame of Pujol and Fick
(Source: Pujol and Fick, 2010)
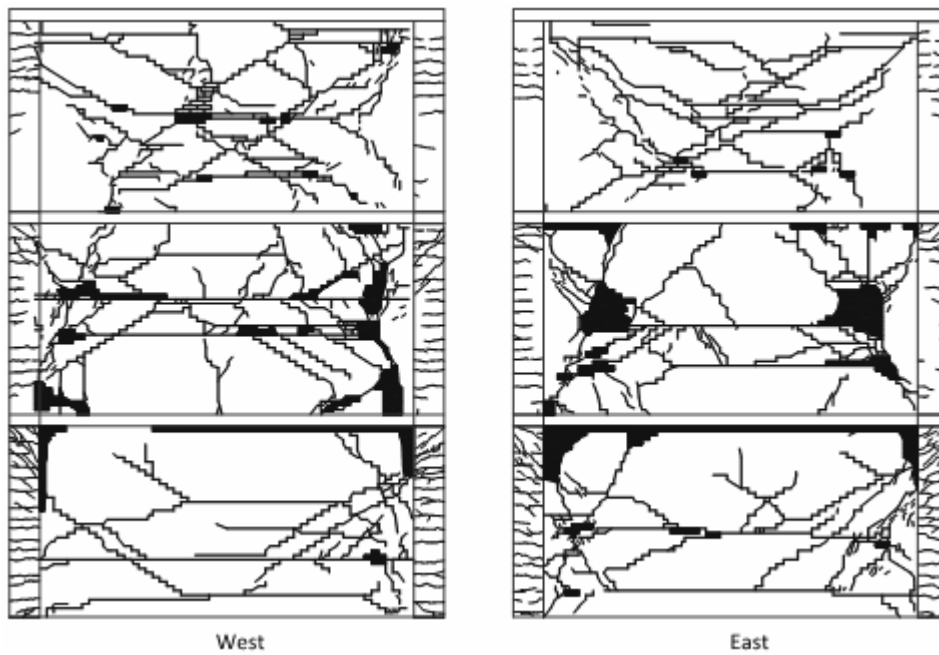
Figure 1.6. Crack patterns of the infilled bays
(Source: Pujol and Fick, 2010)

Mohammadi et al. (2011) conducted a two-phase study to investigate the efficiency of various methods to improve the ductility of infilled frames. The first stage

included three techniques, namely, cornerless infill, column fuse and infill fuse. Six 2/3-scale, single-bay, single-story steel frames were constructed. The frames were infilled with three-ply panels composed of masonry and concrete materials. The specimens were subjected to five loading cycles of drift ratios ranging from 0.5% to 2.5% and pushed to failure, if possible. Two frames were used for testing each method – one frame with a regular infill configuration and one frame with the proposed method. The first method, that is cornerless infill, was achieved by removing the masonry from the corners of the panel. The purpose in this method was to transfer the failure to the beams, which are normally weaker than the columns. However, corner crushing took place below the openings in the top corners. The strength and stiffness of the system was observed to be significantly lower than those of the regularly-infilled frame. The results indicated that the technique was not satisfactory in improving the ductility. The second technique was to provide fuses in the columns to make them yield before the infill panel reaches the cracking load. The method prevented infill crushing, but did not improve the ductility of the system. In the third method, horizontal sliding surfaces were formed by slitting the infill panel horizontally. Two steel plates with a thin grease layer in between were placed between the partitions. The fused specimen exhibited a more ductile behavior and prevented the infill damage to take place. The infill wall remained intact up to the story drift ratio of 7.1%. The method yielded satisfactory results and in the second phase of the study, the improvements in this technique were investigated.

The infill fuse technique found to have disadvantages, as well. Therefore, some improvements were proposed. The first disadvantage was possible shear failure in the columns due to the compression stresses in the regions close to the contact surfaces. The second deficiency was a potential out-of-plane failure of the infill panel. In order to fix these defects, a frictional sliding fuse (FSF) was designed. The FSF was composed of one sliding steel plate between two fixed steel plates. The sliding plate was bolted to the fixed plates in such a way to allow for sliding in the longitudinal direction while constraining the out-of-plane movement. It is also possible to adjust the sliding strength using the bolts. The infill walls were also chamfered in the mid-height in order to prevent infill-frame interaction in the slide region. Two single-bay, single-story, 1/3-scale steel frames were constructed to test the enhancements made for the infill fuse technique. The details of the specimen are presented in Figure 1.7. The frames were infilled with fibrous concrete and the FSF was placed in the mid-height of the infill wall. The FSF of the first specimen, was set for a sliding strength of 51 kN and the FSF

of the second specimen, was set for 73 kN to investigate the effect of sliding strength. The specimens were subjected to in-plane, quasi-static, cyclic loading tests. The results indicated that the stiffness and the strength of the specimens increased in accordance with the FSF sliding strengths. In addition, the first specimen was loaded in the out-of-plane direction and remained stable.
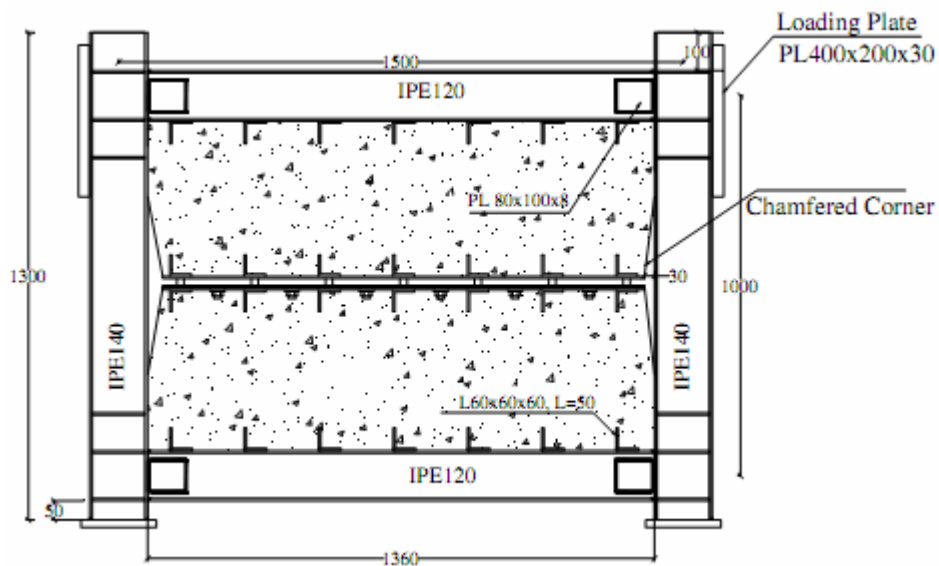
Figure 1.7. Details of the specimen
(Source: Mohammadi et al., 2011)

Preti et al. (2012) investigated the behavior of infilled frames with horizontal sliding joints in the infill walls. Four single-bay, single-story, large-scale steel frames were constructed. Two of them were filled with hollow clay bricks and the other two were filled with adobe. Sliding joints were provided in one of the each set of frames. The average compression strength of the hollow clay bricks was 12.1 MPa and 2.3 MPa in parallel and perpendicular directions to the holes, respectively. The mortar compressive strength was 5 MPa. Two sliding joints were formed by two couples of shaped steel foils of 2 mm thickness. The thickness of the bricks and the plaster was 200 mm and 10 mm, respectively. In the adobe infill, solid adobe bricks and mud mortar were used. The compressive strengths of the adobe units and the mortar were measured to be 2.3 MPa and 2.8 MPa, respectively. Three sliding joints were provided in the adobe infill using straight wooden boards. Thickness of the adobe units was 120 mm. The adobe infill was not plastered to observe crack patterns accurately. The specimens were subjected to a cyclic loading program and were pushed up to a drift level of 2.5%, if possible. In the first test, it was noticed that the contact between the infill and the

upper beam limited the sliding mechanism. Therefore, the contact removed in all the specimens to ensure an effective sliding movement. The test results yielded that the sliding joints improved the ductility of the infilled frames, while reducing the infill damage. The adobe infills reached to large deformations with ignorable damage, due to low stiffness and strength of the material.

1.3. Objective and Scope

The main objective of the study is to investigate the effects of the changes in the stiffness of the infill walls on the seismic response of reinforced concrete frames. Specifically, change of interstory drift distribution with the change in stiffness of the infill walls is investigated. The stiffness distribution along the height of the structure is controlled by varying stiffness of the infill walls in elevation. Different infill retrofitting and weakening methods are assumed to be applied at different floor levels to control the stiffness distribution. Thus, distribution of interstory drift ratio is targeted to be controlled to mitigate concentration of drift at lower levels in the structure.

An analytical software was selected for the study. The software was calibrated and validated by simulating a series of previously performed experiments in the first stage of the study.

In the second stage, a five-bay, five-story, planar reinforced concrete frame was designed. The frame is aimed to have common deficiencies observed in the residential buildings in Turkey. A pushover analysis of the designed frame was performed according to the Turkish Earthquake Code (TEC2007) and the structure was determined to be in the pre-collapse region. Afterwards, two types of infilled frames were obtained by placing infill walls into the two bays of the frame. Stiffness of the infill walls were the main parameters of the study. The infill walls of the first infilled frame (IF-1) had a uniform stiffness and strength distribution along the height of the frame. In the second infilled frame (IF-2), the stiffness and strength of the infill walls had a decreasing profile from the bottom to the top story. A series of nonlinear dynamic analyses were performed with the bare and the infilled frames. Seismic response and the drift distribution of the frames are determined and compared. Moreover, pushover analyses of the infilled frames were performed to determine the influence of stiffness variations in the infill walls on the performance of the structures.

CHAPTER 2

MODELING THE NONLINEAR BEHAVIOR OF RC FRAMES WITH INFILL WALLS

2.1. Introduction

A numerical study is performed to estimate the hysteretic control parameters and verify the selected nonlinear analysis program. Four RC frames were analyzed using IDARC-2D Version 7.0. Details and properties of the modeled frames are presented in this chapter. Brief explanations of the hysteretic behavior and infill models implemented in the program are also given. Afterwards, numerical model, selected control parameters and loading histories are presented. The chapter ends with comparison of the numerical and the experimental results.

2.2. Frames

An experimental study was conducted in Izmir Institute of Technology (IYTE) Structural Mechanics Laboratory by Çankaya (2011) to investigate dynamic behavior of infilled frames. Four single-bay, 1/5-scale, four-story, planar RC frames with and without infill walls (Figure 2.1) were subjected to pseudo-static cyclic loading. Infill walls were present in two of the frames. Another parameter of the study was the reinforcement detailing. One frame from the each set of bare and infilled frames had brittle reinforcement details, while others had ductile reinforcement details. Brittle detailing was obtained by insufficient splice lengths for longitudinal column reinforcement, large stirrup spacing, and 90° stirrup hooks. Ductile detailing was determined according to the Turkish Earthquake Code (TEC2007). Brittle and ductile reinforcement details are presented in Figure 2.2 and Figure 2.3, respectively.
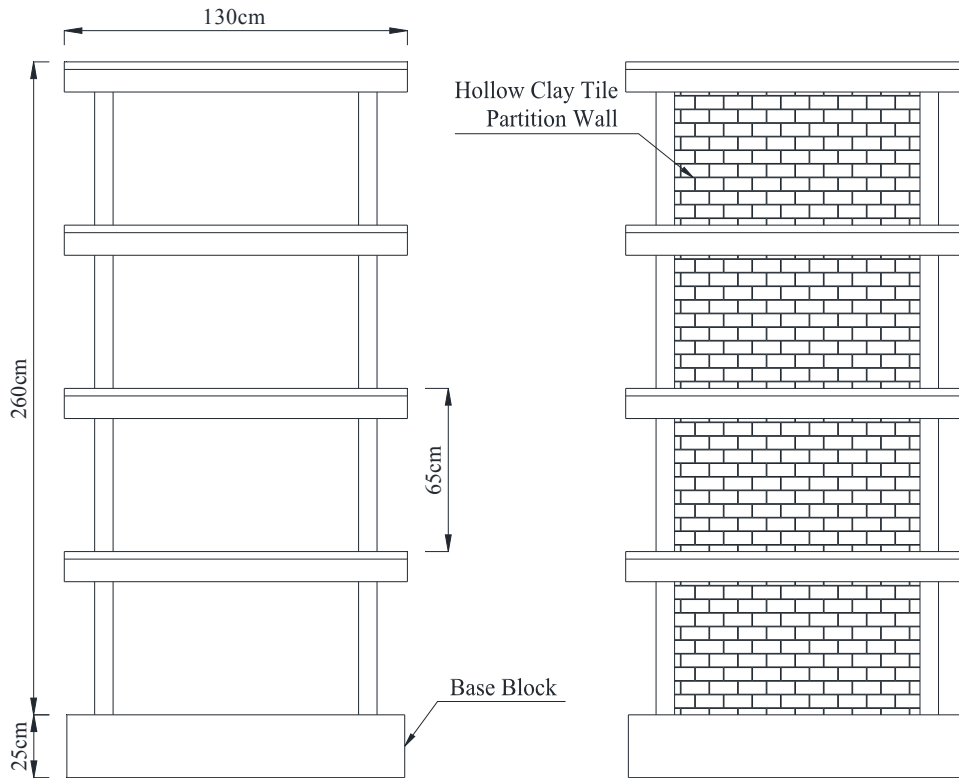
Figure 2.1. Overview of the frames used in the experiments and analyses

Frame #1 and #2 were the bare frames with brittle and ductile reinforcement detailing, respectively. Frames #3 and #4 were the infilled frames with brittle and ductile reinforcement detailing, respectively, Table 2.1.

Table 2.1. Frame definitions

| FRAME NO | EXPERIMENT PARAMETERS | |
	Presence of Infill Walls	Reinforcement Detailing
#1	No	Brittle
#2	No	Ductile
#3	Yes	Brittle
#4	Yes	Ductile

3 E3@3CM 2 cm 6 E3@5CM 11 E3@3CM 6 E3@5CM

LOAD
TRANSFER
ROD , Ø16 Ø 18 PVC PIPE

2 BEAM REINFORCEMENT DETAILS

Ø8 Logitidunal
Reinforcement Bars

Beam section 2

E1,
TYPICAL

4CM SPACING

20 CM
DEVELOPMENT
LENGTH

BOTTOM-TOP,
TYPICAL

Ø8 Logitidunal
Reinforcement Bars

Column section 1

Ø5
10.5 cm
5.5 cm

E3 TYPE TRANSVERSE
REINFORCEMENT

Ø5
8.5 cm
5.5 cm

E1 TYPE TRANSVERSE
REINFORCEMENT

2 cm

Joint Zone
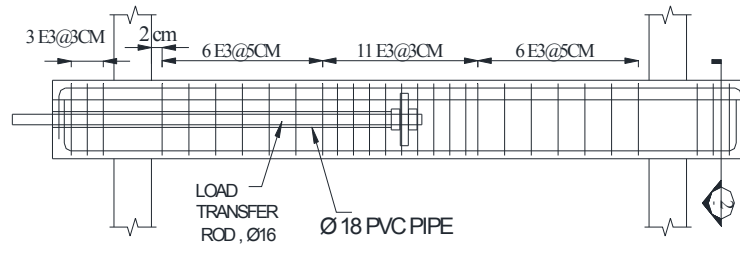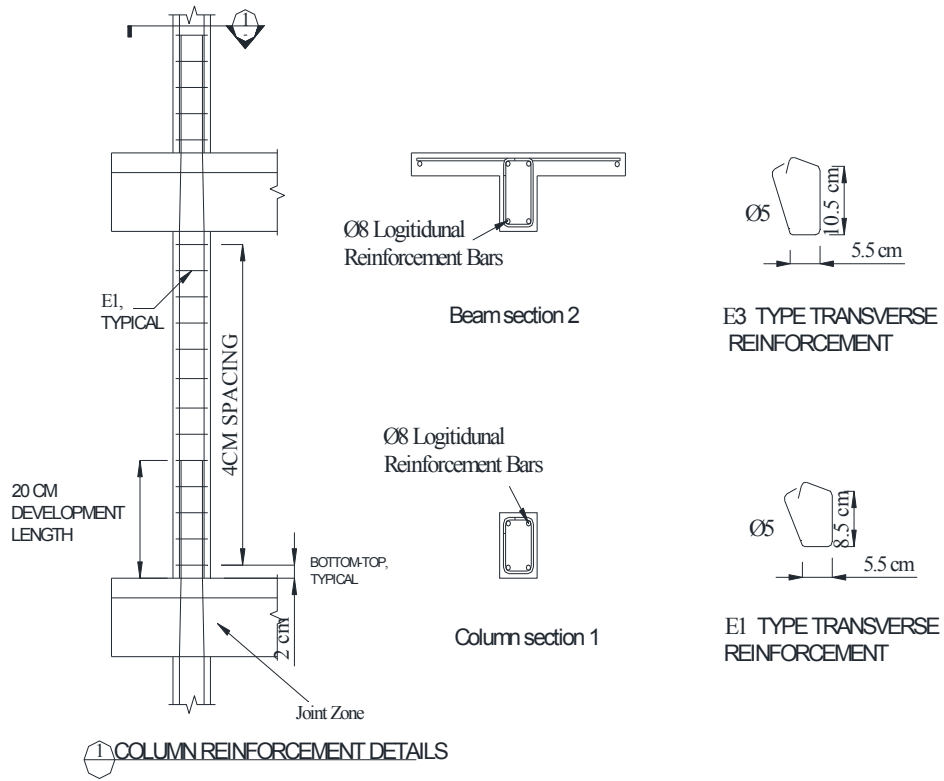
1 COLUMN REINFORCEMENT DETAILS

Figure 2.2. Reinforcement details of the frames with ductile reinforcement
(Source: Çankaya, 2011)
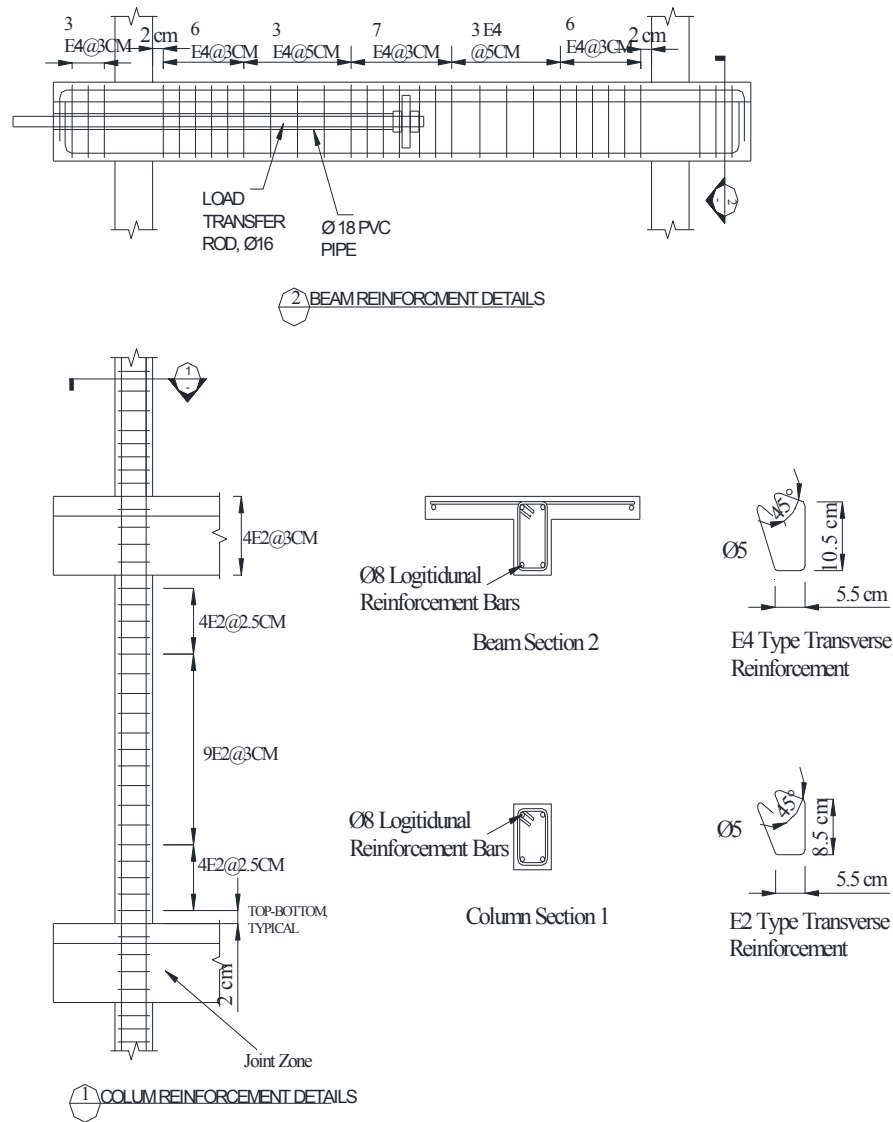
Figure 2.3. Reinforcement details of the frames with brittle reinforcement
(Source: Çankaya, 2011)

Material properties used in the numerical analyses are taken from the test results of Çankaya (2011). 8 mm deformed bars that were used as longitudinal reinforcement in columns and beams had an average yield stress of 470 MPa. Test results of 5 mm cold-drawn plain bars, which were used as shear reinforcement, showed that they had an average yield stress of 420 MPa. Although their ultimate strain values were below the defined limits of Turkish RC Code (TS500, 2000), these values were accepted to be valid, since no stirrup failure was observed during the tests.

Compressive strength values of the concrete were obtained from the results of the cylinder compression tests which were performed on the day of each experiment.

The specimens had 42.6, 36.1, 37.1 and 24.7 MPa compressive strengths for Frames #1 to #4, respectively.

In the experiment, hollow clay tiles of 57 x 100 x 130 mm were used in the infill walls. Two types of tests were performed for determining the compressive and shear strengths of the clay tile prisms. In the first test, three prisms containing two tiles combined with mortar were subjected to axial loading along the holes. The compressive strengths were measured to be 3.6, 5.4 and 5.0 MPa. In the second test, three diagonal compression tests were performed. The shear strengths of the prisms were obtained as 0.16, 0.22 and 0.47 MPa and 0.86, 0.84 and 0.57 MPa for Frame #3 and Frame #4, respectively.

2.3. Software

IDARC-2D (Inelastic Damage Analysis of Reinforced Concrete) Version 7.0 is selected to perform analyses of the presented study. This program is an analytical software for the inelastic evaluation of buildings under dynamic, static and quasi-static loading.

The program was developed as a research tool at the State University of New York at Buffalo. The main purpose in developing the program was to overcome numerous constrictions encountered in many other analytical programs. IDARC presents several hysteretic behavior models and gives users the possibility to adjust the parameters of those models to capture the actual behavior of structures. The details of the hysteretic behavior models can be found in Section 2.3.1.

Moreover, the program is capable of modeling shear walls, edge columns, transverse beams, rotational inelastic springs, viscoelastic and friction dampers and infill walls. The latter is also the main subject of this study. Explanation of the infill model is presented in Section 2.3.2.

2.3.1. Hysteretic Behavior Models

IDARC includes six types of hysteretic response models. The models are as follows:

- Three-parameter Park model

- Tri-linear steel model

- Bilinear hysteretic model

- Kelvin model

- Maxwell model

- Smooth hysteretic model

Each model is used to model the behavior of different structural elements. Beams, columns, rotational inelastic springs and shear walls can be modeled using the three-parameter Park model, tri-linear steel model or bilinear hysteretic model. Viscoelastic dampers can be modeled using either the Kelvin or the Maxwell model. Hysteretic dampers, friction dampers and infill walls are modeled using the smooth hysteretic model.

Since, the frames analyzed in this study consisted of reinforced concrete beams, columns and masonry infill walls, only the three-parameter Park model and the smooth hysteretic model will be mentioned herein.

2.3.1.1. Three-parameter Park Model

In order to represent the nonlinear cyclic behavior of reinforced concrete members, a complicated yet simple-to-adjust model is essential. The three-parameter Park hysteretic model (Park et al., 1987) satisfies this need by introducing parameters α, β and γ to represent and control stiffness degradation, strength deterioration (β_1 for ductility-based, β_2 for energy-based) and pinching effects in hysteretic cycles, respectively. Figure 2.4 shows the effects of those parameters on a hysteretic curve. Additionally, the typical ranges are presented in Table 2.2 to form an understanding about the values of those parameters.
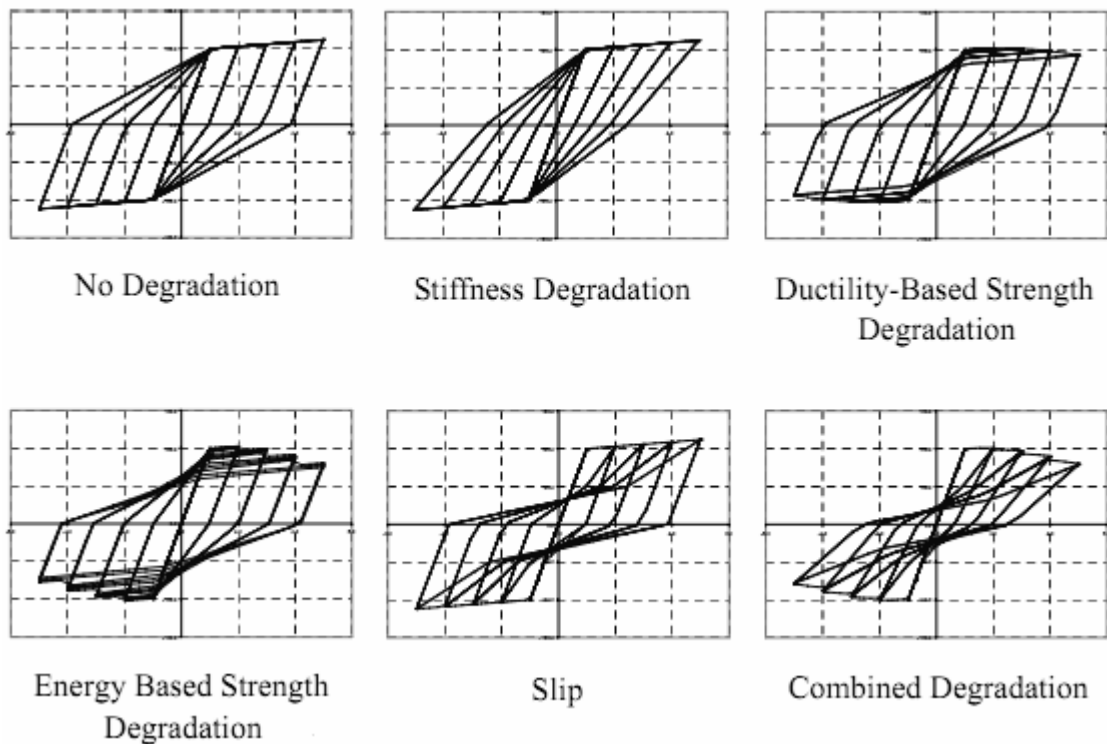
Figure 2.4. Effects of control parameters on hysteretic behavior
(Source: IDARC User's Guide, 2010)

Table 2.2. Typical range of values for three-parameter Park model
(Source: IDARC User's Guide, 2010)

PARAMETER	MEANING	VALUE	EFFECT
α	Stiffness Degrading Parameter	4.00	Severe Degrading
		10.00	Moderate Degrading
		15.00	Mild Degrading
		200.00	No Degrading
β_1	Strength Degrading Parameter (ductility-based)	0.60	Severe Degrading
		0.30	Moderate Degrading
		0.15	Mild Degrading
		0.01	No Degrading
β_2	Strength Degrading Parameter (energy-based)	0.60	Severe Deteriorating
		0.15	Moderate Deteriorating
		0.08	Mild Deteriorating
		0.01	No Deteriorating
γ	Slip or Crack-closing Parameter	0.05	Severe Pinched Loops
		0.25	Moderate Pinching
		0.40	Mild Pinching
		1.00	No Pinching

2.3.1.2. Smooth Hysteretic Model

The smooth hysteretic model (Reinhorn et al., 1995) used for infill walls in IDARC is based on the Bouc-Wen model (Bouc, 1967; Baber and Noori, 1985). This model takes into account hysteretic effects such as stiffness degradation, strength deterioration and pinching which are characteristics of infill walls subjected to lateral-load reversals. A list of the parameters used by the model and their default values are presented in Table 2.3. Detailed information about the calculation steps can be found in Valles et al. (1996).

Table 2.3. Control parameters of the smooth hysteretic model
(Source: IDARC User's Guide, 2010)

PARAMETER	MEANING	DEFAULT VALUE
A	Parameters that control the shape of generated hysteretic loops	1.00
β		0.10
γ		0.90
η	Parameter controlling the stiffness decay	2.00
α	The ratio of the post-yield stiffness to the initial stiffness	0.01
IS	Flag to indicate the presence of slip in hysteresis	1.00
A_s	Control parameter for slip length	0.30
Z_s	Parameter controlling the sharpness of the slip	0.10
$\overline{Z}$	Offset value for slip response	0.00
s_k	Control parameter to vary the rate of stiffness decay	0.10
s_{p1}	Parameters to control the rate of strength deterioration	0.80
s_{p2}		1.00
μ_u	Ductility capacity of infill panel	5.00

2.3.2. Infill Wall Model

The analytical models that represent the behavior of the infill walls may be categorized into two main groups as micro-models and macro-models.

Micro-models are based on the finite element method. In this approach, detailed modeling of the infill walls is established by modeling masonry units, mortar and interface elements separately to represent the behavior of the infill wall more accurately. On the other hand, major computational effort and calibration of high amount of parameters are the disadvantages of the method. Therefore, this approach may be effective for local analyses such as frame-infill interaction or failure modes of the walls, but impractical for global analyses.

Macro-models use equivalent struts to model the contribution of the infill walls to the response of the infilled frame. This method replaces the infill panel by two diagonal, compression-only struts as seen in Figure 2.5. This approach is advantageous since the masonry is a very heterogeneous material and it is hard to predict the material properties of the constituent members accurately. Besides, it is possible to obtain mechanical properties of the infill walls from prism tests to model the equivalent struts. IDARC utilizes macro-modeling for infill walls.
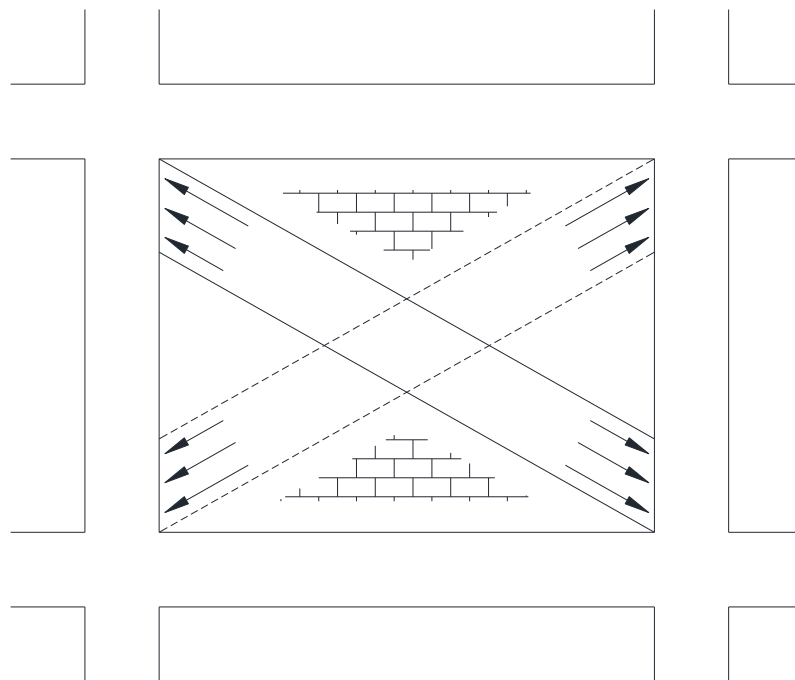
Figure 2.5. Equivalent strut model

The model used by the program idealizes the stress-strain relationship of the infill panel using a parabolic function up to the peak stress f'_m. Then, the stress drops linearly with increasing strains until a constant value (Madan et al., 1997), Figure 2.6.
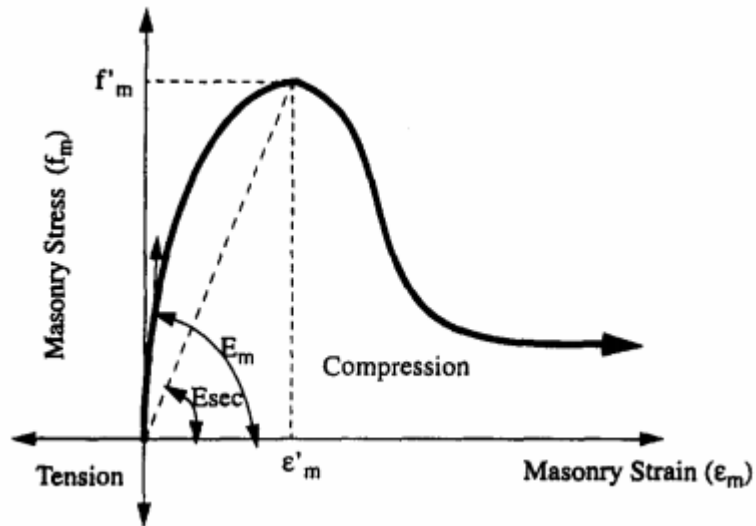
Figure 2.6. Strength envelope for equivalent strut
(Source: Madan et al., 1997)

The lateral force-deformation relationship of the constitutive model is defined by a bilinear envelope. The first branch is formed by the initial elastic stiffness and the yield force V_y and there on, the second branch is formed by the post-yield stiffness until the maximum force V_m, Figure 2.7. Calculation of these values is based on the method developed by Saneinejad and Hobbs (1995). This method models the elastoplastic behavior of infilled frames while considering various factors such as infill panel aspect ratio, plastic moment capacities of related beams, columns and joints and shear stresses at the infill-frame contact surfaces.
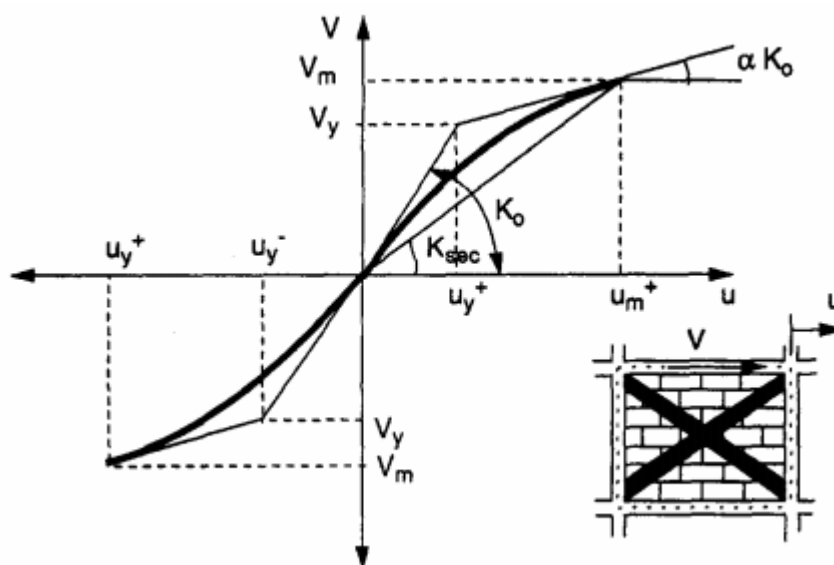
Figure 2.7. Lateral force-deformation relationship for infill wall
(Source: Madan et al., 1997)

22

The infill model uses the smooth hysteretic model described in the previous section to represent the cyclic behavior.

2.4. Numerical Model

In the process of setting up the numerical models of the tested frames, the moment-curvature relationship of each beam and column type was defined in IDARC. Typical tri-linear moment - curvature envelope used by the program is shown in Figure 2.8. The moment - curvature curve for each element type was calculated by performing section analysis. Spreadsheet developed by Ersoy and Özcebe (2001) is used for this purpose. Afterwards, the curves were simplified as tri-linear envelopes for data entry.
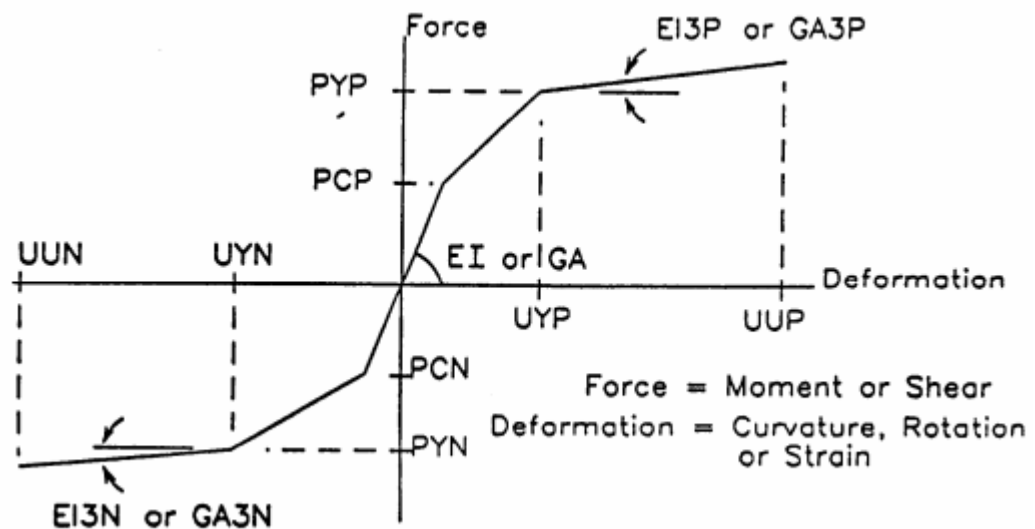
Figure 2.8. Tri-linear envelope used by IDARC
(Source: IDARC User's Guide, 2010)

For modeling the hysteretic behavior of the reinforced concrete members, a parametric study was performed on the bare frames. The parameters of the three-parameter Park model were calibrated for matching the numerical results to the experimental results. The selected parameters are presented in Table 2.4 for each frame.

Table 2.4. Adapted control parameters

| PARAMETER	FRAME #1	FRAME #2	FRAME #3	FRAME #4
α	200.00	200.00	200.00	200.00
β_1	0.01	0.01	0.01	0.01
β_2	0.01	0.01	0.01	0.01
γ	0.20	0.50	0.20	0.15

The infill model of IDARC uses the prism strength for calculating the strength envelope of the infill panel. The prism strength of the infill walls were obtained from the compression tests which had been performed by Çankaya (2011). Since, the results of compression tests showed a wide distribution, a value in vicinity of the results that yielded the best fit is selected. Since no experimental data is available, other parameters, such as cracking modulus of masonry, maximum strain of the prism and shear strength of masonry bed joints, are calculated using the formulae proposed by IDARC (IDARC User's Guide, 2010).

The hysteretic parameters of the infill walls were set to the default values (Table 2.3) of IDARC except the ductility capacity of the infill wall which is set to 15.0 and 13.0 to fit the experimental results for Frame #3 and Frame #4, respectively.

The analyses were performed using displacement-controlled quasi-static loading histories obtained from the experimental results. Since the program limits the number of data points in quasi-static analysis, the number of data points that represent the actual loading histories were decreased to fit the limits. During this process, the loading profile did not change significantly. Simplified loading histories for the bare and infilled frames are presented in Figure 2.9 - Figure 2.12, respectively.
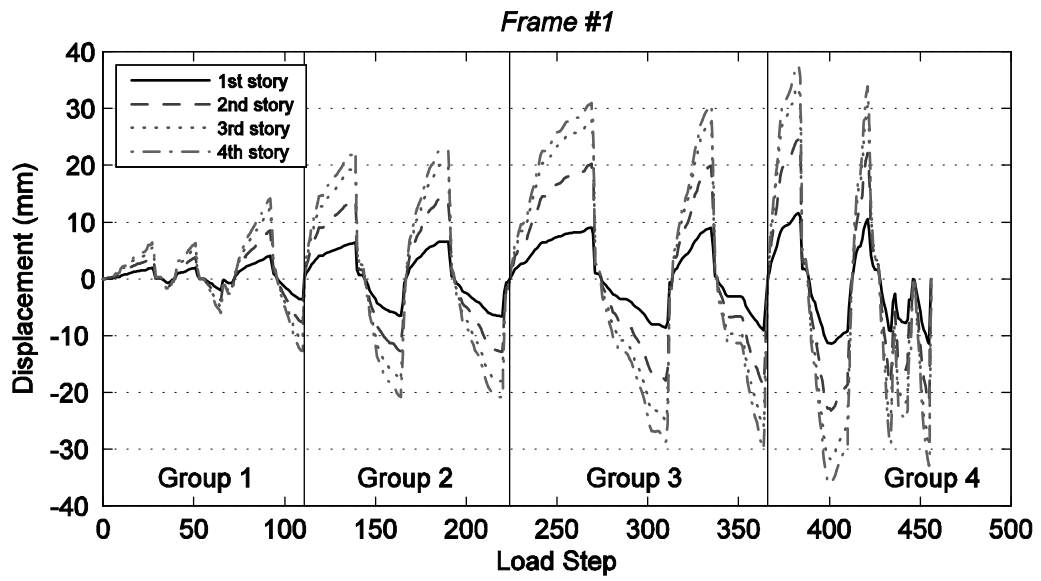
Figure 2.9. Loading history of Frame #1
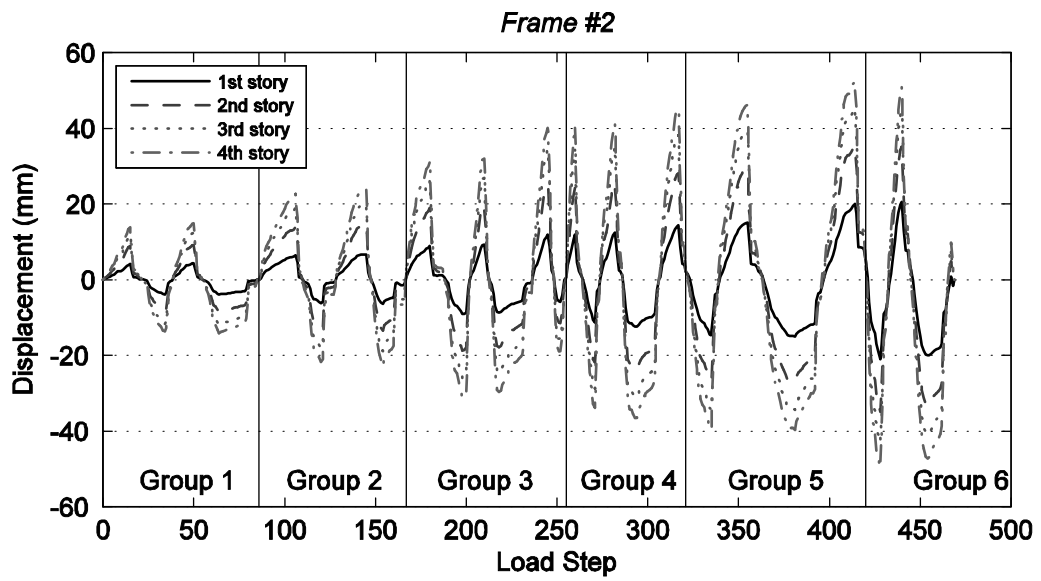
Figure 2.10. Loading history of Frame #2
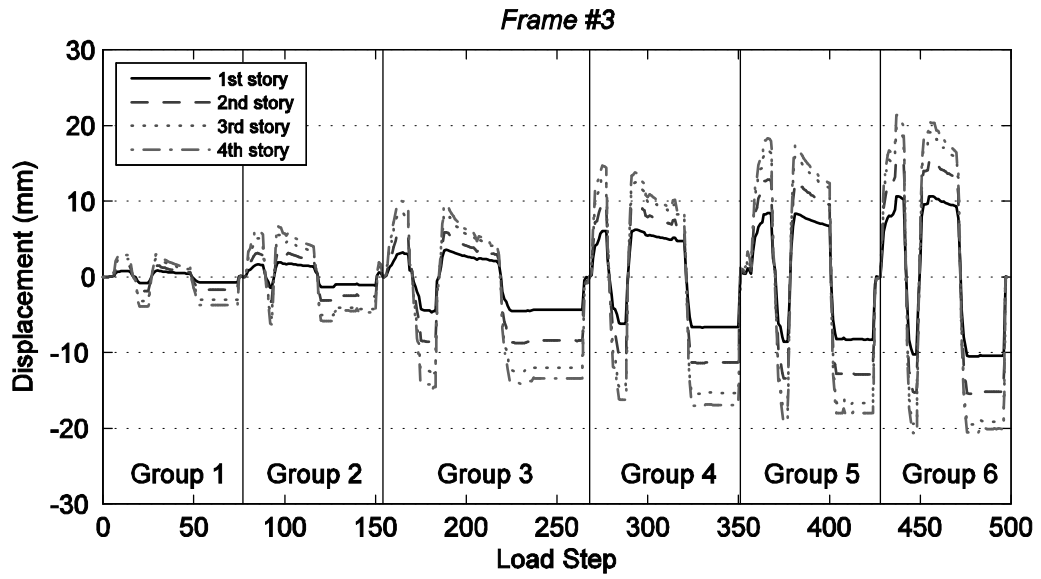
Figure 2.11. Loading history of Frame #3
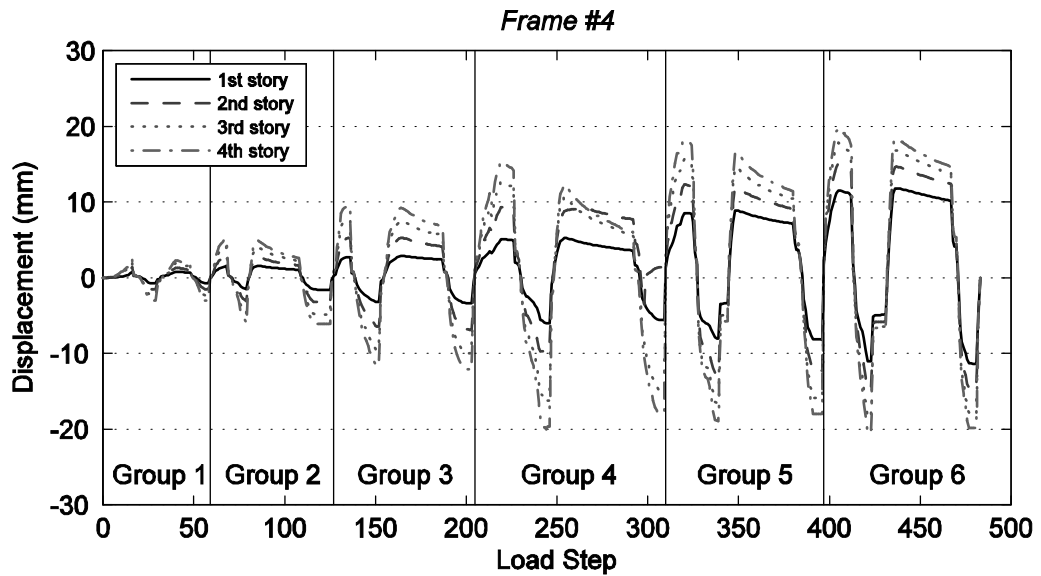
Figure 2.12. Loading history of Frame #4

2.5. Analysis Results

Computed shear force - displacement relationships and the average stiffness changes of the tested and analyzed frames will be presented in this section in a

comparative fashion. In order to provide clear graphics, the hysteresis curves and average stiffness changes were also grouped by the loading groups defined in Figure 2.9 - Figure 2.12. In the experimental study, only the hysteresis curves of the first stories were presented. Therefore, the comparisons, herein, contain the global shear force and the first story displacement relationships.

Figure 2.13 presents the experimental and analytical hysteresis curves of Frame #1 grouped by the loading groups. The horizontal axes of the curves are the absolute drifts of the first story and the vertical axes are the total shear forces on the frame.
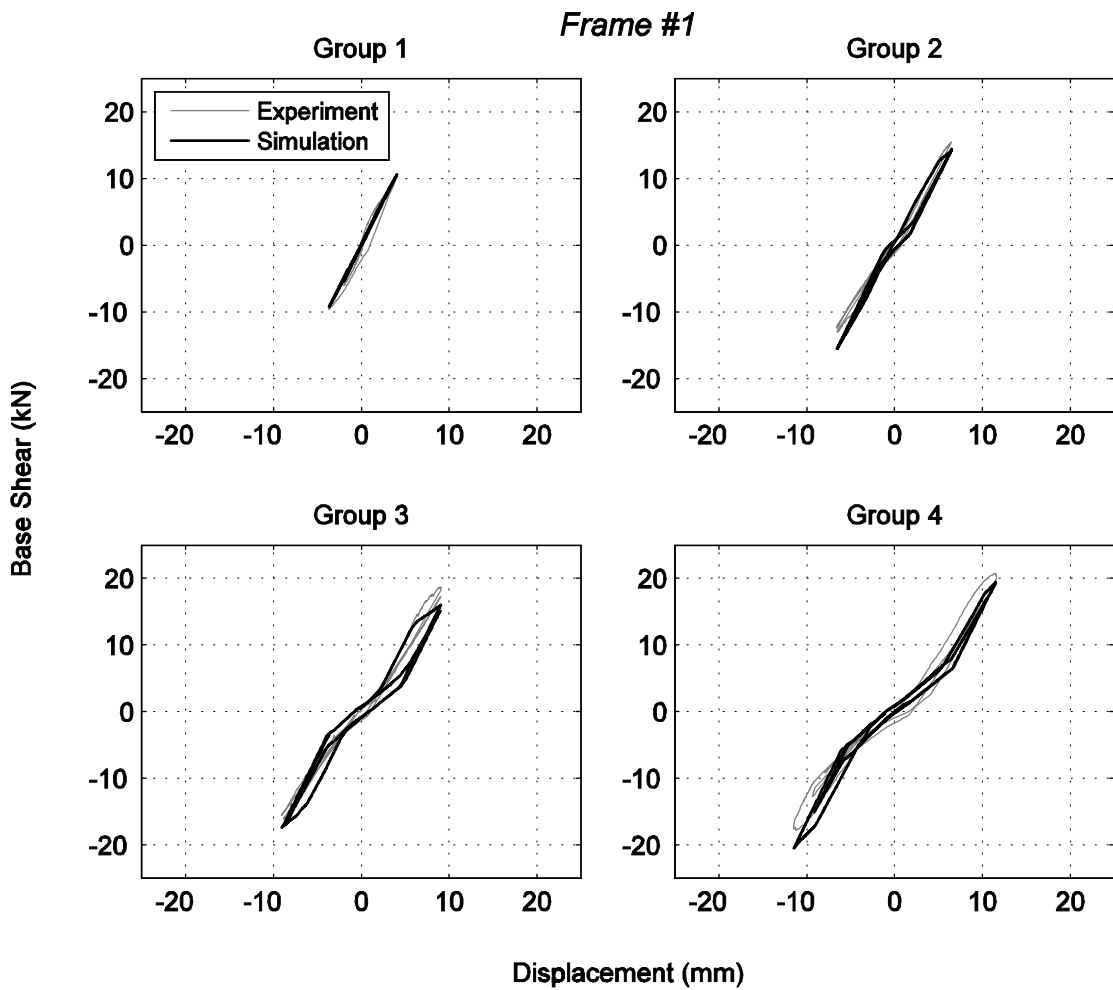
Figure 2.13. Hysteresis curves of Frame #1 grouped by the loading groups

In the first loading group, both initial stiffness and maximum base shear values at the maximum displacements show a good agreement.

In the second loading group, pinching behavior starts in both experimental and analytical systems. Sharper strength degradation is observed in the simulation for the

27

positive region of the hysteresis. On the contrary, stiffness degradation in the experiment is larger in the negative region. As a result, base shear at maximum displacement in the analysis is lower than the experimental results in the positive region, while it is higher in the negative region. The positive base shear at maximum displacement is 7% lower and the negative base shear at maximum displacement is 19% higher than the experimental results.

In the third loading group, the same effects on strength and stiffness degradations can be observed. The pinching is significant. The positive base shear at maximum displacement is 16% lower and the negative base shear at maximum displacement is 10% higher in the simulation.

In the fourth loading group, pinching continues to show a good agreement between the two systems. The positive base shear at maximum displacement is 5% lower and the negative base shear at maximum displacement is 15% higher than the experimental results.

The changes in the average stiffness values grouped by the loading groups are presented in Figure 2.14.
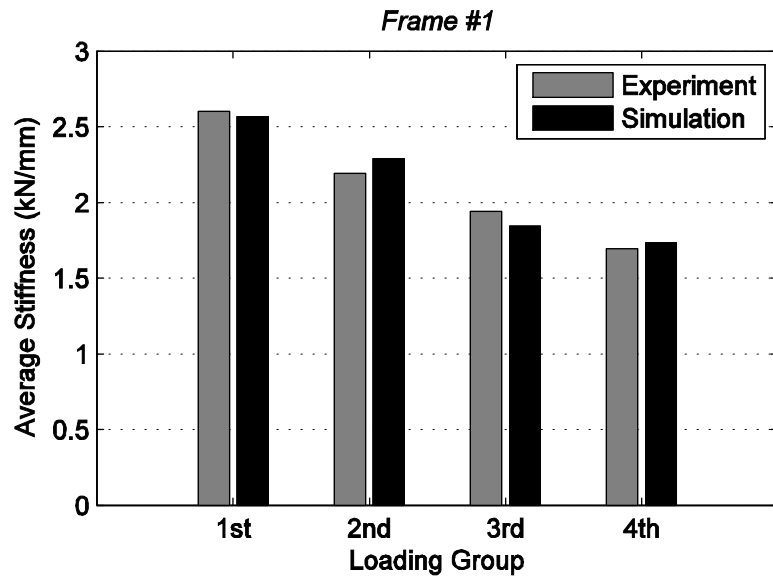
Figure 2.14. Average stiffness values of Frame #1 grouped by the loading group

The difference of the average stiffness values between the experimental and the analytical results is nearly 1% in the first loading group. In the second group, the

average stiffness is 4% higher in the simulation and in the third loading group, it is 5% lower. In the fourth group of loading the difference is 2%.

In Figure 2.15, complete hysteresis curves of the first story for Frame #1 are presented. The horizontal axis is the interstory drift ratios of the first story and the vertical axis is total base shear on the frame. The overall behavior matches closely with the experimental results. In addition, it can be seen that the pinching behavior observed in the experiment may be modeled by selecting the proper parameter for the slip.
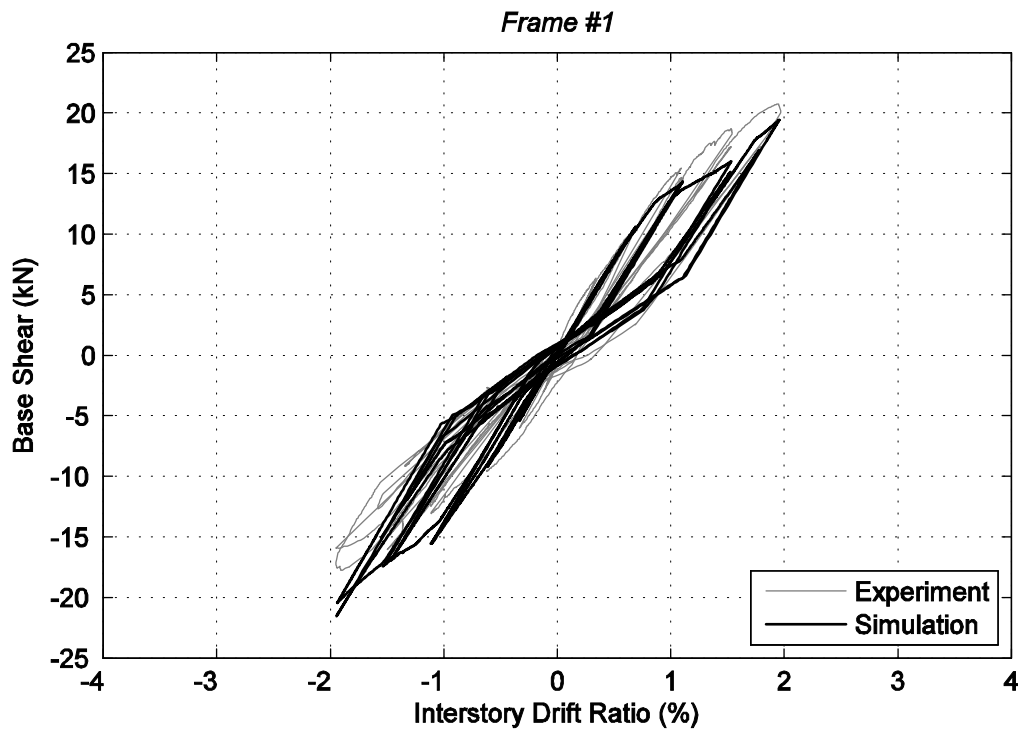
Figure 2.15. Hysteresis curves of the first story, Frame #1

The hysteresis curves of Frame #2, obtained from the experiment and the simulation, are presented in Figure 2.16. Similar to the previous frame, the curves are grouped by the loading groups defined in Figure 2.10.
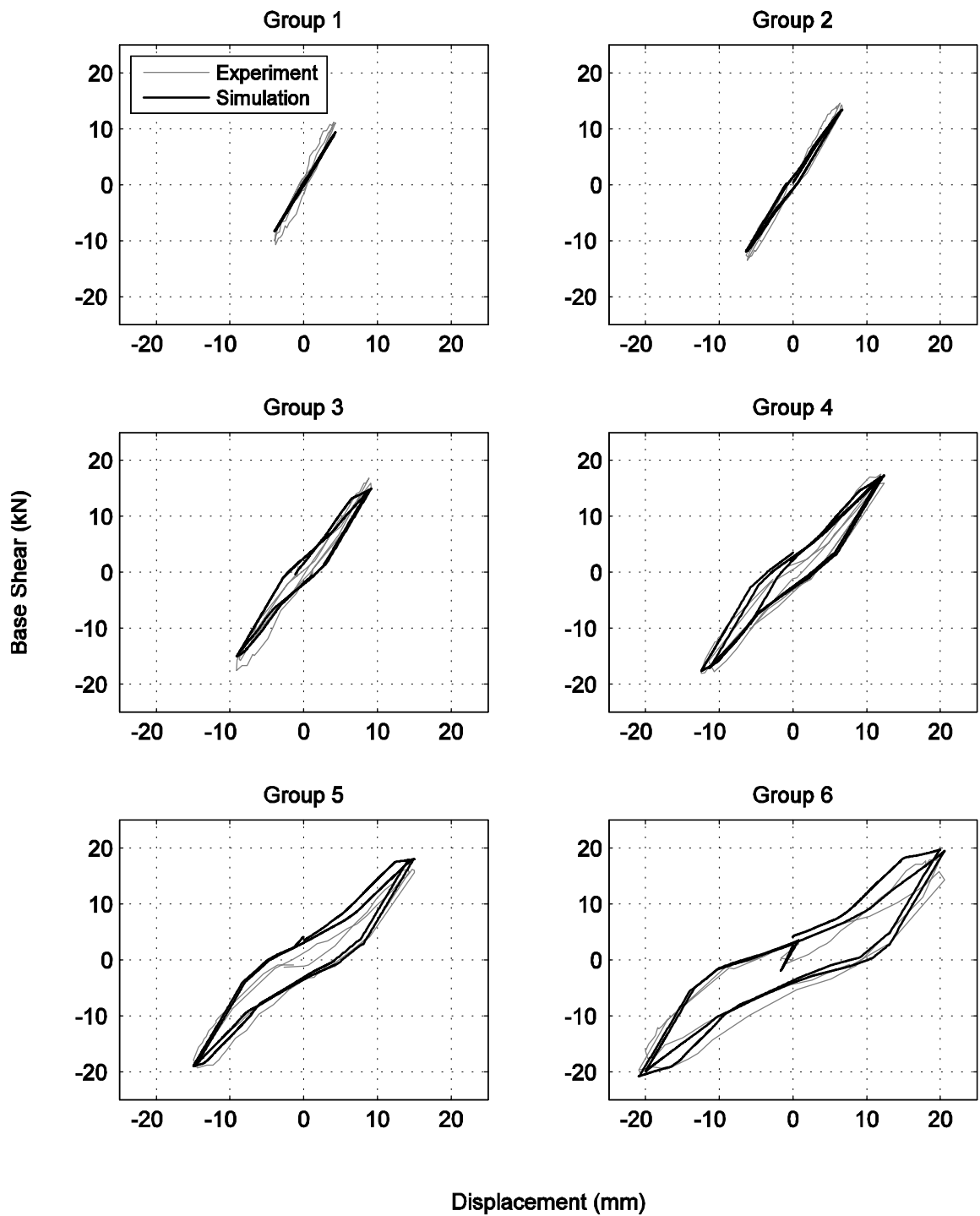
Figure 2.16. Hysteresis curves of Frame #2 grouped by the loading groups

In the first loading group, the initial stiffness of the analytical model is slightly lower than that of the experimental system. Thus, the shear forces at the maximum displacements are 20% lower than the experimental results.

Pinching starts in the second loading group. The positive base shear at maximum displacement is 2% higher and the negative base shear at maximum displacement is 6% lower than the simulation.

In the third loading group, strength degradation between the two cycles becomes observable in the experimental results, however IDARC calculates less degradation. In the first cycle, the shear forces at the maximum displacements are 10% lower than those of the experimental system. In the second cycle, the difference decreases to 6% in both directions.

In the fourth and the fifth loading groups, the difference of the shear forces decreases up to 1% between the numerical and experimental results. The pinching behavior matches closely with the experimental results.

In the sixth loading group, experimental system loses its strength slightly more than the numerical system. However, the difference is still tolerable.

In Figure 2.17, the changes in the average stiffness of the frames are compared by the loading groups.
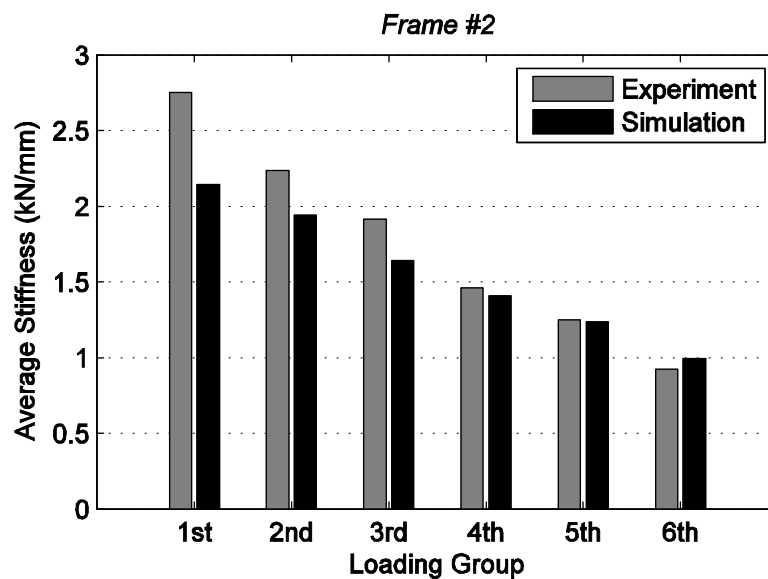
Figure 2.17. Average stiffness values of Frame #2 grouped by the loading group

In the simulation, the average stiffness values are lower than the experimental results in all loading groups, except the sixth group.

In the first five loading groups, the difference decreases from 28% to 1%. In the last group, the average stiffness calculated from the analytical results is 3% higher than that of the experimental results.

Figure 2.18 presents the entire hysteresis curves of the first story for Frame #2. It can be observed from the figure that the simulation shows a close proximity to the experimental results.
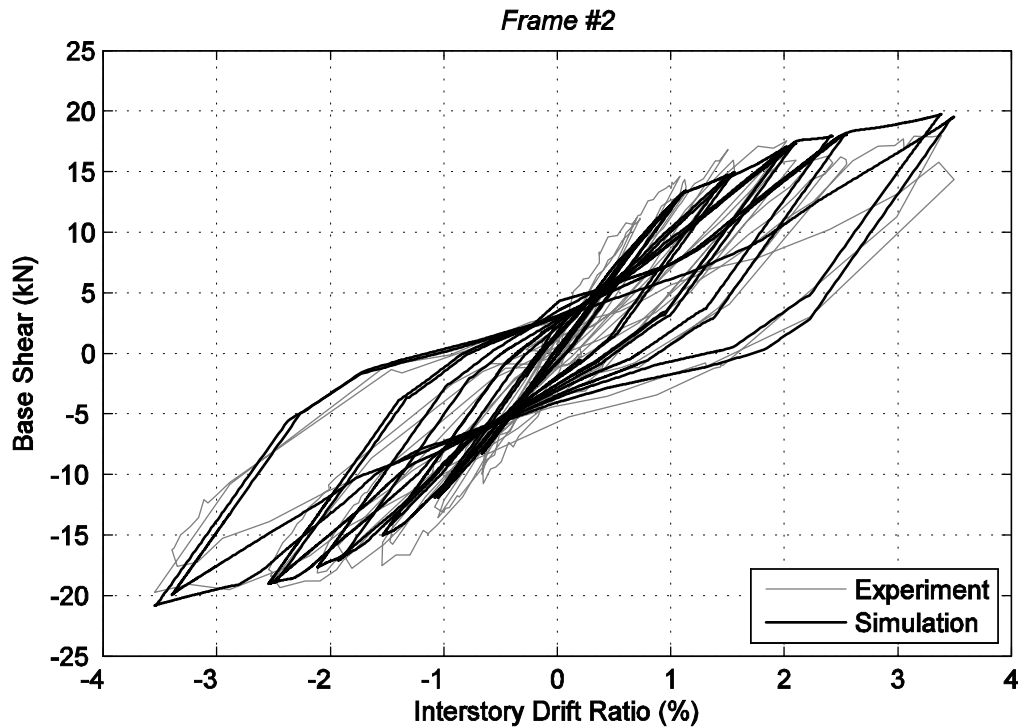
Figure 2.18. Hysteresis curves of the first story, Frame #2

The experimental and the analytical hysteresis curves of Frame #3 can be seen in Figure 2.19, divided by loading groups defined in Figure 2.11.

Figure 2.19. Hysteresis curves of Frame #3 grouped by the loading groups

Observing the first loading group indicates that the initial stiffness of the experimental frame is considerably high at the beginning when it is compared to the analytical model. However, in the second cycle of the first loading group, the stiffness values of the two models are close to each other.

In the second loading group, only the experimental system starts pinching. The shear forces calculated in the analysis at the maximum displacements are higher in both regions of the hysteresis and the difference is 15%.

The shear forces of the analytical model are equal to the forces of the experimental system at maximum displacements in the third loading group. The pinching behavior starts in the analytical model, as well. The difference between the loading paths originates from the parabolic function used by the infill model of IDARC which was described in Section 2.3.2. In the following loading groups, the difference between the loading paths continues. The pinching behavior of the two systems is similar to each other until the end of the loading.

In the fourth loading group, the positive base shear of the analytical model at the maximum displacement is higher than that of the experimental force. However, they are equal in the negative region of the hysteresis.

In the fifth and sixth loading group, the difference between the base shear forces at maximum displacements are nearly 1%, except the first cycles in the negative region. The infill model of IDARC exhibits greater strength degradation in the negative region. Therefore, the negative base shears of the analytical system at the maximum displacement are approximately 20% lower than those of the experimental system.

The changes in the average stiffness for Frame #3 are shown in Figure 2.20 for each loading group.
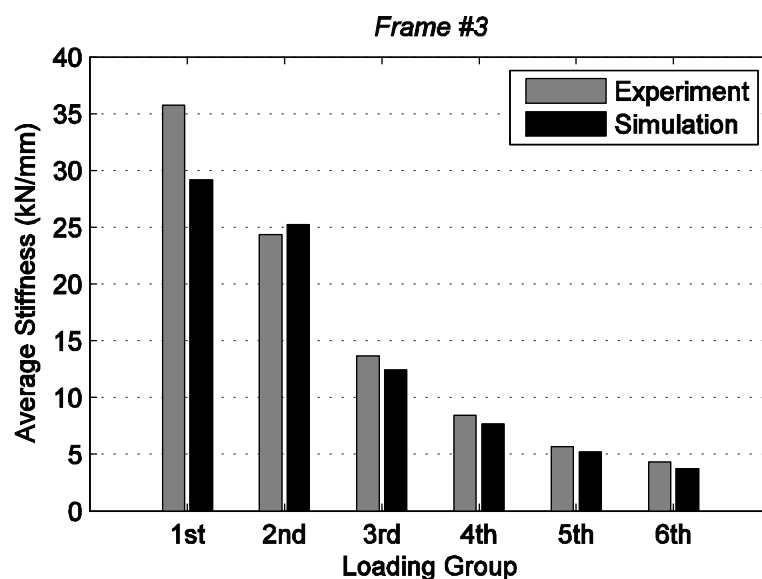
Figure 2.20. Average stiffness values of Frame #3 grouped by the loading group

The average stiffness of the experimental system is 22% higher than that of the analytical system in the first loading group. However, as it was mentioned above, the initial stiffness of the experimental frame is significantly high at the beginning until the second cycle of the first loading group. Depending on this, if the first cycle is neglected, the average stiffness values for the first loading group are approximately equal to each other.

In the second loading group, the average stiffness of the numerical model is 3% higher than that of the experimental system. In all the remaining loading groups, the average stiffness of the analytical system is approximately 8% lower than that of the experimental system.

Hysteresis curves of the first story for Frame #3 are presented in Figure 2.21. It can be observed from the figure that the selected control parameters for the slip behavior simulated the pinching accurately. Moreover, the infill model used by IDARC represents the contribution of the infill wall to the stiffness of the system and the strength degradation at the increasing drift levels satisfactorily.

Figure 2.21. Hysteresis curves of the first story, Frame #3

Figure 2.22 presents the experimental and analytical hysteresis curves of Frame #4 grouped by the loading groups defined in Figure 2.12.
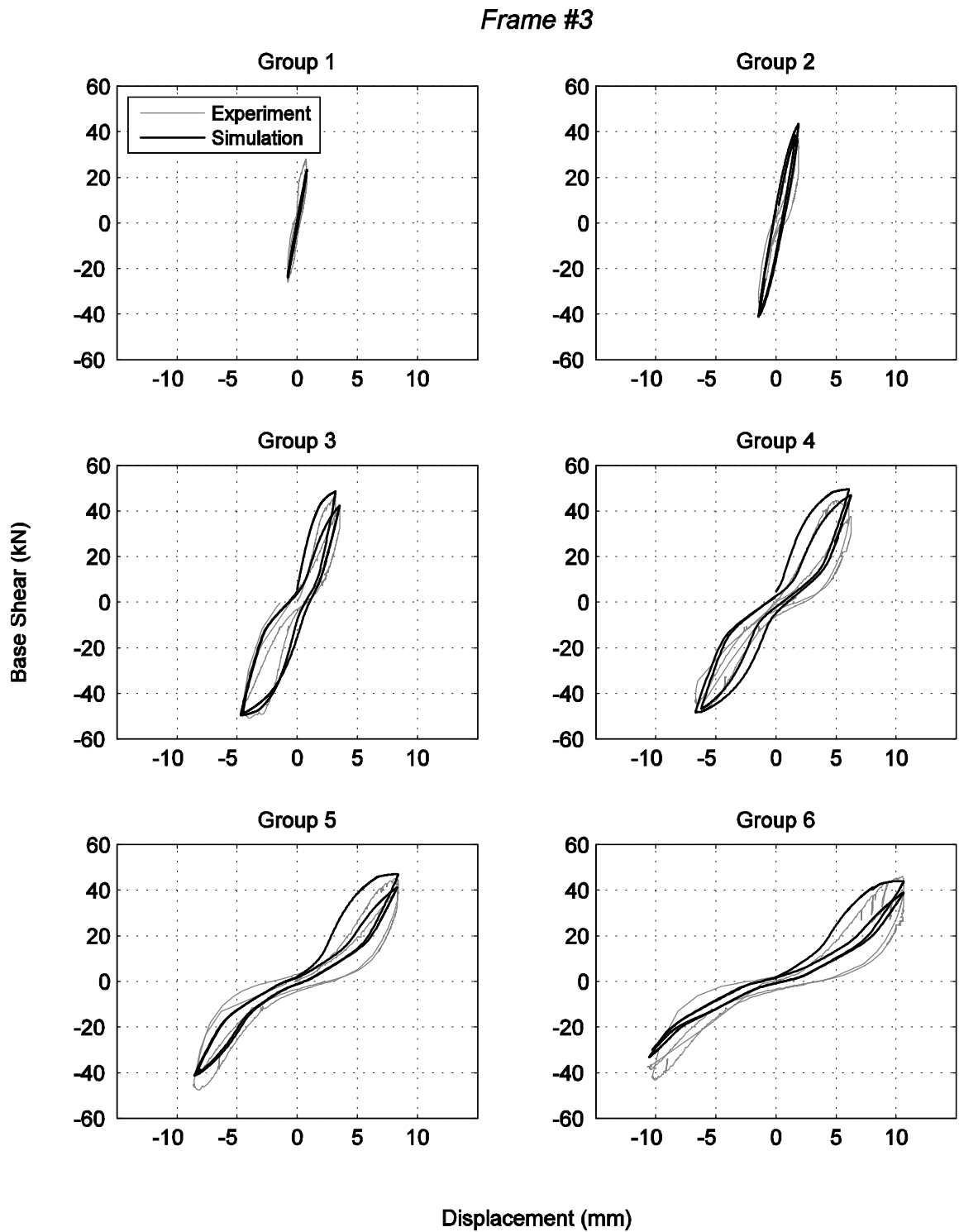

Figure 2.22. Hysteresis curves of Frame #4 grouped by the loading groups

Observing the first loading group points out that the initial stiffness of the experimental frame is noticeably high at the beginning when it is compared to the analytical model, similar to Frame #3. However, in the second cycle of the first loading group, the stiffness values of the two models are close to each other and the difference is nearly 2%.

Similar to Frame #3, only the experimental system starts pinching in the second loading group. Therefore, the base shear at the maximum displacement calculated in the analysis is 13% higher than the experimental results in both regions of the hysteresis.

In the third loading group, the base shear at the maximum displacement is equal in both systems for the positive region. However, in the negative region analysis yields 15% lower results. The pinching starts in the analytical model, as well.

In the fourth loading group, the calculated shear forces at the maximum displacements are 15% lower than the experimental results in the first cycle. Moreover, the maximum lateral force sustained by the numerical model is 15% lower than that of the experimental system. However, values approximate to the experimental results in the second cycle in both regions of the hysteresis.

The calculated base shear at the maximum displacement is nearly equal to the experimental results in the positive region for the fifth loading group; nonetheless the maximum lateral force sustained by the experimental system is still higher than that of the analytical model. In the negative region, strength of the analytical system degraded more than the experimental system. The shear forces at the maximum displacements are 34% and 23% lower in the first and the second cycles, respectively.

In the last loading group, the total shear forces at the maximum displacement are equal in both systems for the first cycle in the positive region. For the second cycle, strength degradation in the experimental system is greater. In the negative region, the analytical system loses its capacity to dissipate energy and the shear forces at the maximum displacements are 43% and 33% lower than those of the experimental frame.

The changes in the average stiffness values of the two systems are presented in Figure 2.23 separately for each loading group for Frame #4.
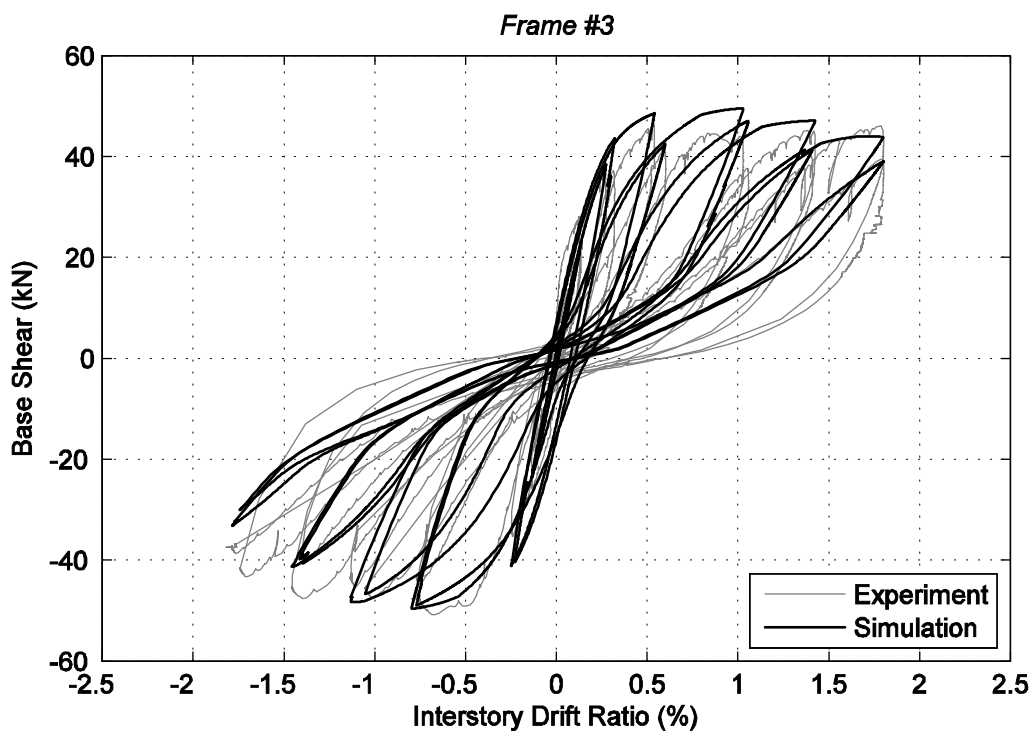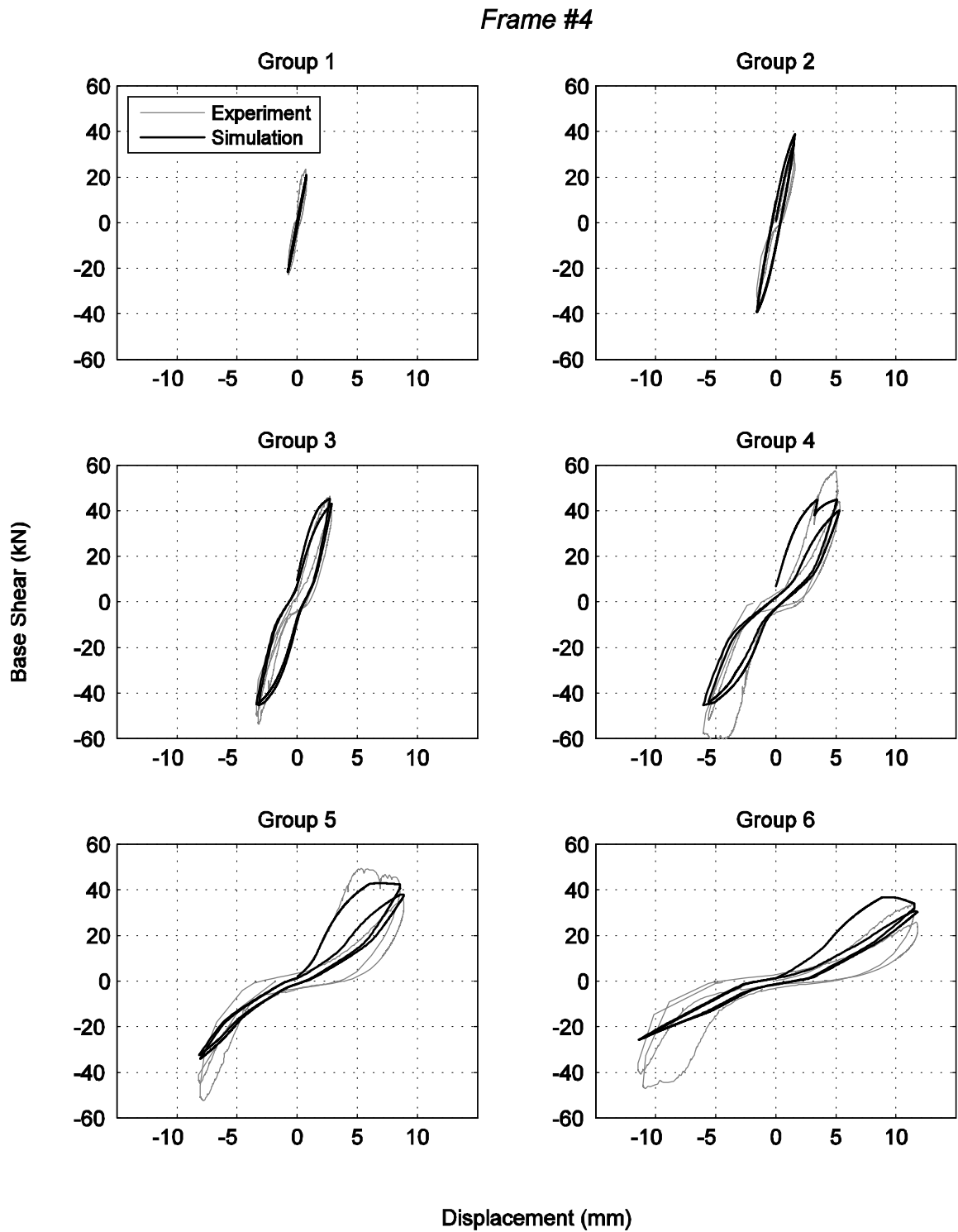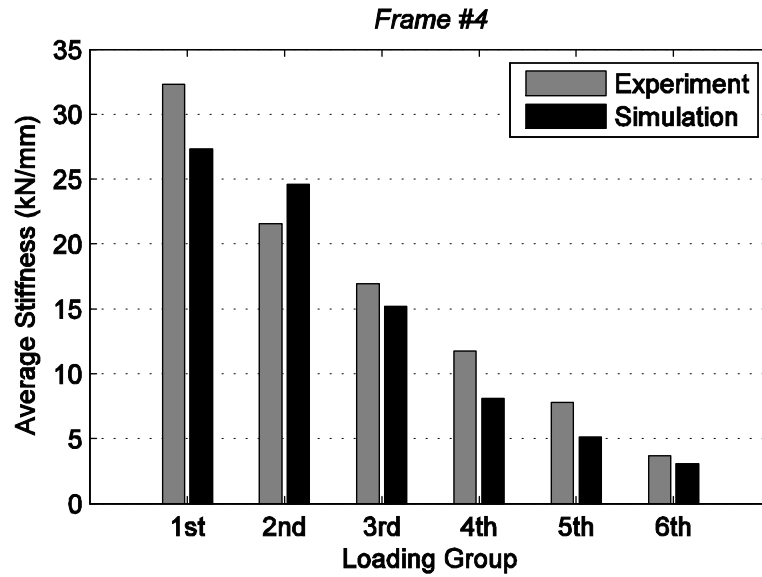
Figure 2.23. Average stiffness values of Frame #4 grouped by the loading group

As mentioned earlier, the initial stiffness of the experimental frame is considerably high at the beginning. Therefore, the average stiffness in the experiment is 18% higher than that in the analysis. If the first cycle of the first loading group can be neglected, the average stiffness values of both frames are equal to each other.

In the second loading group, the average stiffness calculated in the analysis is 14% higher.

The average stiffness values observed in the experiments in the third, fourth, fifth and the sixth loading groups are 11%, 45%, 33% and 16% higher, respectively.

In Figure 2.24, complete hysteresis curves of the first story for Frame #4 are presented.
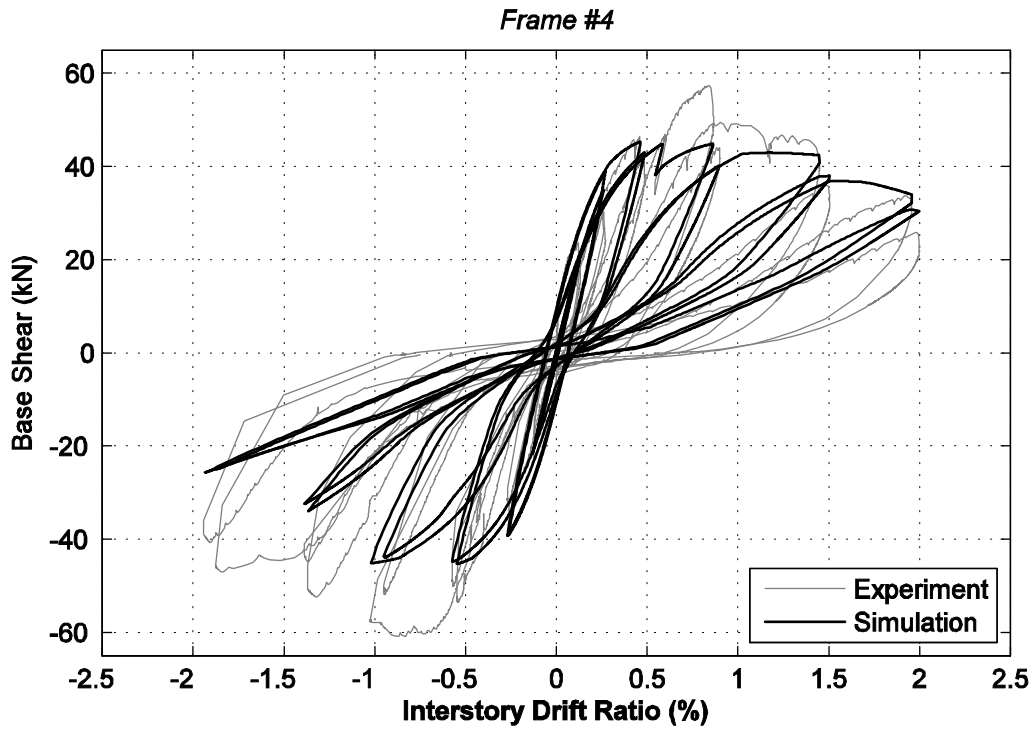
Figure 2.24. Hysteresis curves of the first story, Frame #4

In the experiment, Frame #4 exhibited a different failure mechanism than Frame #3. Shear cracks appeared at the upper ends of the first story columns due to the compression applied by the infill wall in the third loading group. In the next loading groups, heavy shear damages developed in those regions and the upper stories started to move as a rigid body (Çankaya, 2011). Since the shear modulus of the columns are accepted infinitely high in IDARC by default, the program failed to model the failure mechanism observed in the experiment.

CHAPTER 3

EFFECT OF INFILL WALLS ON THE DRIFT DISTRIBUTION OF INFILLED RC FRAMES

3.1. Introduction

The effect of infill wall stiffness variations on the seismic behavior of reinforced concrete frames is aimed to be investigated in this study. A planar, five-bay, five-story reinforced concrete frame was designed to have common deficiencies observed in the residential buildings in Turkey for this purpose. Then two different infilled frames were obtained by filling the bare frame with infill walls in two bays. All the frames were analyzed using nonlinear dynamic and pushover analysis methods. Then, the results were compared in terms of interstory drift distributions.

Firstly, the effect of stiffness variations throughout the elevation of linear systems was investigated by performing linear modal analysis on four different multi-degree-of-freedom (MDOF) systems. Considering that first mode is dominant on the drift behavior, first modal shapes of the systems are used to compare drift distributions. Then, the details and the properties of the designed and analyzed frames are presented. Dynamic analyses of the three frames followed. Brief information about the selected ground motions and their normalization is given. Results of the dynamic analyses are discussed. Afterwards, information about the pushover procedure is presented. As the last section, results of the pushover analyses are discussed.

3.2. Linear-Simple MDOF Systems

Previous studies have shown that under seismic demands, drift concentration in lower stories of infilled frames may cause major damages. It is anticipated that a well-organized stiffness distribution along the height of the building may help mitigating the concentration phenomena. In this study, the stiffness variation of the structure is aimed to be controlled by the infill walls.

In order to understand the effects of stiffness variations throughout the elevation of the structures, four linear MDOF systems were constructed. The MDOF systems had varying stiffness distributions which represent the effect of infill walls with various stiffness properties at every level. Assumed mass and stiffness properties of the MDOF systems are given in Figure 3.1.
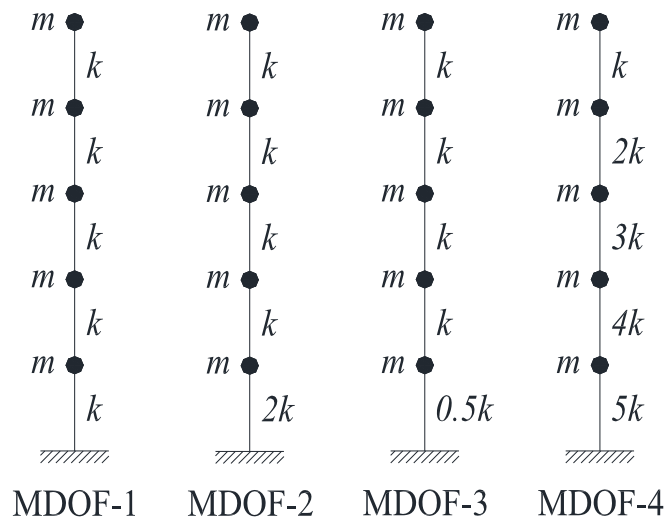
Figure 3.1. Selected multi-degree-of-freedom systems

The stiffness of a story with typical infill panels is represented with a stiffness of k. The increasing stiffness values correspond to stories with either thicker infill walls or infill walls those were reinforced using different methods. The decreasing values correspond to stories with weaker infill walls whose stiffness values were assumed to be reduced using different techniques.

Linear modal analyses were performed to determine the natural periods and the modal shapes of the systems. Considering that deflected shapes of the selected systems are dominated by the first modes of the systems, interstory drift ratios were observed based on the first modes of the systems. First mode vibration periods of the systems are given in Table 3.1. The period of MDOF-1 was calculated as 0.51 seconds. Existence of a strong first floor reduced the period of MDOF-2 to 0.46 seconds. In MDOF-3, the first story was assumed to be a soft story, thus the period increased to 0.60 seconds, as expected. MDOF-4 has a descending stiffness distribution from the first to the top floor. This distribution reduced the period to 0.25 seconds.

Table 3.1. First mode vibration periods of the MDOF systems

	MDOF-1	MDOF-2	MDOF-3	MDOF-4
Period (sec)	0.51	0.46	0.60	0.25

The interstory drift ratios of the MDOF systems are presented in Figure 3.2. In order to make a comparison of the interstory drift distributions, the ratios were normalized with respect to the maximum interstory drift which was observed in the first story of MDOF-3. The first story interstory drift of the MDOF-3 was normalized such that its value is unity. Note that, the absolute values of the drift ratios do not have any importance here. Distributions of the ratios are the key. It can be observed from the figure that a soft first floor causes significant increase on the drift of the first story. On the contrary, a strong first floor limits the drift of the first story, however the drifts of the upper floors increase when they are compared to those of MDOF-1. The stiffness distribution of MDOF-4 caused a more balanced interstory drift profile and distributed the total drift among the individual floors. Thus, it reduced the drift concentration in the lower floors.
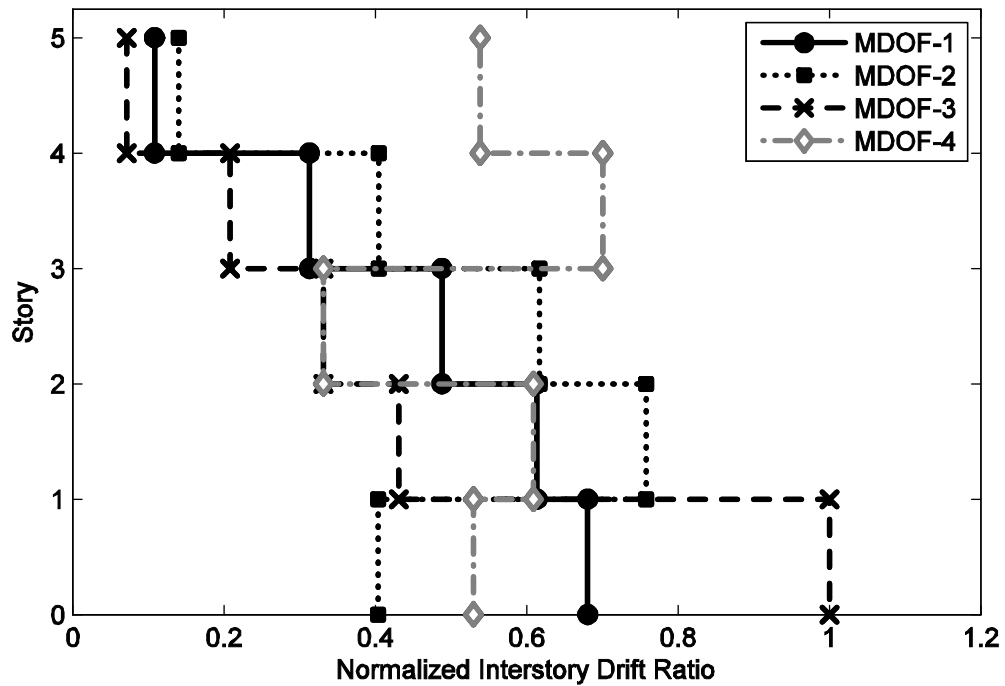

Figure 3.2. Interstory drift ratios of the MDOF systems

The target structures of the study presented are the typical residential buildings in Turkey. Considering that generally the first mode governs the dynamic response of such frames, modifying the first mode shape may help controlling the interstory drifts. For this purpose, infill walls were utilized to change the first mode shape by altering the stiffness distribution along the height of the structure.

3.3. Model Frames

Three frames were analyzed in this study. Initially, a bare frame was designed and modeled. Afterwards, two infilled frames with different infill wall properties were modeled to observe the effects of change in infill wall stiffness values.

3.3.1. Bare Frame

A planar, five-bay, five-story reinforced concrete frame was designed. Characteristic properties of the residential buildings in Turkey were considered during the design process in light of building stock assessment studies (Bal et al., 2007; Bal et al., 2008; Inel et al., 2009). The designed bare frame (BF) is assumed to be located in a building that is symmetrical in both directions. The plan of the building and an overview of the designed frame are presented in Figure 3.3 and Figure 3.4, respectively.

The frame has 5.0 m beam span and the story height is taken as 3.0 m. All columns have 50x50 cm rectangular cross section, while beams were designed to have "T" sections. Beams of the outer bay have 105x12 cm flange, 25x38 cm web dimensions. Other beams have 85x12 cm flange, 25x38 cm web dimensions. Dimension details of the members are given in Figure 3.5.

Proportioning of the selected frame is based on the following material properties: the compressive strength of the concrete was assumed to be 20 MPa. The modulus of elasticity of the concrete was calculated as 28 500 MPa using the formula proposed by Turkish RC Code (TS500, 2000). The yield stress and the modulus of elasticity of the steel were taken as 420 MPa and 200 000 MPa, respectively.

A uniform dead load of 0.45 t/m^2 and live load of 0.20 t/m^2 were assumed on the slabs. Gravitational loads from the slabs were calculated by a triangular distribution to the beams and as axial loads to the columns.
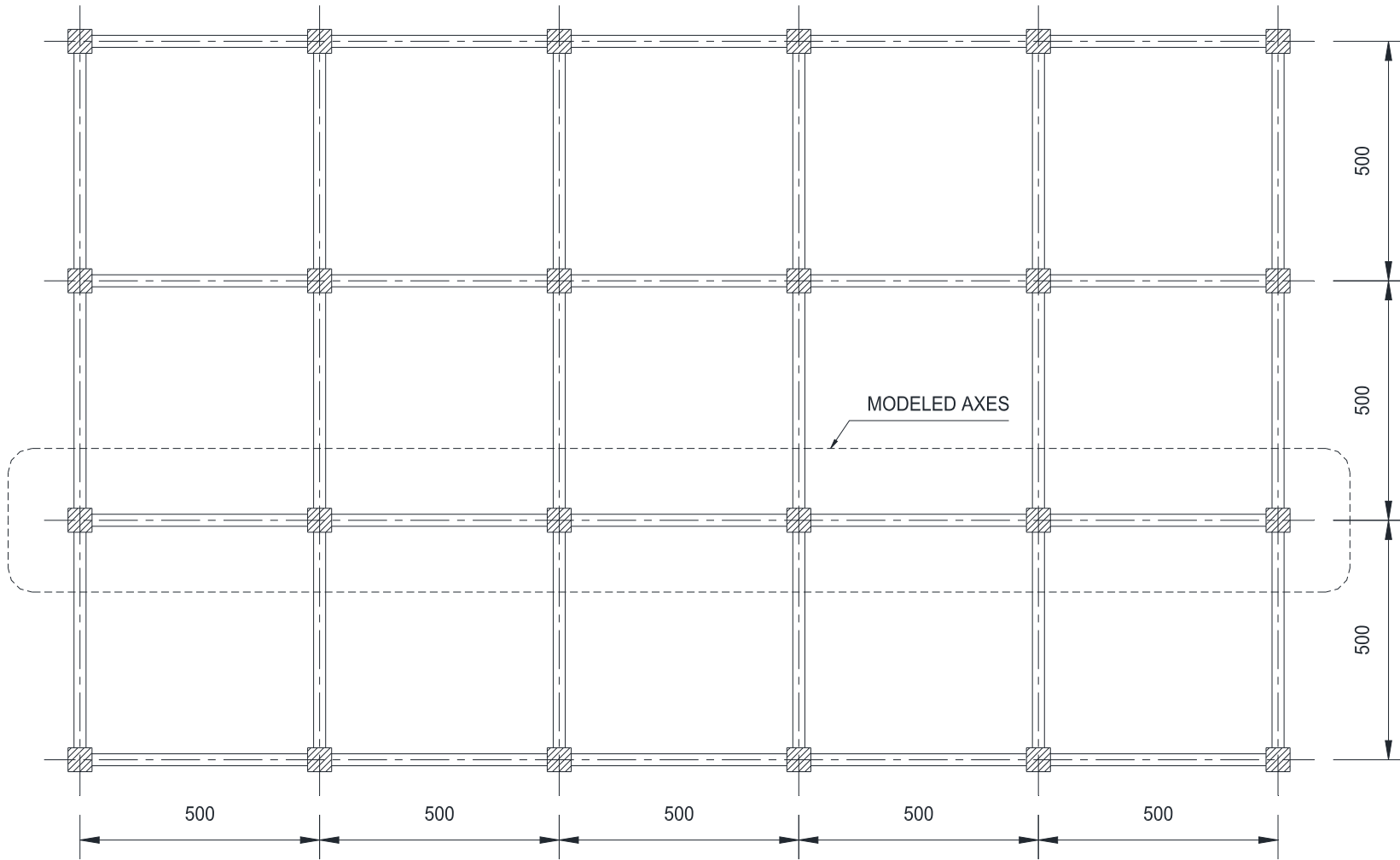
Figure 3.3. Plan of the designed frame

(All dimensions are in centimeters)

MODELED AXES

500

500

500

500

500

500

500

500

C5	B3	B4	B4	B4	B3
	C10	C10	C10	C10	C5
C4	B3	B4	B4	B4	B3
	C9	C9	C9	C9	C4
C3	B1	B2	B2	B2	B1
	C8	C8	C8	C8	C3
C2	B1	B2	B2	B2	B1
	C7	C7	C7	C7	C2
C1	B1	B2	B2	B2	B1
	C6	C6	C6	C6	C1

300 300 300 300 300

500 500 500 500 500
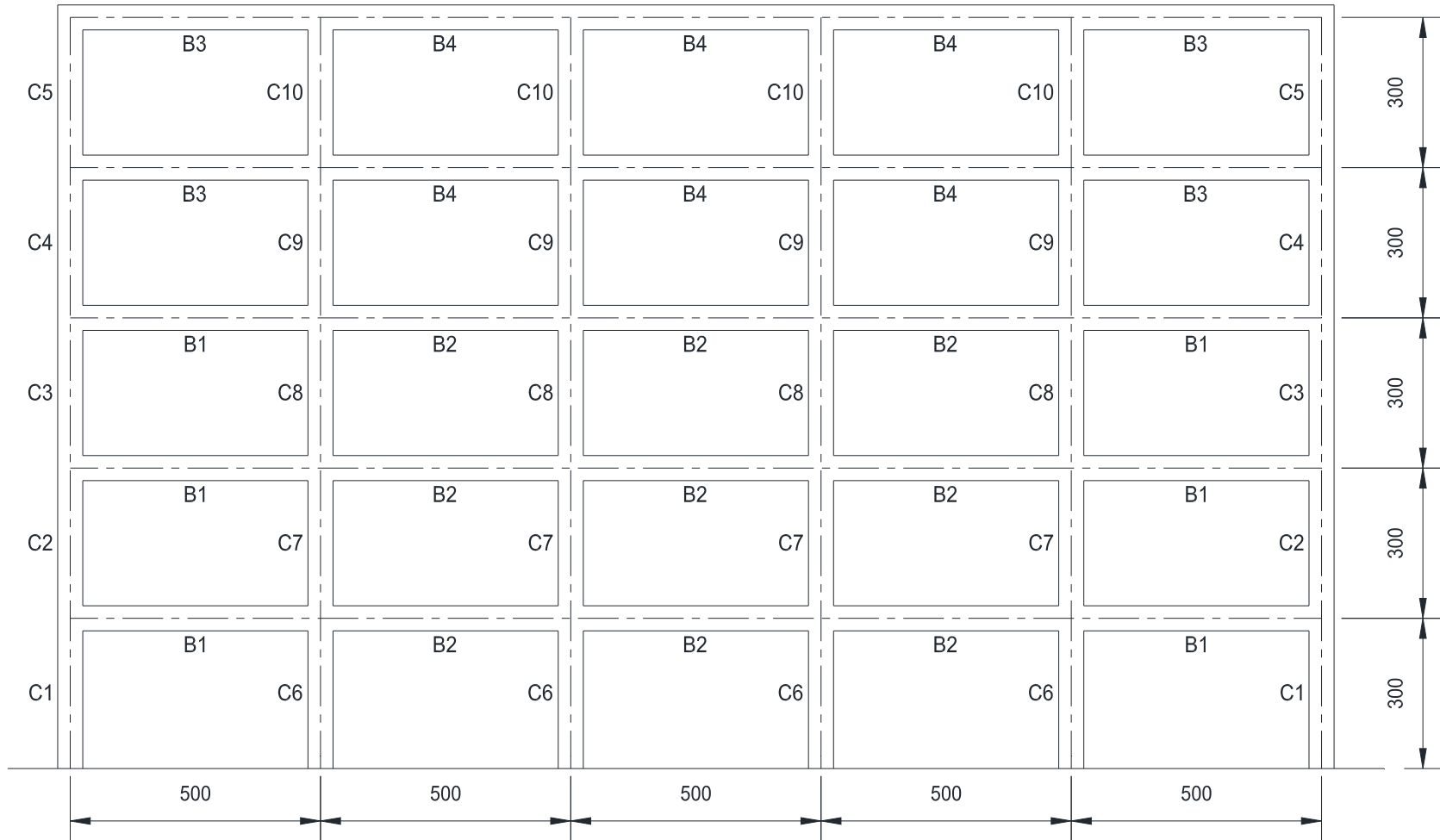
(All dimensions are in centimeters)

Figure 3.4. Overview of the designed frame and element types
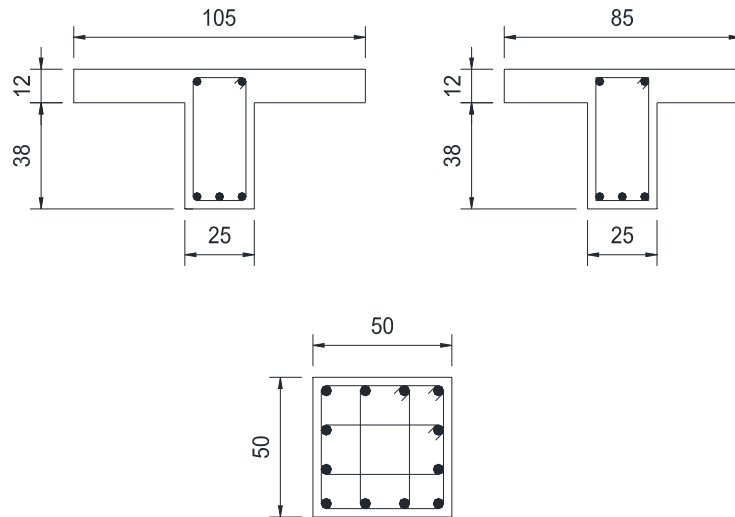
(All dimensions are in centimeters)

Figure 3.5. Dimension details of the outer and inner beams and columns, respectively

The reinforcement details are determined according to the Turkish Earthquake Code (TEC2007) and Turkish RC Code (TS500, 2000). In order to represent the common deficiencies of the residential buildings in Turkey, calculated stirrup spacing for the confinement regions was increased to twice of the code designed values in all the members. Modified stirrup spacings are in accordance with the observed values in the residential buildings (Inel et al., 2009). The reinforcement details of the beams and the columns are presented in Table 3.2 and Table 3.3, respectively.

Table 3.2. Reinforcement details of the beams

LOCATION OF REINFORCEMENT		BEAM TYPE			
		B1	B2	B3	B4
	Bottom	3Ø16	3Ø14	3Ø12	2Ø14
Left	Top	4Ø16 + 2Ø12	5Ø14 + 2Ø12	2Ø16 + 2Ø12	3Ø12 + 2Ø12
	Stirrup	Ø8 / 192 mm	Ø8 / 192 mm	Ø8 / 192 mm	Ø8 / 192 mm
	Bottom	3Ø12	3Ø12	3Ø12	3Ø12
Midspan	Top	2Ø12	2Ø12	2Ø12	2Ø12
	Stirrup	Ø8 / 235 mm	Ø8 / 235 mm	Ø8 / 235 mm	Ø8 / 235 mm
	Bottom	3Ø16	3Ø14	2Ø14	2Ø14
Right	Top	4Ø16 + 2Ø12	5Ø14 + 2Ø12	2Ø14 + 2Ø12	3Ø12 + 2Ø12
	Stirrup	Ø8 / 192 mm	Ø8 / 192 mm	Ø8 / 192 mm	Ø8 / 192 mm

Table 3.3. Reinforcement details of the columns

TYPE OF REINFORCEMENT	ALL COLUMNS
Longitudinal	12Ø18
Stirrup	Ø10 / 200 mm

Dynamic properties of the bare frame were determined by linear modal analysis. Period of vibration for the first mode was found to be 0.74 seconds. Pushover analysis was performed to determine the capacity of the frame. Results of the analysis indicated that the designed frame is in the "Collapse Prevention" performance level that is described in the Turkish Earthquake Code (TEC2007) and needs retrofitting. The details of the pushover analysis will be presented in Section 3.5.

3.3.2. Infilled Frames

Two infilled frames, namely IF-1 and IF-2, are modeled for this study. The infilled frames were obtained by placing infill walls into two bays of the bare frame to represent the average infill wall ratio in the literature (Bal et al., 2008; Inel et al., 2009), Figure 3.6.
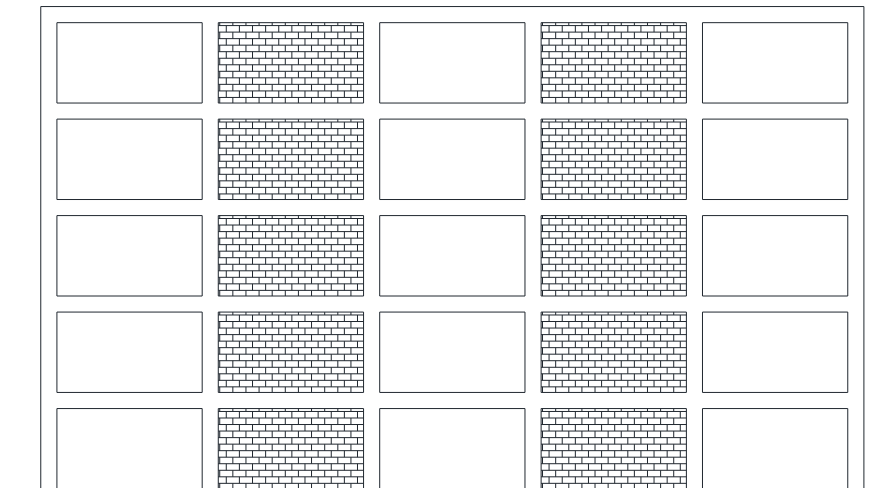

Figure 3.6. Overview of the infilled frames

IF-1 is supposed to represent the common infill wall practices observed in the residential buildings in Turkey. Hollow clay tiles with dimensions of 19x19x13.5 cm were assumed for the infill walls. Total infill panel thickness was assumed as 23 cm with 2 cm of plaster on each side. Weight of an individual infill panel was calculated as 4.5 tons depending on the information given by the manufacturers. The prism strength of an infill panel was assumed to be 3 MPa depending on the literature (Paulay and Priestley, 1992) and other properties needed by IDARC were calculated using the default formulae proposed by the program itself (IDARC User's Guide, 2010). Then, the infill wall stiffness and strength values were calculated by IDARC using the method described in Section 2.3. The initial stiffness of an individual infill panel is approximately 80 kN/mm and the lateral yield force is 420 kN.

In the second infilled frame, that is IF-2, it was aimed to have a pre-organized stiffness distribution throughout the height of the building by modifying the infill walls of IF-1. In Section 3.2, it is observed that a descending stiffness distribution proportional to the building height is advantageous in terms of linear interstory drift profile. Depending on this observation, the infill panels in IF-2 were aimed to have the stiffness properties in a descending fashion, where the strongest infill walls are located in the first story. The stiffness values of the infill walls of IF-2 were determined to be 2.0, 1.6, 1.2, 0.8 and 0.4 times of the stiffness of the infill panels used in IF-1. In this distribution, the lower three stories were assumed to be reinforced using different methods to obtain the mentioned stiffness values. On the contrary, the upper two stories were assumed to be weakened using various techniques mentioned in the literature (Mohammadi et al., 2011; Preti et al., 2012). Since the modifying methods affect the strength properties of the infill walls, the yield strength of the reinforced panels were assumed to be increased by 40%, 30% and 20% in the first, second and third floors, respectively. In the fourth and fifth stories, the yield strength values were assumed to be decreased by 20% and 40%, respectively. These factors were selected arbitrarily, since no specific modifying method was selected. Then, it is also considered that IF-1 and IF-2 should have the same initial period to keep the seismic demand same for both systems, therefore the response of the two systems can be comparable. To achieve the same periods, the initial stiffness of the infill walls of IF-1 increased by 10%. The first mode periods of the infilled frames were calculated as approximately 0.5 seconds by linear modal analysis. The initial stiffness and yield strength values of the infill walls are presented in Table 3.4.

Table 3.4. Initial stiffness and yield strength values of the infill walls

STORY	IF-1		IF-2	
	Initial Stiffness (kN/mm)	Yield Force (kN)	Initial Stiffness (kN/mm)	Yield Force (kN)
5	88	420	32	252
4	88	420	65	336
3	88	420	97	504
2	88	420	129	546
1	88	420	161	588

3.4. Dynamic Analysis

Nonlinear dynamic analyses were performed to calculate the seismic response of the three frames which were described in Section 3.3. Initially, a total of ten earthquakes were selected and applied to BF and IF-1 to determine the most critical ground motions. Then, the selected earthquakes were applied to IF-2 to investigate the consequences of the organized stiffness distribution.

3.4.1. Ground Motions

A total of ten ground motions were selected to perform the dynamic analyses. The records were taken from the works of Lepage (1997). Information about the selected ground motions is given in Table 3.5 in terms of location and date, station name, component and characteristic period of the ground motion, record duration and peak ground acceleration. Ground acceleration histories for original records are presented in Figure 3.7. The selected ground motions exhibit a wide range of characteristic periods ranging from 0.35 seconds to 1.14 seconds.
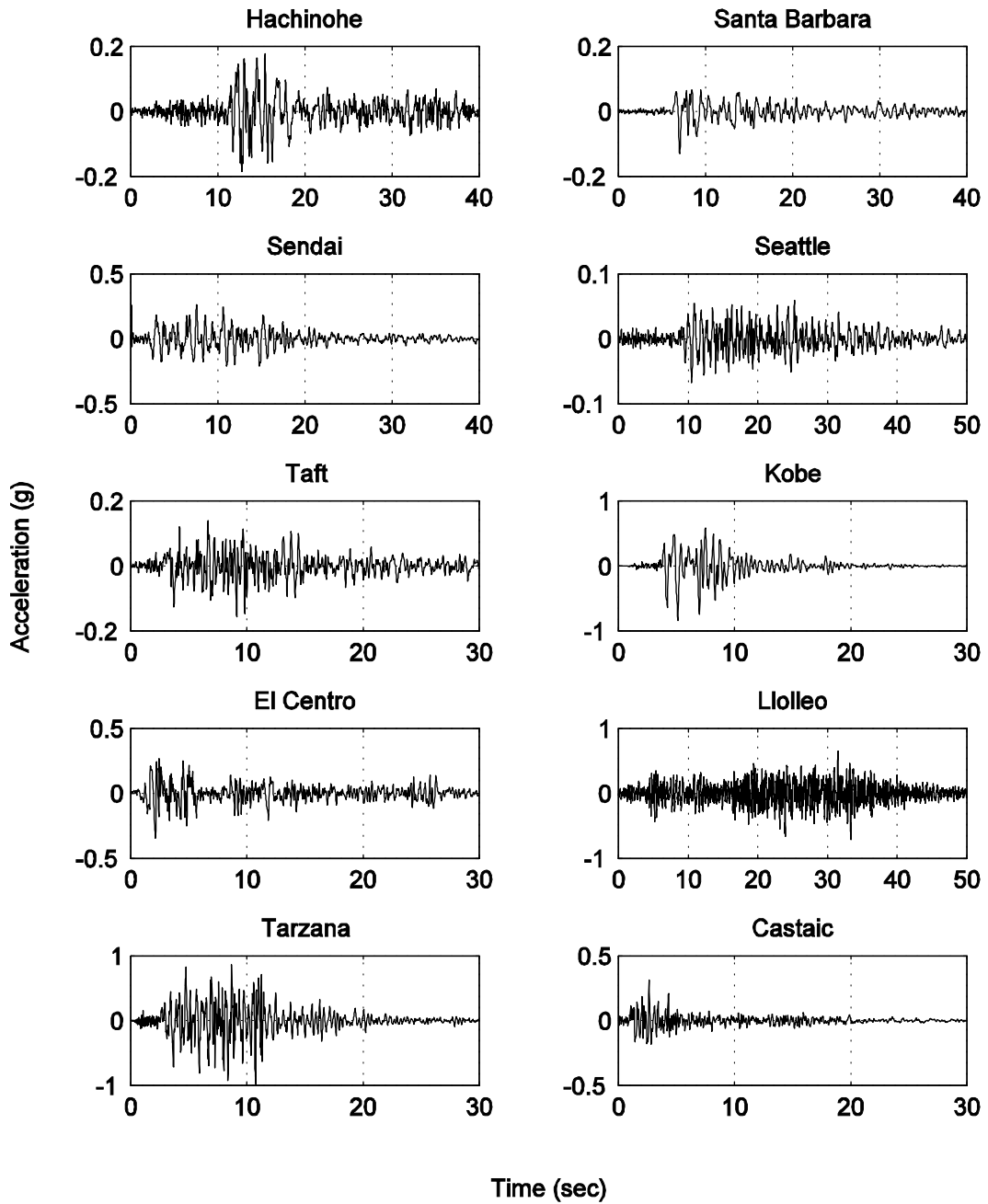
Figure 3.7. Original acceleration records for the ground motions considered in the study

The idealized displacement and acceleration response spectrum for each ground motion was calculated for 2% damping factor. The idealized response spectra were calculated using the following expressions proposed by Lepage (1997):

$$S_a = \begin{cases} F_a \cdot \alpha \cdot g \\ F_a \cdot \alpha \cdot g \cdot \dfrac{T_g}{T} \end{cases} \qquad \text{for} \qquad \begin{array}{l} T < T_g \\ T \geq T_g \end{array} \qquad (3.1)$$

$$S_d = \begin{cases} \dfrac{F_a \cdot \alpha \cdot g}{(2\pi)^2} \cdot T^2 \\ \dfrac{F_a \cdot \alpha \cdot g \cdot T_g}{(2\pi)^2} \cdot T \end{cases} \qquad \text{for} \qquad \begin{array}{l} T < T_g \\ T \geq T_g \end{array} \qquad (3.2)$$

where,

$F_a =$ Acceleration amplification factor. A value of 3.75 for oscillators, with 2% damping ratio, is representative of a wide range of earthquakes;

$g =$ Acceleration of gravity;

$\alpha =$ Peak ground acceleration expressed as a coefficient of the acceleration of gravity;

$T_g =$ Characteristic period for ground motion. Period at which the nearly constant acceleration region ends.

Equation 3.1 and Equation 3.2 are based on the assumptions that for periods lower than T_g, the acceleration response of the structures are nearly constant and for periods higher than T_g, velocity response is nearly insensitive to period variation.

Table 3.5. Ground motions considered in the study

EARTHQUAKE	STATION	COMPONENT	CHARACTERISTIC PERIOD T_g (sec)	RECORD DURATION (sec)	PEAK GROUND ACCELERATION (g)
Tokachi-Oki 16.05.1968	Hachinohe	EW	1.14	40	0.19
Kern County 21.07.1952	Santa Barbara	S48E	1.03	40	0.13
Miyagi-Ken-Oki 12.06.1978	Sendai	NS	0.95	40	0.26
Western Washington 13.04.1949	Seattle	S02W	0.89	50	0.07
Kern County 21.07.1952	Taft	N21E	0.72	30	0.16
Hyogo-Ken-Nanbu 17.01.1995	Kobe	NS	0.70	30	0.83
Imperial Valley 18.05.1940	El Centro	NS	0.55	30	0.35
Chile 03.03.1985	Llolleo	N10E	0.50	50	0.71
Northridge 17.01.1994	Tarzana	NS	0.44	30	0.99
San Fernando 09.02.1971	Castaic	N21E	0.35	30	0.32

The selected ground motions were normalized with respect to El Centro 1940 NS scaled to 0.4 g peak ground acceleration using Equation 3.2. For the selected scale, S_d corresponds to $205T$. The peak ground acceleration values of other ground motions were then scaled to yield the same result so that the displacement demand of all ground motions would be targeting the designated displacement spectrum. The peak ground accelerations used to normalize each record are presented in Table 3.6. It can be observed from the table that lower values of peak ground acceleration correspond to higher values of characteristic periods for ground motion. Therefore the product of α times T_g is constant for all the ground motions.

Table 3.6. Ground motion parameters for normalized records

EARTHQUAKE	CHARACTERISTIC PERIOD (sec)	PEAK GROUND ACCELERATION (g)
Hachinohe 1968 EW	1.14	0.19
Santa Barbara 1952 S48E	1.03	0.21
Sendai 1978 NS	0.95	0.23
Seattle 1949 S02W	0.89	0.25
Taft 1952 N21E	0.72	0.31
Kobe 1995 NS	0.70	0.31
El Centro 1940 NS	0.55	0.40
Llolleo 1985 N10E	0.50	0.44
Tarzana 1994 NS	0.44	0.50
Castaic 1971 N21E	0.35	0.63

Linear displacement response spectra for each ground motion that was normalized to have the scaled peak ground accelerations is presented in Figure 3.8 for 2% damping factor. Linear displacement response spectra for 5% and 10% damping factors are given in Appendix A.
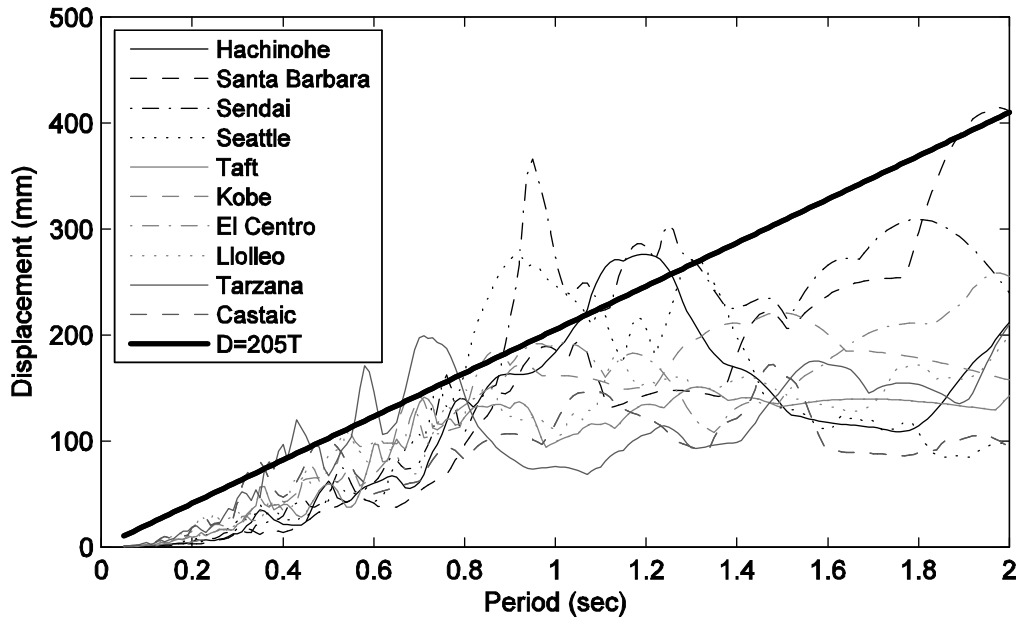
Figure 3.8. Linear displacement response spectra for normalized ground motions for 2% damping

3.4.2. Numerical Model

The nonlinear dynamic analyses were performed using IDARC-2D. Based on the section and reinforcement details given in Section 3.3 for each element type, moment - curvature relationship of the frame members were determined using the spreadsheet developed by Ersoy and Özcebe (2001). Then, the curves were simplified as tri-linear envelopes for data entry. Hysteretic behavior parameters for the reinforced concrete members are taken from the calibration results presented in Section 2.4. Lumped weights were calculated by considering the member weights and the gravitational loads.

Infill wall properties are taken from the properties mentioned in Section 3.3.2. The hysteretic parameters of the infill walls are taken same as the ones of Frame #3 discussed in Chapter 2.

3.4.3. Analysis Results

The first dynamic analysis series included the frames BF and IF-1. The total of ten ground motions was applied to the systems to determine the ground motions with high demand. Roof displacement histories, base shear-roof displacement hysteresis

curves and interstory drift ratios at the moment of maximum roof displacements are compared. In Figure 3.9, roof displacement histories of BF and IF-1 are given for each analysis. It is observed that the infill walls limit the roof displacement of IF-1 up to a certain point in most earthquakes. However, in some earthquakes, that are Sendai, Seattle, Kobe and El Centro, the roof displacement of IF-1 is almost equal to or higher than that of the bare frame. It should be noted that smaller peak displacements are expected from the frame with infill wall due to the shortened period of the frame.
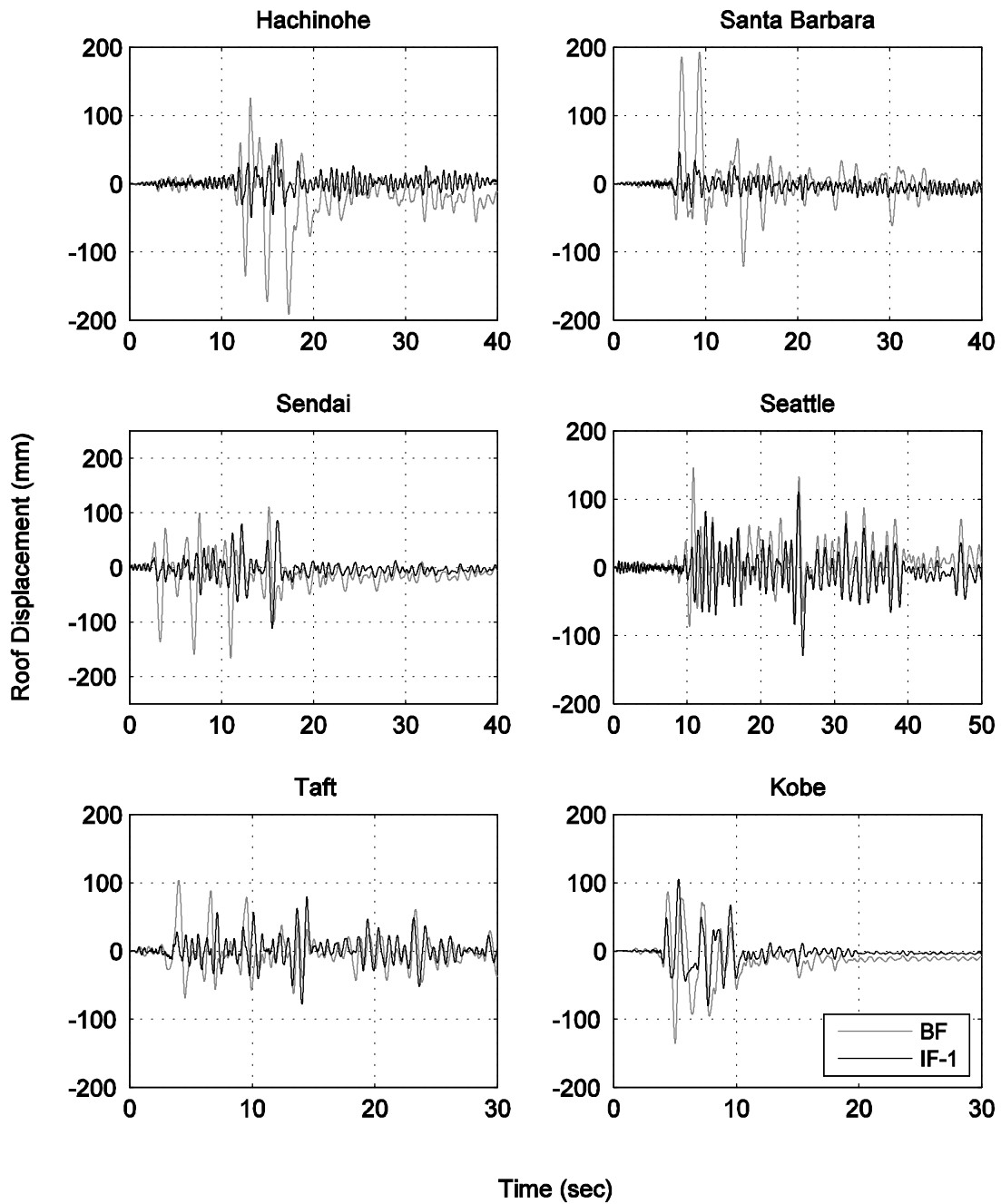

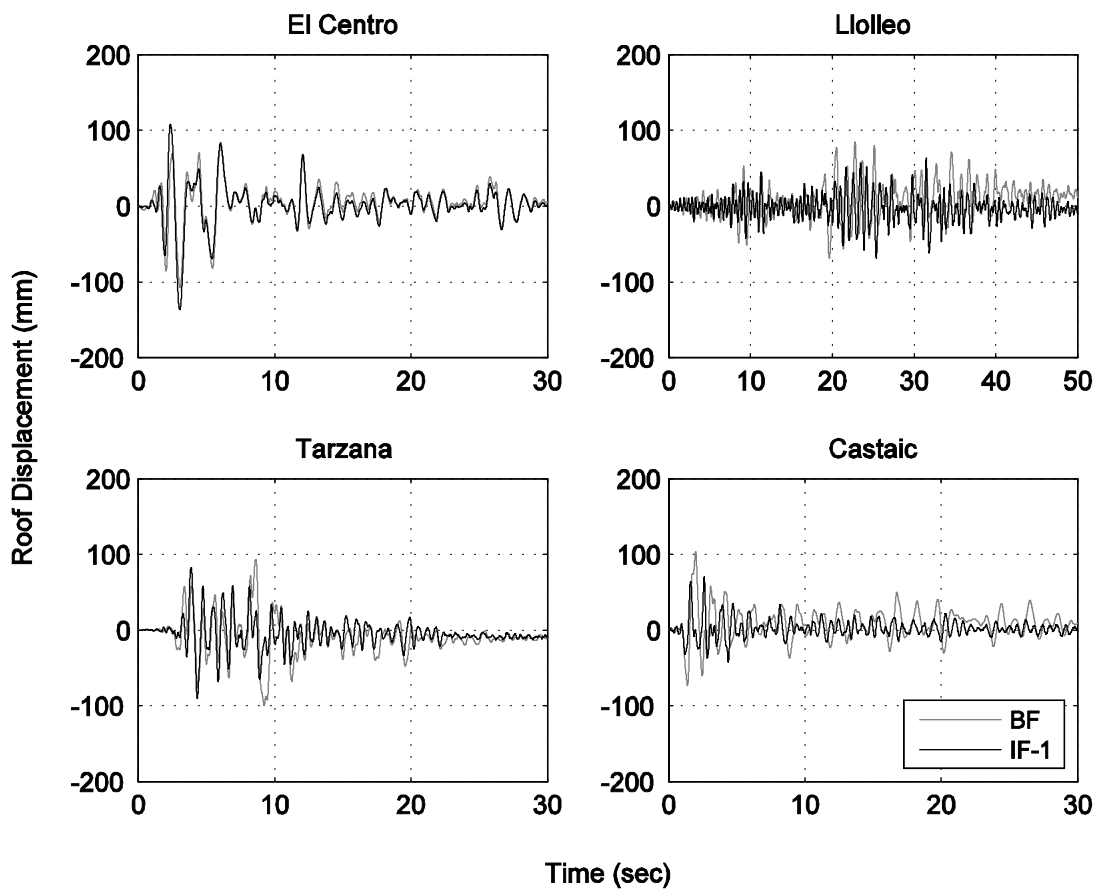Figure 3.9. Roof displacement histories of BF and IF-1

Figure 3.9 (cont.)

The same effects can be observed in Figure 3.10, where the total base shear versus the roof displacement plots are presented. It can be seen from the plots that the infill walls increase the total stiffness and the strength of the frame significantly. However, in some earthquakes, the stiffness of IF-1 decreases dramatically and higher displacement values are encountered. Upon observation of the individual infill wall hystereses at these frames, it was seen that the infill walls at the lower stories were in the post-peak region of their response. Noting that, infill wall stiffness and strength decreased seriously at this stage and soft-story mechanisms formed in IF-1. This situation explains the higher roof displacements of IF-1, which was mentioned above.
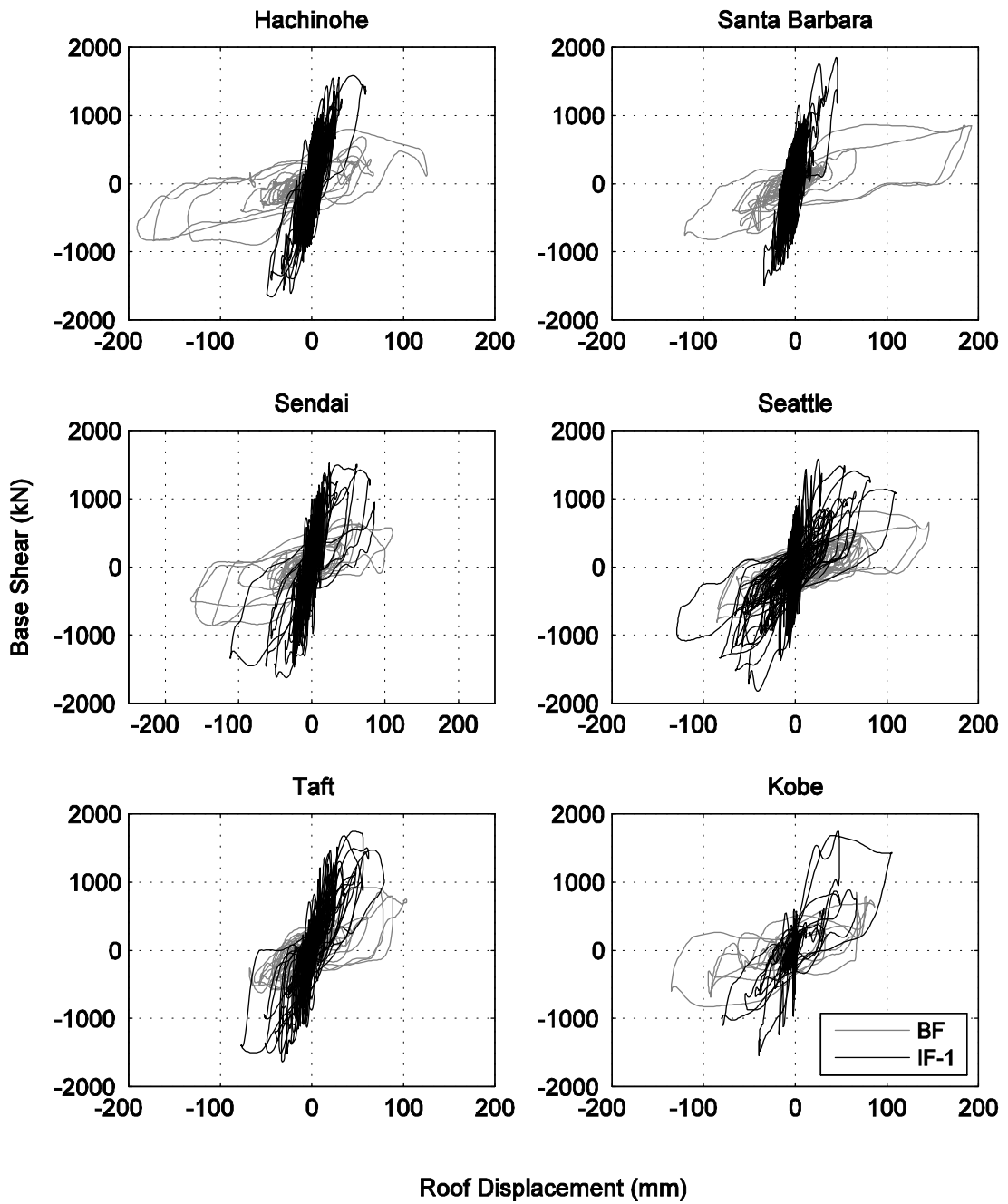
Figure 3.10. Base shear-roof displacement curves of BF and IF-1
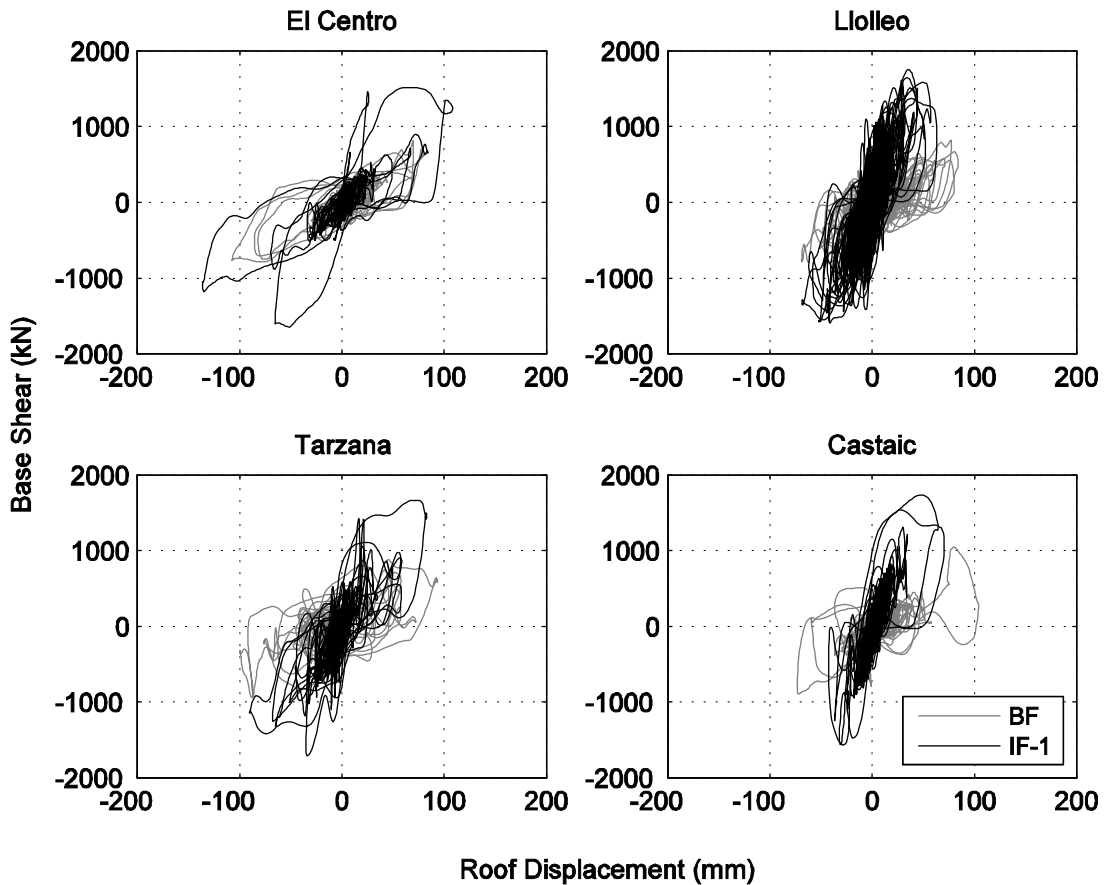
(cont. on next page)

Figure 3.10 (cont.)

Interstory drift distribution of BF and IF-1 can be seen in Figure 3.11. The interstory drift distributions of IF-1 are better when they are compared to those of the BF for the earthquakes in which the infill walls restricted the roof displacement. On the other hand, the interstory drift ratios of the lower stories in IF-1 are beyond the ones that in BF for the ground motions which create demands beyond the infill wall capacities. The soft-story mechanisms were formed due to the drift concentrations in the lower stories in these frames. Based on these observations, dynamic analyses of IF-2 were carried out with Sendai 1978 NS, Seattle 1949 S02W, Kobe 1995 NS and El Centro 1940 NS ground motions.
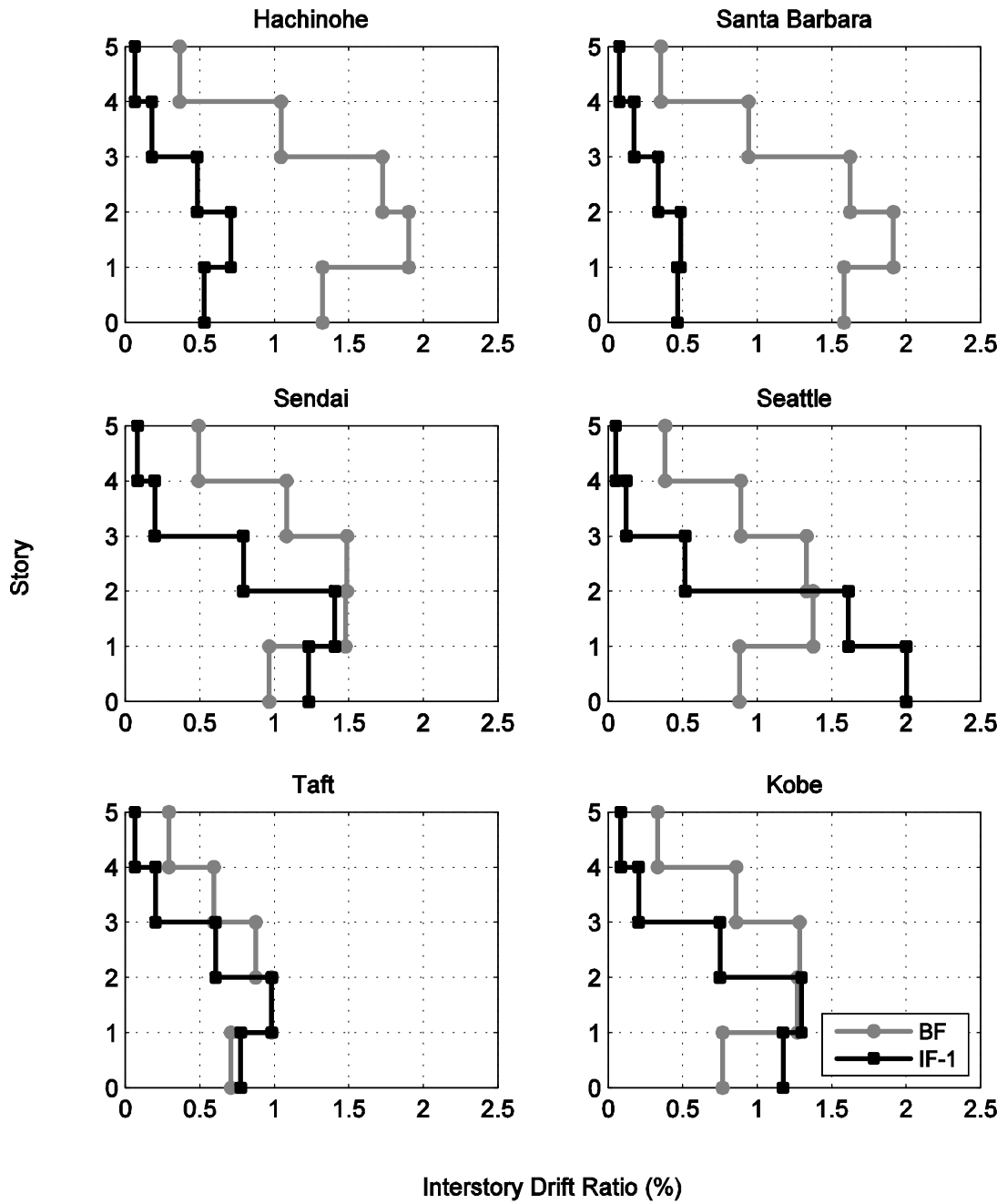
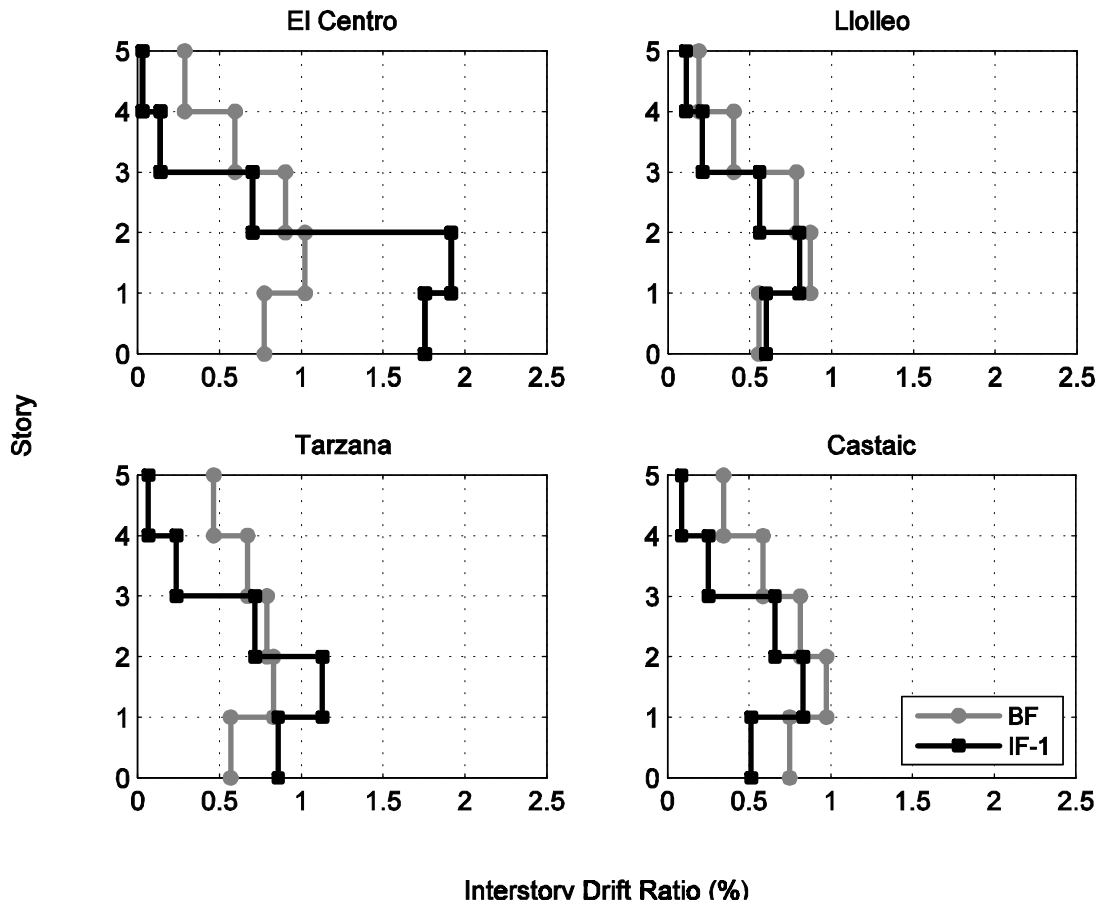Figure 3.11. Interstory drift ratios of BF and IF-1

Figure 3.11 (cont.)

IF-2, whose infill panels have varying stiffness and strength properties which are decreasing with the elevation, was subjected to these four ground motions and the results were compared to those of BF and IF-1. In Figure 3.12 to Figure 3.15, roof displacement histories of IF-1 and IF-2 are presented. As it can be observed from the figures, for the ground motions Sendai and Seattle, the organized stiffness distribution restricted the roof displacements significantly. However, in Kobe and El Centro, the infill walls in the lower stories passed to the post-peak stage. As a result, the maximum roof displacements are approximately equal to those of BF and IF-1.
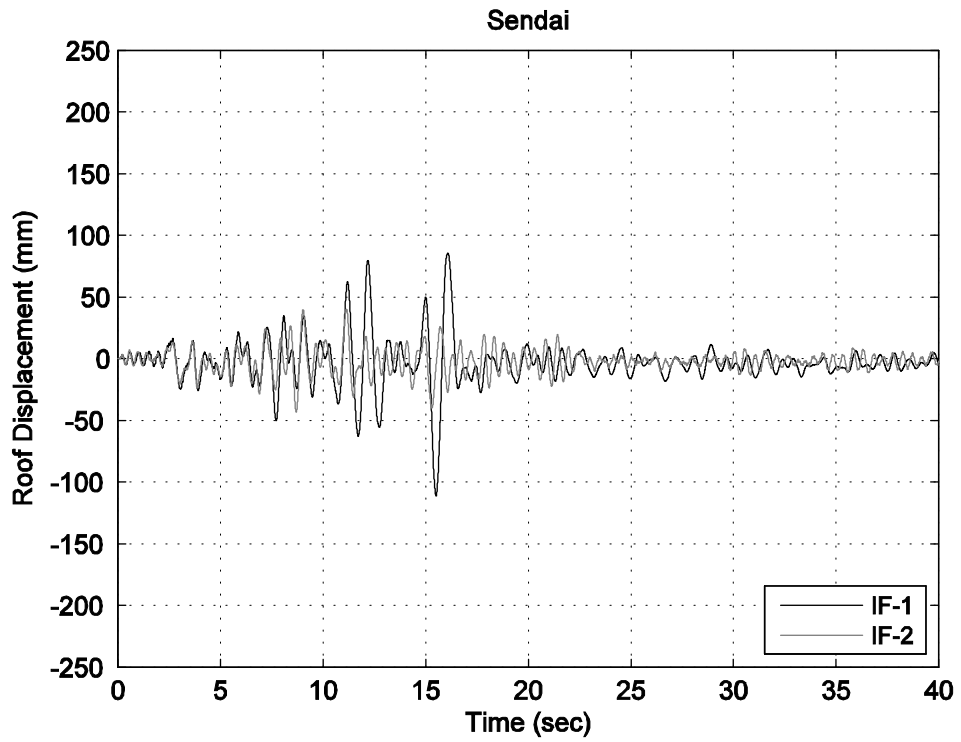
Figure 3.12. Roof displacement history of IF-1 and IF-2 for Sendai earthquake
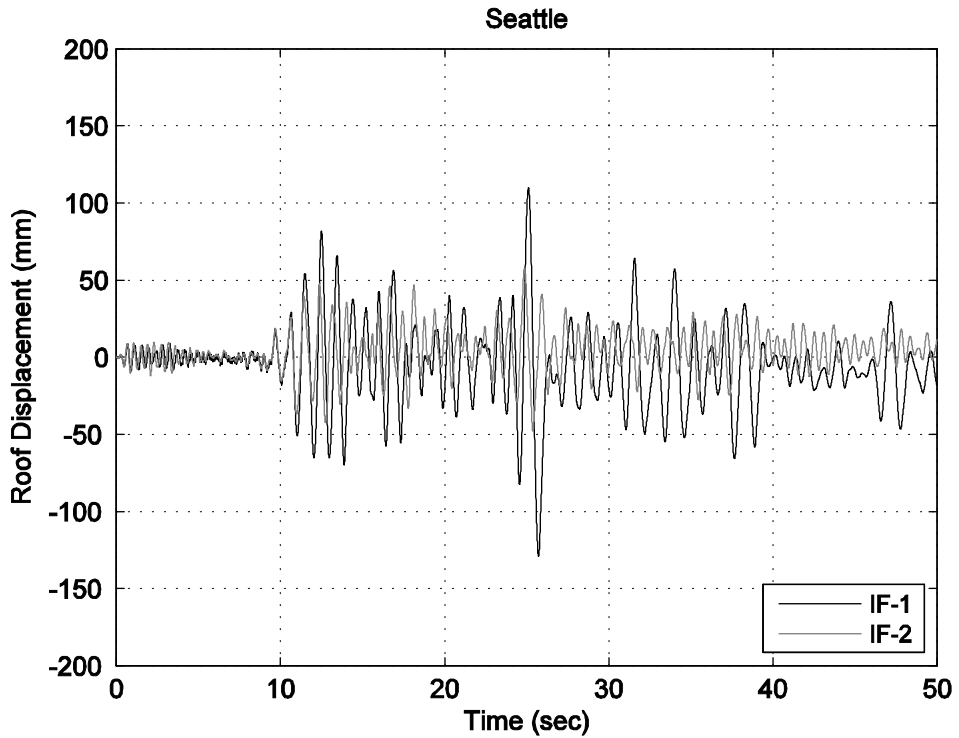

Figure 3.13. Roof displacement history of IF-1 and IF-2 for Seattle earthquake

Figure 3.14. Roof displacement history of IF-1 and IF-2 for Kobe earthquake

Figure 3.15. Roof displacement history of IF-1 and IF-2 for El Centro earthquake

Total base shear - roof displacement curves for the performed dynamic analyses are presented in Figure 3.16 to Figure 3.19. The maximum roof displacements are lower than those of IF-1, even for Kobe and El Centro, where the infill walls of the lower stories were in the post-peak stage.
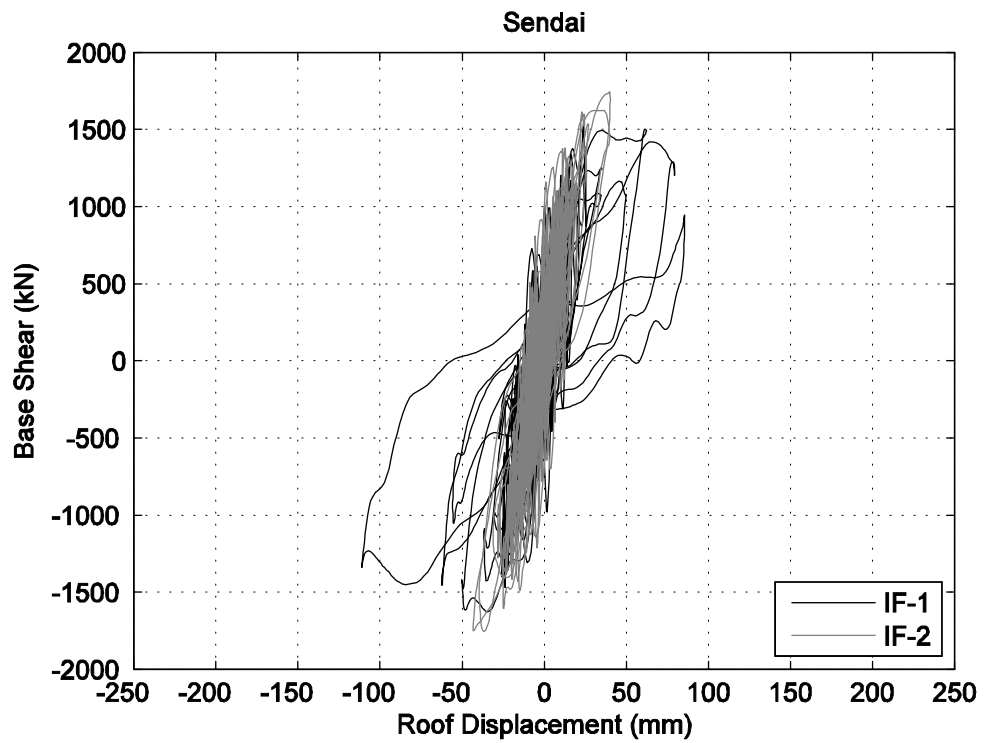
Figure 3.16. Base shear-roof displacement curves of IF-1 and IF-2 for Sendai earthquake
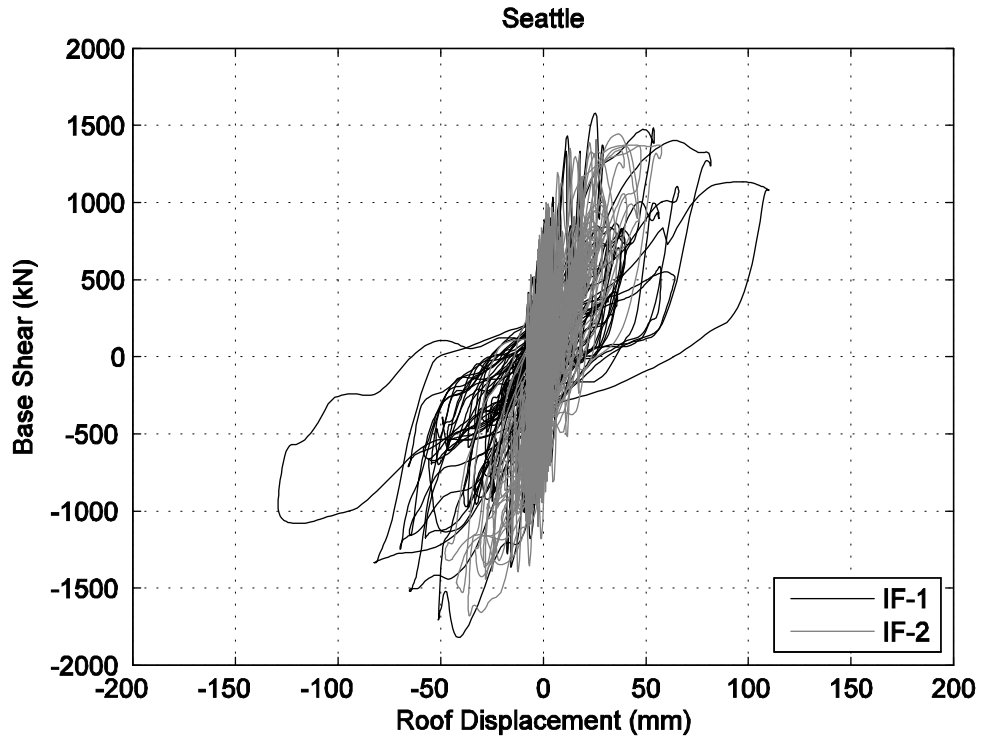
Figure 3.17. Base shear-roof displacement curves of IF-1 and IF-2 for Seattle earthquake
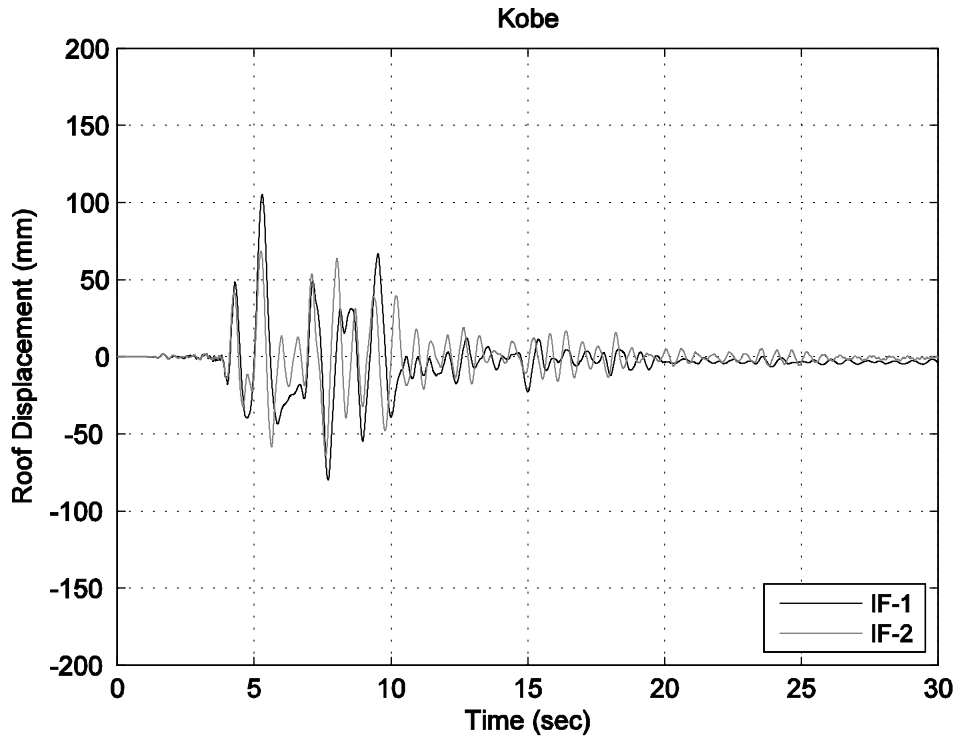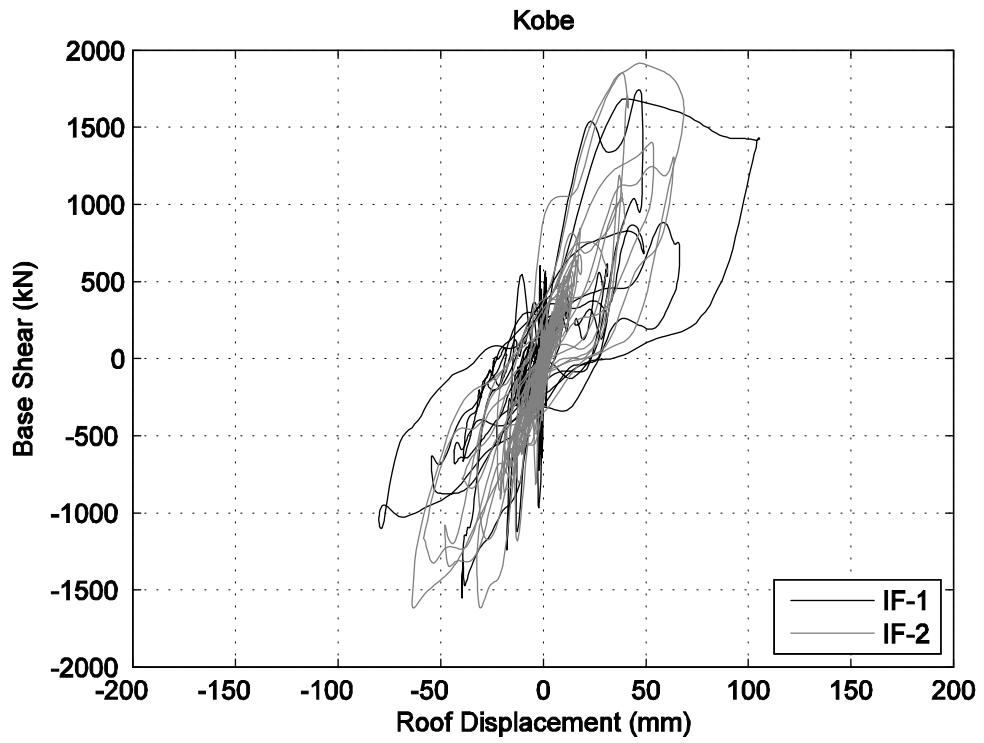

Figure 3.18. Base shear-roof displacement curves of IF-1 and IF-2 for Kobe earthquake
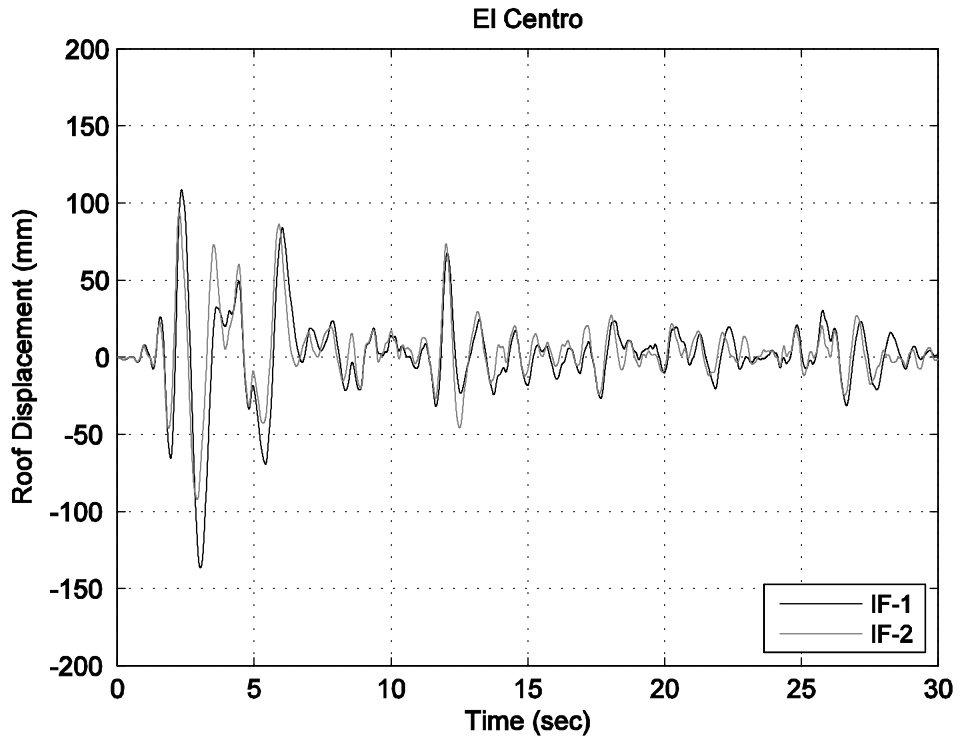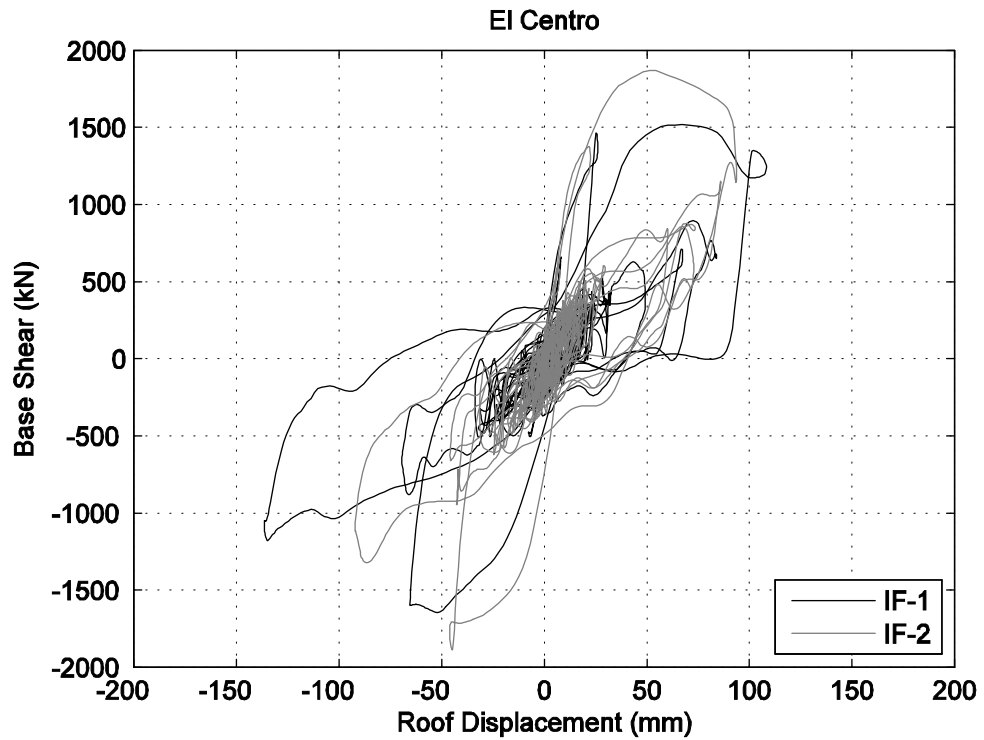
Figure 3.19. Base shear-roof displacement curves of IF-1 and IF-2 for El Centro earthquake

The interstory drift ratios of BF, IF-1 and IF-2 are compared in Figure 3.20 to Figure 3.23. In Sendai and Seattle earthquakes, the interstory drift distribution yielded a more balanced profile for IF-2. In Kobe and El Centro, the interstory drift ratios decreased in the lower stories, even though the infill walls in those stories had passed to the post-peak stage.

Figure 3.20. Interstory drift ratios of BF, IF-1 and IF-2 for Sendai earthquake

Figure 3.21. Interstory drift ratios of BF, IF-1 and IF-2 for Seattle earthquake

Figure 3.22. Interstory drift ratios of BF, IF-1 and IF-2 for Kobe earthquake

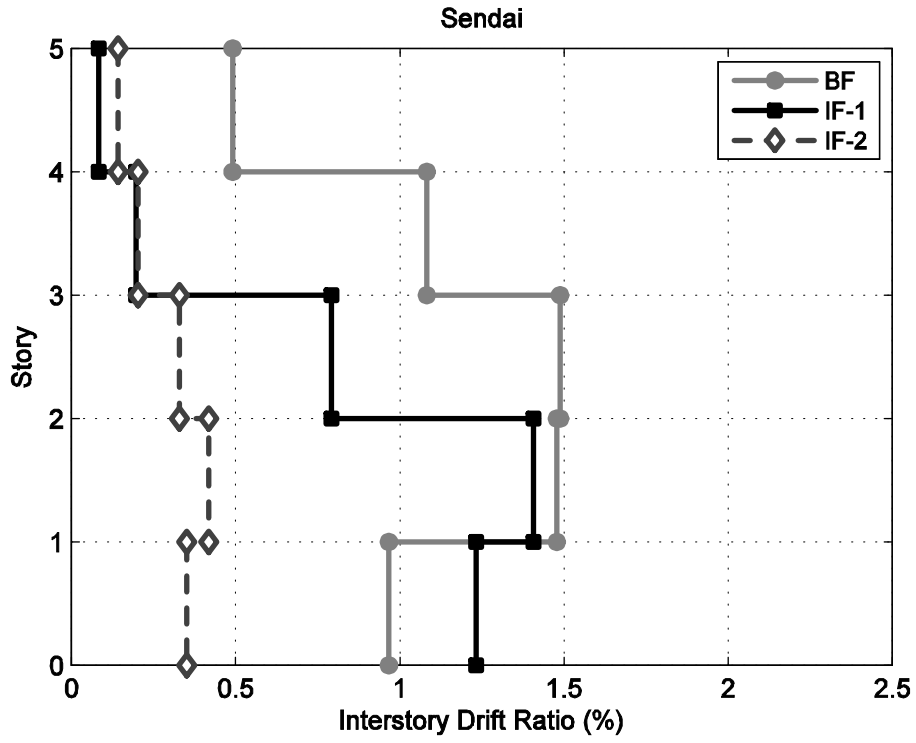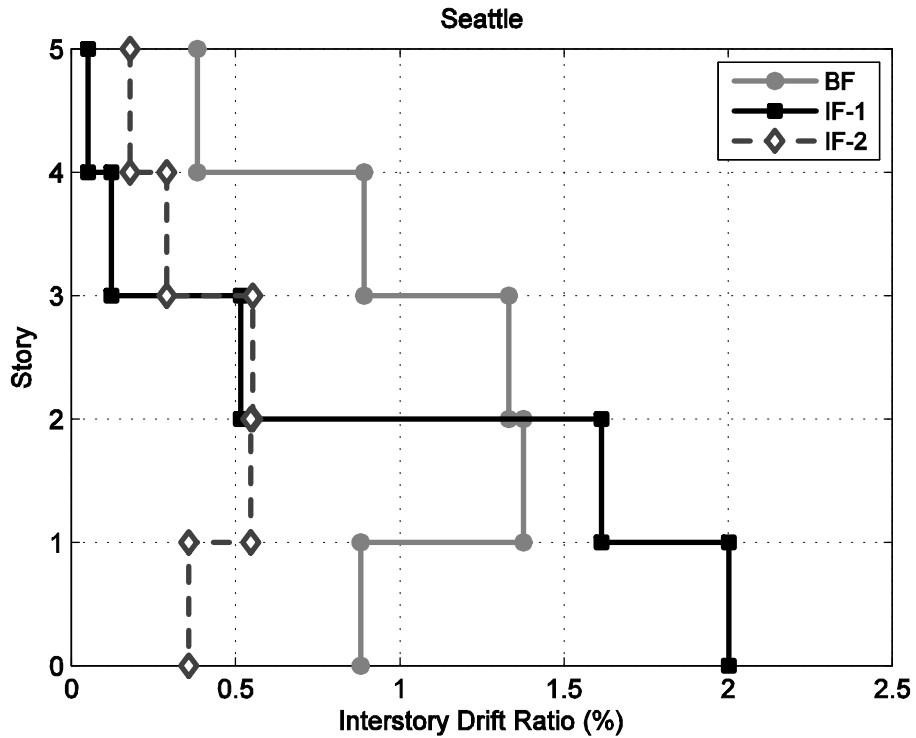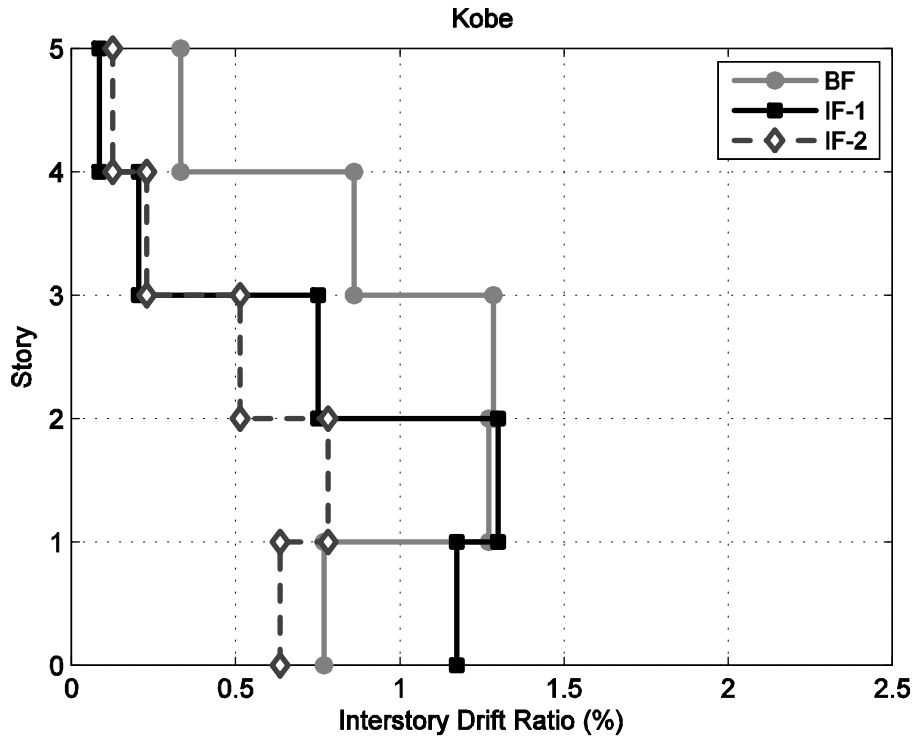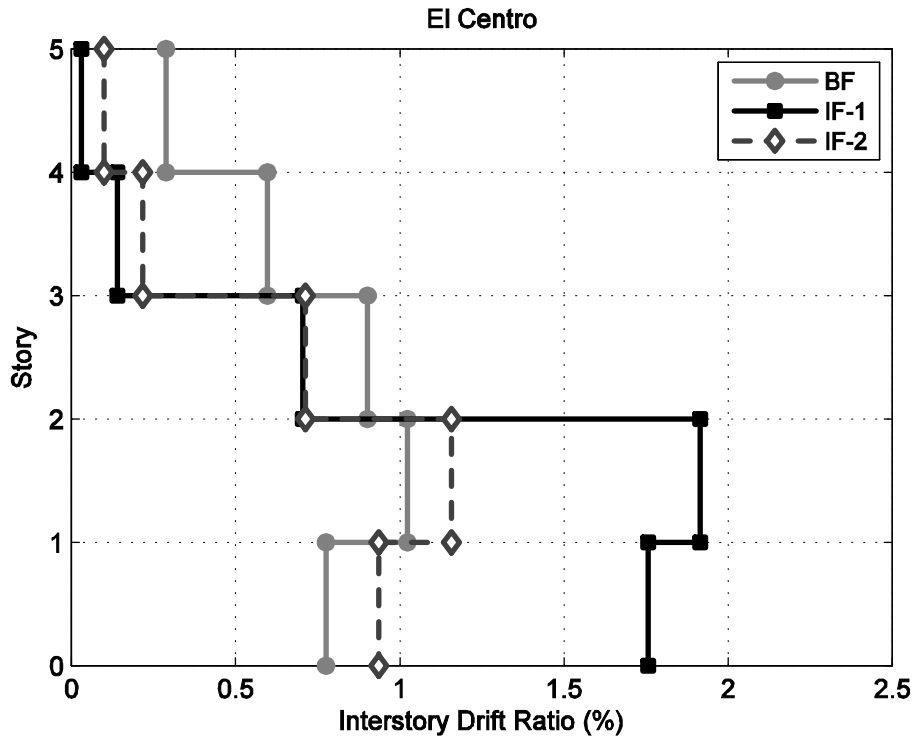Figure 3.23. Interstory drift ratios of BF, IF-1 and IF-2 for El Centro earthquake

The interstory drift ratios of the infilled frames are given in Table 3.7 as absolute values and proportional to each other and to the bare frame in story basis.

Table 3.7. Proportional interstory drift ratios of the infilled frames in story basis

SENDAI						
Story	**Interstory Drift Ratios (%)**			**Relative Ratios**		
	BF	**IF-1**	**IF-2**	**IF-1/BF**	**IF-2/BF**	**IF2/IF-1**
5	0.49	0.08	0.01	0.16	0.03	0.18
4	1.08	0.19	0.20	0.18	0.18	1.05
3	1.49	0.79	0.33	0.53	0.22	0.42
2	1.48	1.41	0.42	0.95	0.28	0.30
1	0.97	1.23	0.35	1.27	0.36	0.28

SEATTLE						
Story	**Interstory Drift Ratios (%)**			**Relative Ratios**		
	BF	**IF-1**	**IF-2**	**IF-1/BF**	**IF-2/BF**	**IF2/IF-1**
5	0.38	0.05	0.18	0.13	0.47	3.60
4	0.89	0.12	0.29	0.14	0.33	2.38
3	1.33	0.52	0.55	0.39	0.41	1.06
2	1.38	1.61	0.55	1.17	0.40	0.34
1	0.88	2.00	0.36	2.27	0.41	0.18

KOBE						
Story	**Interstory Drift Ratios (%)**			**Relative Ratios**		
	BF	**IF-1**	**IF-2**	**IF-1/BF**	**IF-2/BF**	**IF2/IF-1**
5	0.33	0.08	0.13	0.24	0.39	1.63
4	0.86	0.20	0.23	0.23	0.27	1.15
3	1.28	0.75	0.51	0.59	0.40	0.68
2	1.27	1.30	0.78	1.02	0.61	0.60
1	0.77	1.17	0.64	1.52	0.83	0.55

EL CENTRO						
Story	**Interstory Drift Ratios (%)**			**Relative Ratios**		
	BF	**IF-1**	**IF-2**	**IF-1/BF**	**IF-2/BF**	**IF2/IF-1**
5	0.29	0.03	0.10	0.10	0.34	3.33
4	0.60	0.14	0.22	0.23	0.37	1.57
3	0.90	0.70	0.71	0.78	0.79	1.01
2	1.02	1.92	1.16	1.88	1.14	0.60
1	0.78	1.76	0.94	2.26	1.21	0.53

It has to be noted that, the maximum displacements calculated by IDARC are below the values estimated by Lepage's upper envelope formula. The estimates were calculated by using the formula proposed by Lepage (1997):

$$D_{max} = \frac{F_a \cdot \alpha \cdot g \cdot T_g}{(2\pi)^2} \cdot T \tag{3.3}$$

The formula estimates the maximum nonlinear drift response of the reinforced concrete structures.

3.5. Pushover Analysis

The pushover analyses were performed to determine the performance of the three frames which were described in Section 3.3. Since the infill model in IDARC does not work in pushover analysis, SAP2000 was used for the pushover analyses of the frames.

The analyzed frames were assumed to be located in the first seismic zone and on a Z3 type of local site. Depending on these assumptions, the effective ground acceleration coefficient was taken as 0.40 and the characteristic periods for the soil type were 0.15 and 0.60 seconds according to Turkish Earthquake Code (TEC2007).

The lateral force pattern was calculated according to the equivalent earthquake loads procedure and assigned to the frames at the floor levels. Initially, the frames were pushed to failure and the capacity curves were obtained. Using the procedures described in Section 7 of Turkish Earthquake Code (TEC2007), seismic displacement demand was determined. Afterwards, the frames were pushed to the demanded displacements and the performance levels were determined.

In Turkish Earthquake Code (TEC2007), limit strains for concrete and reinforcing steel were defined for each damaged-limit state. The strain values of the frame elements at the end of the analyses were determined from the rotations observed at each element based on the moment - curvature relationships.

3.5.1. Numerical Model

In SAP2000, linear behavior of the elements is determined through section and material properties. Therefore, these properties were defined for the reinforced concrete members according to the information given in Section 3.3. The nonlinear behavior of the reinforced concrete members was defined by assigning plastic hinges in both ends of each member. These hinges were determined according to the tri-linearly simplified moment-curvature relationships of the members, as in IDARC. In Turkish Earthquake Code (TEC2007), strain limits for concrete and reinforcement steel were determined for each damage region. Using these strain limits, limit curvatures for each damage region were calculated for each plastic hinge and defined in SAP2000. Therefore, it is possible to determine the damage region of each reinforced concrete member and the performance of the structure.

The infill walls were modeled as compression-only equivalent struts in SAP2000. The linear properties of the infill panels were defined so that the initial stiffness values correspond to those of the ones defined in IDARC. For determining the nonlinear behavior of the infill walls used in the infilled frames, displacement-controlled incremental quasi-static analyses were performed in IDARC for each infill wall. Then, the results were simplified as tri-linear curves and defined as plastic hinges in the middle of each equivalent strut.

3.5.2. Analysis Results

The pushover curves of the three frames are presented in Figure 3.24. It can be seen that the presence of the infill walls substantially increased the strength and stiffness of the frame. The maximum base shear versus the frame weight ratio is 0.17 for the bare frame. This ratio increases to 0.27 and 0.29 for IF-1 and IF-2, respectively. The maximum shear force is reached in relatively small displacements for the infilled frames compared to the bare frame. The initial stiffness of IF-1 and IF-2 is 2.80 and 3.07 times that of the BF, respectively.
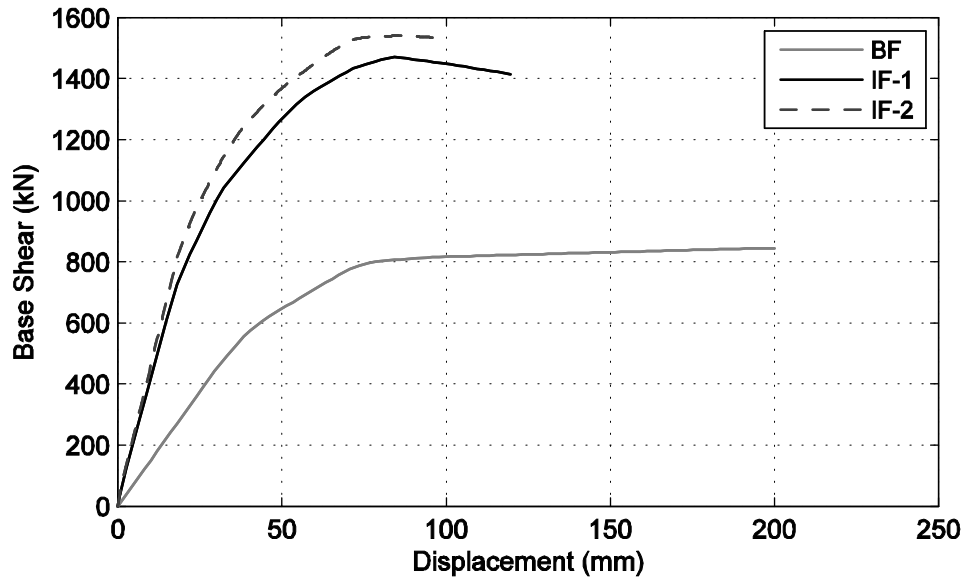
Figure 3.24. Pushover curves of BF, IF-1 and IF-2

Maximum displacement demands of the infilled frames are smaller compared to that of the bare frame. They are approximately 12 cm for IF-1 and 10 cm for IF-2, while nearly 20 cm for BF.

The plastic hinge states observed at the end of the analyses are shown in Figure 3.25 for BF, IF-1 and IF-2, respectively.
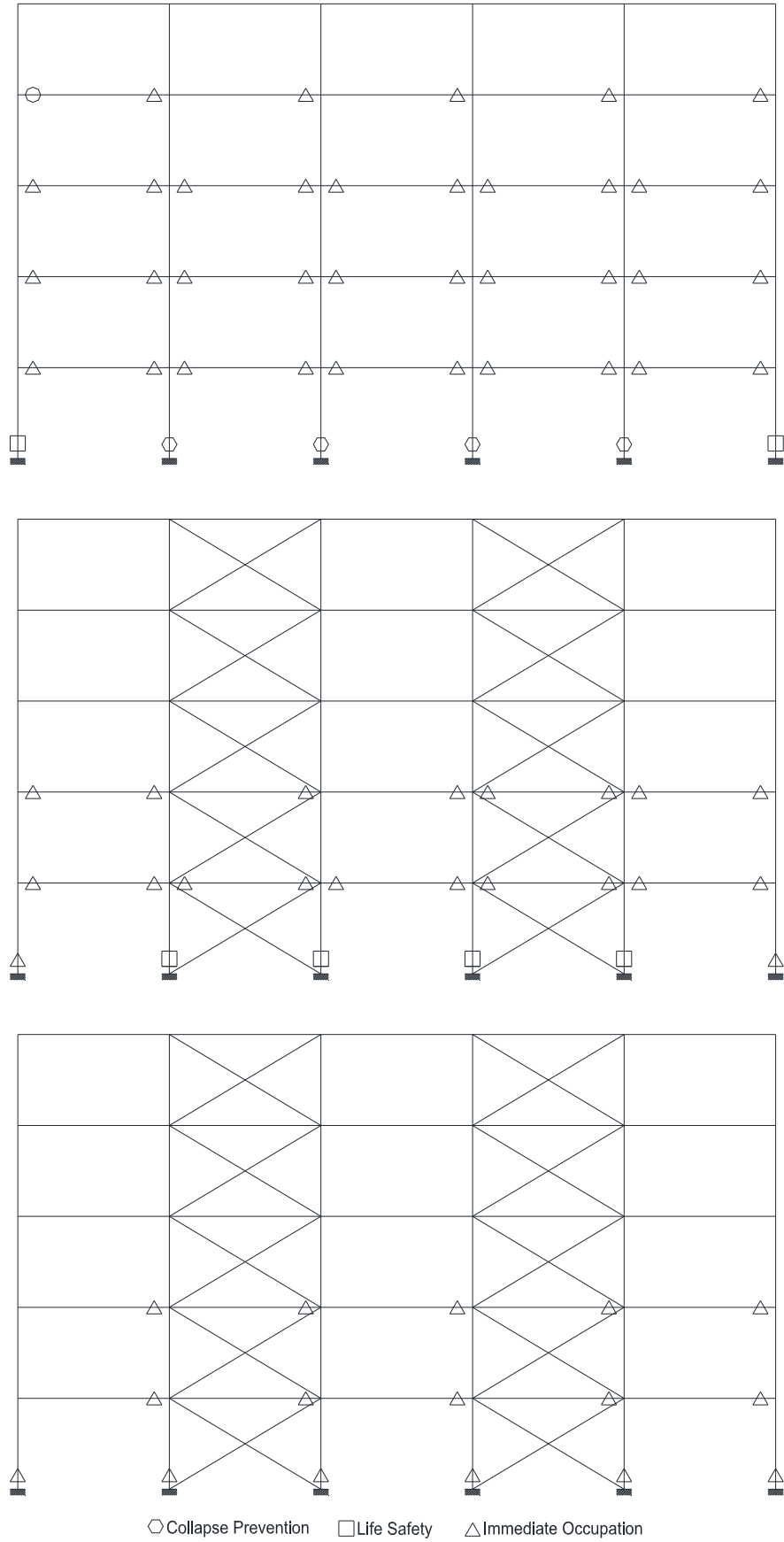
Figure 3.25. Plastic hinge states of BF, IF-1 and IF-2 at code displacement demands

As it can be seen from the Figure 3.25, the inner columns of the first story are highly damaged in BF. According to the damage limits defined in Turkish Earthquake Code (TEC2007), the bare frame is determined to be in "Collapse Prevention" performance level and it does not satisfy the life safety requirements. In Figure 3.25, damages in the columns of the first story of IF-1 are lower than those of the bare frame. The evaluation of the damage levels observed in the plastic hinges reveals that IF-1 is in "Life Safety" damage zone. In Figure 3.25, damages in the first story columns of BF-2 are observed to decrease. The damage zone of IF-2 is determined as "Immediate Occupation" after evaluating the plastic hinge states.

Interstory drift ratios for the analyzed frames are presented in Figure 3.26 at the code displacement demands. The maximum interstory drift is observed in the second story of BF as 1.78%. In IF-1, the interstory drift increase of the lower stories is larger than that of BF. However, the maximum interstory drift ratio, which is 1.30% is smaller than that of BF. In IF-2, the maximum interstory drift is observed in the second story as 0.95%. The interstory drifts of the lower floors decreased in IF-2 when those of the upper floors increase when compared to IF-1. This leads the frame to have a more balanced interstory drift distribution while preventing the drifts to concentrate in the lower stories.
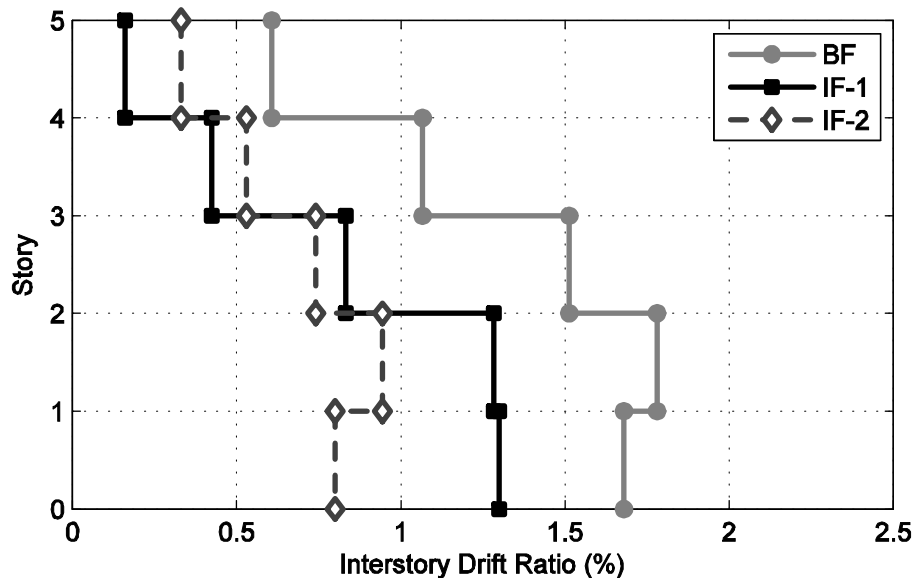
Figure 3.26. Interstory drift ratios of BF, IF-1 and IF-2 for pushover analysis

The interstory drift distributions of the three frames at various displacement levels are given in Figure 3.27 to Figure 3.29. The selected displacements cover a range starting from 20% below the code displacement demand and ending at 10% above, where the code displacement demand is the design target for a particular frame.

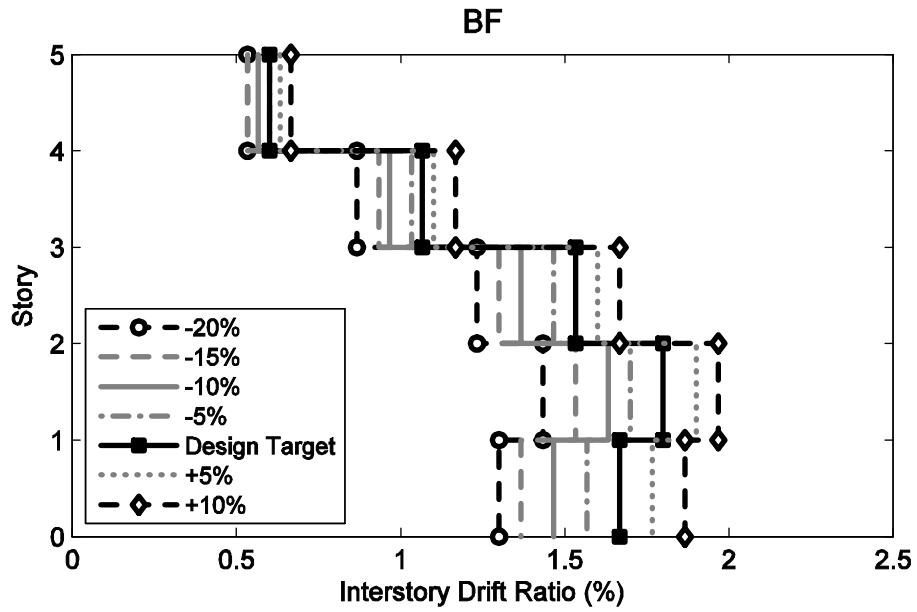Figure 3.27. Interstory drift ratios of BF at various stages of the pushover analysis
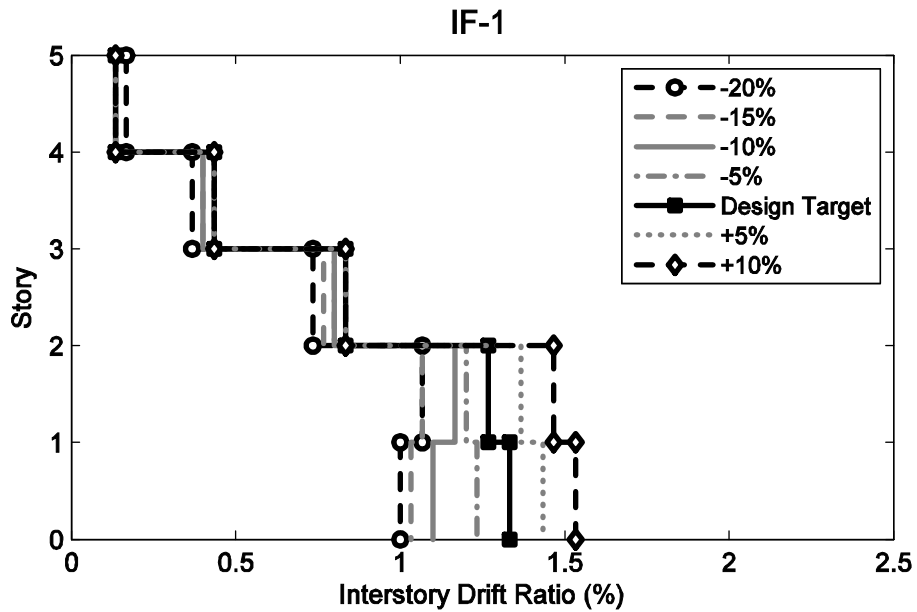

Figure 3.28. Interstory drift ratios of IF-1 at various stages of the pushover analysis
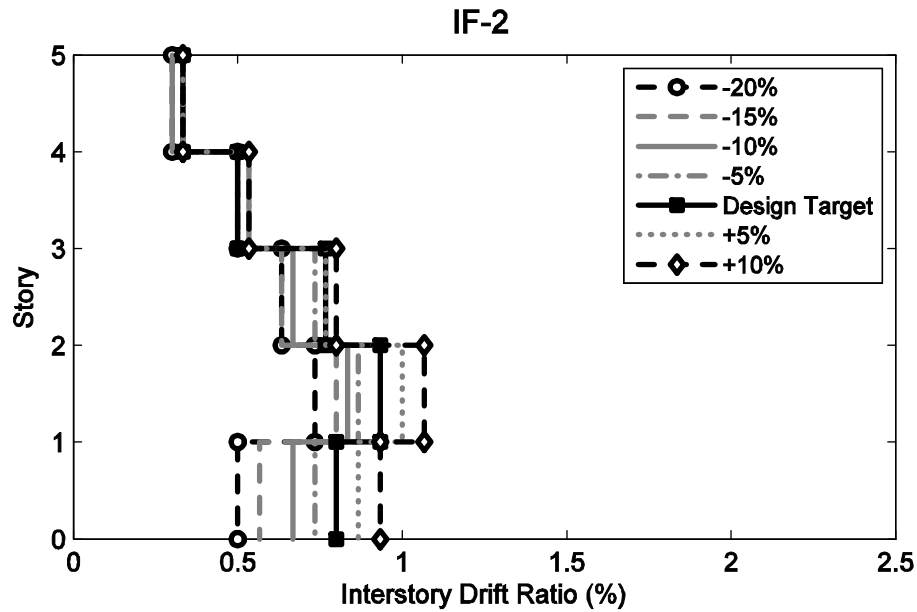
Figure 3.29. Interstory drift ratios of IF-2 at various stages of the pushover analysis

In the bare frame, the interstory drift ratios of the upper stories increase parallel to the displacement level. Concentration of deformations to the lower stories with increasing drift levels is observed.

In IF-1, the drift concentration at the first story happens to be more significant at higher displacement levels. This is the manifestation of stronger soft story effects with increasing drift levels.

In IF-2, even though there is still a concentration at the lower stories, it can be observed from the figure that higher levels also contribute to total drift at higher demand levels. Decreased drift concentrations at the lower levels and the decrease in the total displacement demand due to the decreased period of the structure make it possible for the frame to satisfy the design targets.

CHAPTER 4

CONCLUSIONS

4.1. Summary and Conclusions

In this study, effect of stiffness variations of the infill walls to the seismic behavior of RC structures was investigated in terms of interstory drift distributions. An analysis software, IDARC-2D, was selected for the analytical study. The program was calibrated and verified by simulating previously conducted experimental tests on RC frames with and without infill walls. Afterwards, a planar, five-bay, five-story RC frame was designed with insufficient confinement at the hinge regions. Two modified frames were obtained by filling two bays of the bare frame (BF) with infill walls. The infill walls of the first infilled frame (IF-1) had a uniform stiffness and strength distribution along the height of the frame. In the second infilled frame (IF-2), the stiffness and strength of the infill walls had a decreasing profile from the bottom to the top story. By this distribution, drift concentration at the lower stories was aimed to be mitigated.

The three frames were analyzed using nonlinear dynamic and pushover analysis procedures. Initially, BF and IF-1 were subjected to ten ground motion records which are normalized in terms of drift demand. Four critical ground motions were selected and applied to IF-2. Afterwards, pushover analyses of three frames were performed to determine the capacities and the interstory drift distributions. The results were compared and evaluated in terms of interstory drift distributions.

The implications inferred from the study may be listed as follows:

- The selected software can simulate the global behavior of bare and infilled frames with accuracy provided that the hysteretic control parameters are calibrated cautiously. However, the program did not have simulation capability of the shear failure in the columns due to the compression applied by the infill walls.

- The existence of infill walls increased the stiffness and strength of the frame substantially. The base shear capacities of the infilled frames were increased by approximately 100%. Moreover, the initial stiffness values of the infilled frames were as high as three times of the bare frame initial stiffness. Since, the maximum displacement induced by strong ground motions is sensitive to stiffness (Shimazaki and Sozen, 1988; Lepage, 1997); with decreasing periods, the displacement demand for the infilled frames decreased. However, the drift concentration in the lower stories of IF-1 caused a soft-story mechanism in some of the selected ground motions and the upper stories moved together almost as a rigid body.

- In some of the selected ground motions, the interstory drift ratio of the lower stories of IF-1 exceeded those of BF. The organized stiffness distribution managed to limit these drifts up to a certain point in IF-2. The drifts observed in the lower stories of IF-2 were even smaller than those of BF, except El Centro ground motion. The maximum interstory drift levels of IF-2 in El Centro are about the bare frame demands. Still, it can be concluded that the selected distribution was proved to be advantageous in controlling drift distribution of the frames.

- In the pushover analyses, the existence of an organized stiffness distribution revealed a better interstory drift distribution along the elevation of the frame. The evaluation of the hinge states revealed that the selected stiffness distribution improved the performance of the frame when it compared to those of BF and IF-1.

The results indicate that controlling the stiffness distribution along the height of the buildings by infill walls which have varying stiffness properties may help mitigating drift concentrations in the lower stories and improving the seismic performance. Another implication is that the existence of infill walls changes the behavior and damage distribution of the structures significantly. Therefore, expected behavior in structural designs which ignore the infill walls may not be the actual behavior and unforeseen damages may occur in the buildings. This implication shows the necessity of taking the infill walls into account in the design process.

4.2. Future Recommendations

The current study indicated that a well-organized stiffness distribution along the elevation of structures can be controlled by infill walls which have varying structural properties. These variations can be obtained by applying different reinforcing or weakening methods to the infill walls. Infill wall reinforcing techniques has been studied widely. On the other hand, studies on the weakening techniques that improve the ductility of the infill walls by decreasing the strength and stiffness values have started recently. Strengthening and weakening methods could be used together to ensure the targeted stiffness and strength distribution in the frames. Therefore, analytical and experimental studies should be performed with such techniques to verify the effectiveness of the proposed method.

In this study, effects of stiffness variation in the elevation of the frames were investigated analytically on a planar frame. Real-life experiments should be performed to verify the analytical results.

REFERENCES

Baber, T. T., & Noori, M. N. (1985). Random Vibration of Degrading, Pinching Systems. *Journal of Engineering Mechanics, 111*(8), 1010-1026.

Baber, T. T., & Wen, Y. K. (1981). Random Vibration of Hysteretic Degrading Systems. *Journal of Engineering Mechanics, ASCE, Vol. 107*.

Bal, I. E., Gulay, F. G., Gorgulu, O., & Baysal, T. (2007). Adana Bölgesindeki B/A Yapı Stoğu Karakteristiklerinin Hasar Kayıp Tahmin Modelleri Açısından İncelenmesi. *Altıncı Ulusal Deprem Mühendisliği Konferansı*, İstanbul, 411-422 (In Turkish).

Bal, I. E., Crowley, H., Pinho, R., & Gülay, F. (2008). Detailed assessment of structural characteristics of Turkish RC building stock for loss assessment models. *Soil Dynamics and Earthquake Engineering*, *28*(10-11), 914-932.

Bertero, V., & Brokken, S. (1983). Infills in Seismic Resistant Building. *Journal of Structural Engineering, 109*(6), 1337-1361.

Bouc, R. (1967). Forced vibration of mechanical systems with hysteresis. *Proceeding of the 4th Conference on Non-linear Oscillations,* Prague.

Çankaya, M. A., (2011). Dynamic behavior of reinforced concrete frames with infill walls (Master's Thesis). Civil Engineering Department, İzmir Institute of Technology, İzmir, Turkey.

Dolšek, M. M., & Fajfar, P. P. (2008). The effect of masonry infills on the seismic response of a four-storey reinforced concrete frame - a deterministic assessment. *Engineering Structures*, *30*(7), 1991-2001.

Erdem, I., Akyuz, U., Ersoy, U., & Ozcebe, G. (2006). An experimental study on two different strengthening techniques for RC frames. *Engineering Structures*, *28*(13), 1843-1851.

Ersoy, U., & Özcebe, G. (2001). Betonarme: Temel İlkeler, TS-500-2000 ve Türk Deprem Yönetmeliğine (1998) Göre Hesap. *Evrim Yayınevi* (In Turkish).

IDARC User's Guide (2010) from ftp://civil.eng.buffalo.edu/idarc2d/7.0/2-manual.zip

Inel, M. M., Ozmen, H. B., Senel, S. M., & Kayhan, A. H. (2009). Mevcut Betonarme Binaların Yapısal Özelliklerinin Belirlenmesi. *Sakarya Uluslararası Deprem Sempozyumu: "İlk on yılında Marmara Depreminin Öğrettikleri", 1–2 Ekim 2009*, Sakarya, Türkiye, 295-304 (In Turkish).

Lepage A. (1997) A method for drift-control in earthquake-resistant design of RC building structures (Ph. D. thesis). University of Illinois, Urbana.

Madan, A. A., Reinhorn, A. M., Mander, J. B., & Valles, R. E. (1997). Modeling of masonry infill panels for structural analysis. *Journal of Structural Engineering*, *123*(10), 1295-1302.

Mohammadi, M., Akrami, V., & Mohammadi-Ghazi, R. (2011). Methods to improve infilled frame ductility. *Journal of Structural Engineering*, *137*(6), 646-653.

Negro, P. P., & Verzeletti, G. G. (1996). Effect of infills on the global behaviour of R/C frames: Energy considerations from pseudodynamic tests. *Earthquake Engineering and Structural Dynamics*, *25*(8), 753-773.

Park, Y. J., Reinhorn, A. M., & Kunnath, S. K. (1987), IDARC: Inelastic Damage Analysis of Reinforced Concrete Frame - Shear-Wall Structures. *Technical Report NCEER-87-0008*, State University of New York at Buffalo.

Paulay, T. and Priestley, M. J. N. (1992), Seismic Design of Reinforced Concrete and Masonry Buildings. *John Wiley & Sons*, New York.

Preti, M. M., Bettini, N. N., & Plizzari, G. G. (2012). Infill walls with sliding joints to limit infill-frame seismic interaction: Large-scale experimental test. *Journal of Earthquake Engineering*, *16*(1), 125-141.

Pujol, S., & Fick, D. (2010). The test of a full-scale three-story RC structure with masonry infill walls. *Engineering Structures*, *32*(10), 3112-3121.

Reinhorn, A. M., Madan, A. A., Valles, R. E., Reichman, Y., & Mander, J. B. (1995). Modeling of masonry infill panels for structural analysis. *Technical Report NCEER-95-0018,* National Center for Earthquake Engineering Research, State University of New York at Buffalo.

Saneinejad, A., & Hobbs, B. (1995). Inelastic design of infilled frames. *Journal of Structural Engineering*, New York, N.Y, *121*(4), 634-649.

SAP2000 Structural Analysis Program, *Computers and Structures, Inc.*, Berkeley, CA, U.S.A.

Shimazaki K, Sozen M. (1988). Strong ground motion drift and base shear coefficient for RC structures. *In: Proc. 9th world conference on earthquake eng. vol. 5,* 165-70.

TEC2007. Turkish Earthquake Code (2007). Regulations on Structures Constructed in Disaster Regions. *Ministry of Public Works and Settlement*, Ankara (In Turkish).

TS500 (2000). Requirements for Design and Construction of Reinforced Concrete Structures. *Turkish Standards Institution*, Ankara.

Valles, R. E., Reinhorn, A. M., Kunnath, S. K., Li, C., & Madan, A. A. (1996). IDARC2D version 4.0 – a program for the inelastic damage analysis of buildings. *Technical Report NCEER-96-0010,* National Center for Earthquake Engineering Research, State University of New York at Buffalo.

APPENDIX A

LINEAR DISPLACEMENT RESPONSE SPECTRA FOR NORMALIZED GROUND MOTIONS FOR 5% AND 10% DAMPING FACTORS
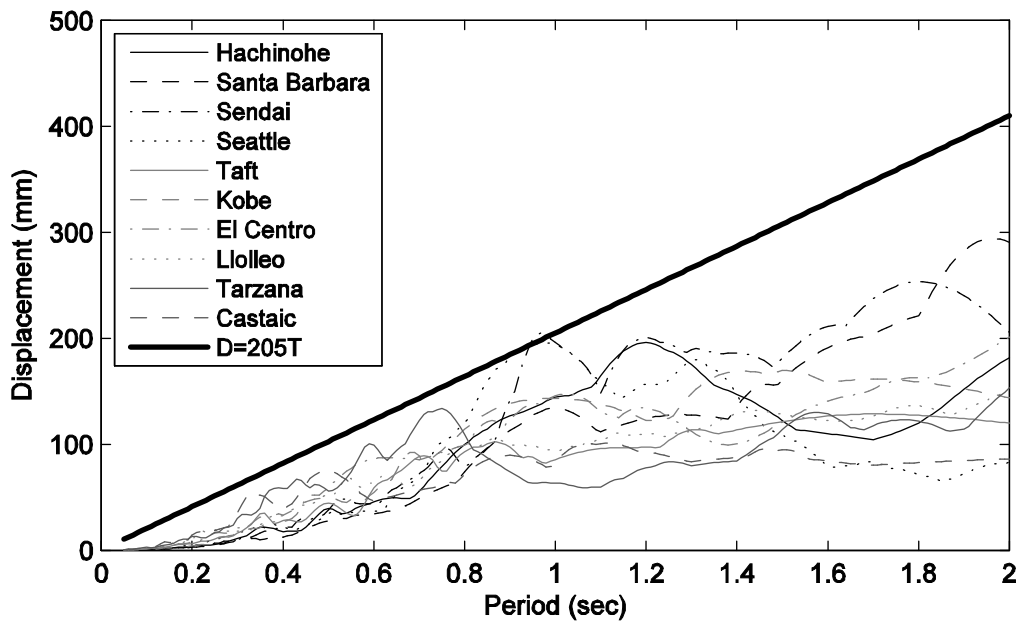

Figure A.1. Linear displacement response spectra for normalized ground motions for 5% damping
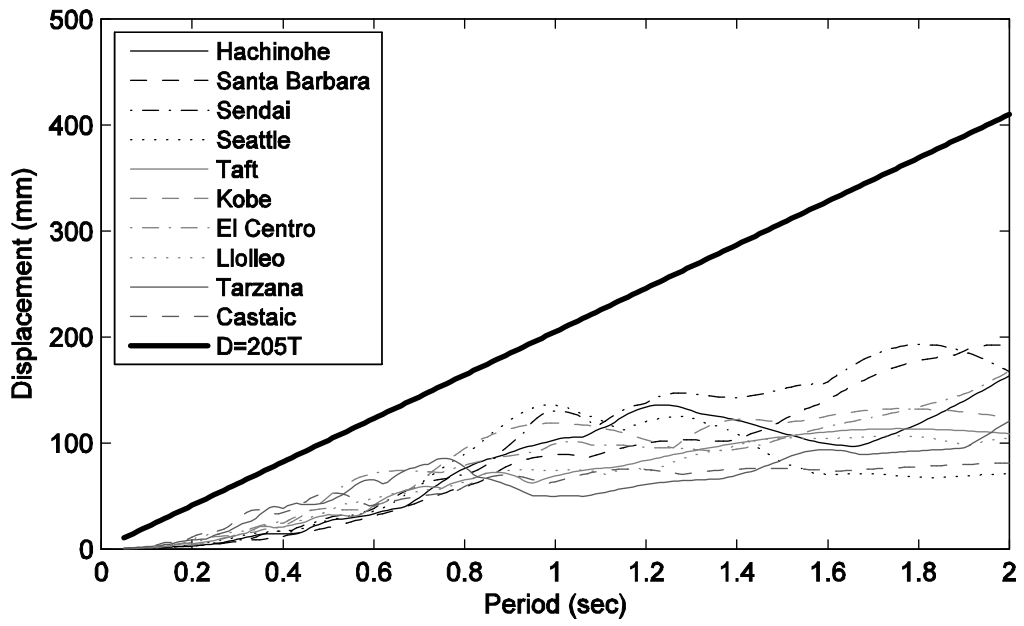
Figure A.2. Linear displacement response spectra for normalized ground motions for 10% damping